THE MESSENGER

EL MENSAJERO

No. 100 – June 2000

We are now celebrating the 100th issue of The Messenger.

The Messenger is one channel of ESO's multimedia approach to providing information about its activities and achievements. Like the European astronomical community, the Messenger looks towards the future, as evi - denced by the first article in this issue, on OWL.

We are ready to publish in the coming years an increasing number of first-class discoveries which will come from innovative technology and from bold, imaginative and efficient observers.

OWL Concept Study

R. GILMOZZI and P. DIERICKX, ESO

ESO is developing a concept of ground-based, 100-m-class optical telescope (which we have christened OWL for its keen night vision and for *OverWhelmingly Large*), with segmented primary and secondary mirrors, integrated active optics and multi-conjugate adaptive optics capabilities. The idea of a 100-m-class telescope originated in 1997, when it was assessed that true progress in science performance after HST and the 8–10-m-class Keck and VLT generations would require an order-of-magnitude increase in aperture size (a similar assessment had been made by Matt Mountain in 1996[1]). The challenge and the science potential seemed formidable – and highly stimulating.

Extremely large telescopes are no new idea: studies for 25-m-class telescopes[2, 3] date back to the mid-70s. Although these studies concluded that such telescopes were already technically feasible, the science case was not as strong as that permitted today by adaptive optics, and underlying technologies were far less cost-effective than they are now. In the late 80's, plans for a 25-m-class telescope were proposed by Ardeberg, Andersen et al.[4]; by 2000 the concept had evolved into a 50-m-class adaptive telescope[5]. Preliminary ideas for a 50-m concept were presented[1] by Mountain et al. in 1996; studies for a 30-m scaled-up version of the Hobby-Eberly telescope

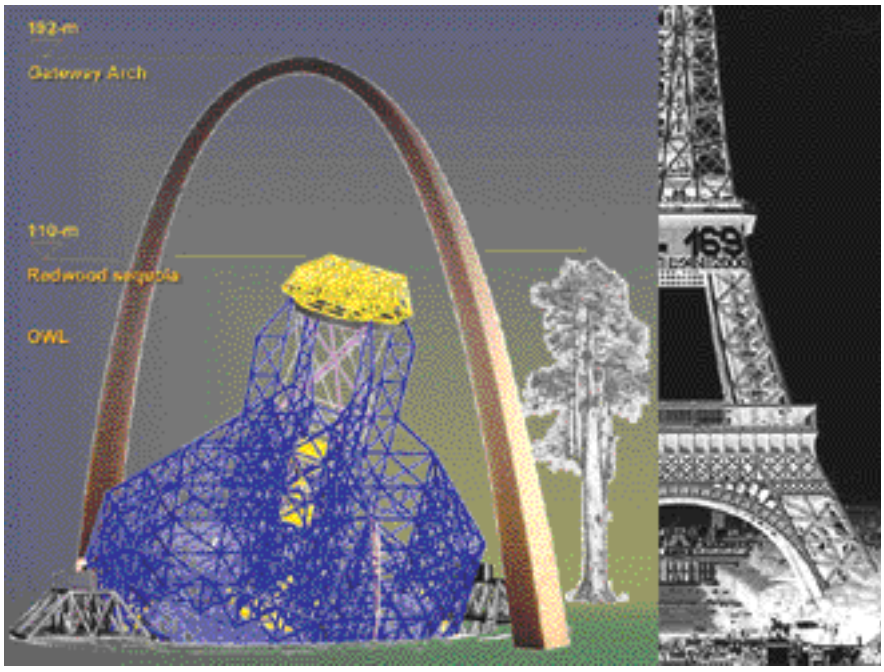

Figure 1: A matter of perspective …

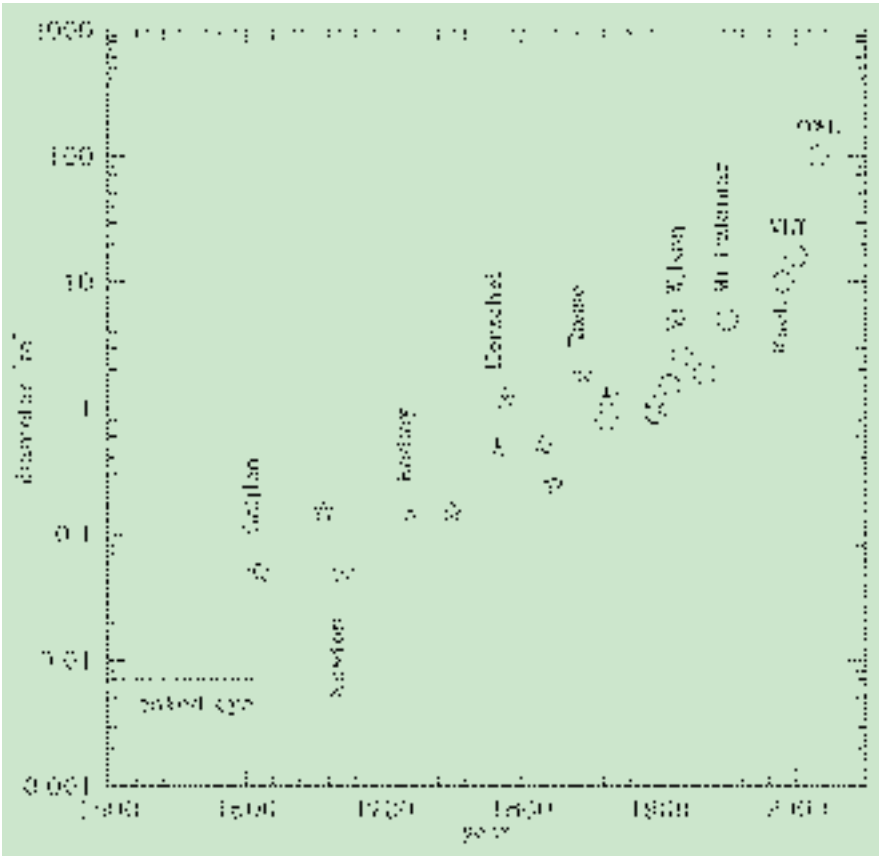

Figure 2: Brief history of the telescope. Stars refer to refractors, asterisks to speculum reflectors, circles to modern glass reflectors. Some telescopes are identified.

have been unveiled[6, 7] by Sebring et al. in 1998 and 1999; and plans for the 30-m California Extremely Large Telescope (CELT) have been unveiled by Nelson et al. at the March 2000 SPIE conference in Munich[8].

As for OWL, initial efforts concentrated on finding suitable optical design and fabrication solutions. The emphasis on optics is evident in the first (1998) publication made about the telescope concept[9], where it was shown that proven mass-production solutions for the telescope optics are readily available. From that point on, further studies progressed as rapidly as permitted by scarcity of resources, strengthening confidence in the concept. Several contributions[10,11,12,13,14] were made at the June 1999 workshop in Bäckaskog, Sweden, where, in particular, the basic concept of the mechanical structure was presented[12]. Industry showed astounding support for extremely large telescope concepts, two major suppliers announcing[15, 16] that they were ready to take orders. Two essential conclusions of this workshop were that, first, extremely large telescopes were indeed feasible, experts arguing about solutions instead of feasibility *per se*, and that, second, the future of high angular resolution belongs to the ground, thanks to adaptive optics.

Preliminary analyses have confirmed the feasibility of OWL's major components within a cost of the order of 1,000 million Euros and within a competitive time frame. A modular design allows progressive transition between integration and science operation, and the telescope would be able to deliver full resolution and unequalled collecting power 11 to 12 years after project funding.

The concept owes much of its design characteristics to features of existing telescopes, namely the Hobby-Eberly for optical design and fabrication, the Keck for optical segmentation, and the VLT for system aspects and active optics control. The only critical area in terms of needed development seems to be multi-conjugate adaptive optics, but its principles have recently been confirmed experimentally, tremendous pressure is building up to implement adaptive capability into existing telescopes, and rapid progress in the underlying technologies is taking place. Further studies are progressing, confirming initial estimates, and a baseline design is taking shape. The primary objective of these studies is to demonstrate feasibility within proven technologies, but provisions are made for likely technological progress allowing either cost reduction or performance improvement, or both.

Why 100 m?

The history of the telescope (Fig. 2) shows that the diameter of the "next" telescope has increased slowly with time (reaching a slope for glass-based reflectors of a factor-of-two increase every ~ 30 years in the last century: *e.g.* Mt. Wilson → Mt. Palomar → Keck).

The main reason for this trend can be identified in the difficulty of producing the optics (both in terms of casting the primary mirror substrate and of polishing it). The advances in material production and in new control and polishing technologies of the last few decades, fostered in part by the requirements set by the present generation of 8–10-m telescopes, offer now the exciting possibility of considering factors much larger than two for the next generation of telescopes. And unlike in the past, they also offer the promise of achieving this *without* implying a lengthy (and costly) programme of research and development (R&D).

At the same time, advances also in adaptive optics (AO) bring the promise of being able to achieve diffraction-limited performance. Though still in its infancy, AO is growing very fast, pushed in part also by customer-oriented applications. New low-cost technologies with possible application to adaptive mirrors (MEMs), together with methods like multi-conjugated adaptive optics (MCAO), new wave-front sensors and techniques like turbulence tomography are already being applied to AO modules for the present generation of telescopes. Although the requirements to expand AO technology to correct the wave front of a 100-m telescope are clearly very challenging (500,000 active elements, enormous requirements on computing power), there is room for cautious optimism. This would allow a spatial resolution of the order of one milliarcsecond, prompting the claim that high angular resolution belongs to the ground. Of course, this is valid only at wavelengths that make sense (*i.e.* $0.3 < \lambda < 2.5$ μm for imaging, $\lambda < 5$ μm for spectroscopy).

Can we afford it (in terms of time and cost)? Another consequence of the recent advances in technology is the fact that we can consider building a next-generation telescope within a reasonable time. Since a large R&D phase is not required (with the exclusion of AO, which is however being performed right now under the requirements set by the current generation of telescopes), 10 to 15 year timelines are appearing reasonable.

The cost issue is evidently one that needs to be addressed (even if a 50- or 100-m telescope is demonstrably feasible from the technical point of view, it will be impossible to build one unless the $D^{2.6}$ cost law can be broken). A "demonstration" that cost can be kept at low values has been put into practice by HET (admittedly accepting reduced performance). The introduction of modular design and mass-production (telescope optics, mechanics) is also a new and favourable factor. Based on this and on extrapolating the experience of the Keck (segmentation) and of the VLT

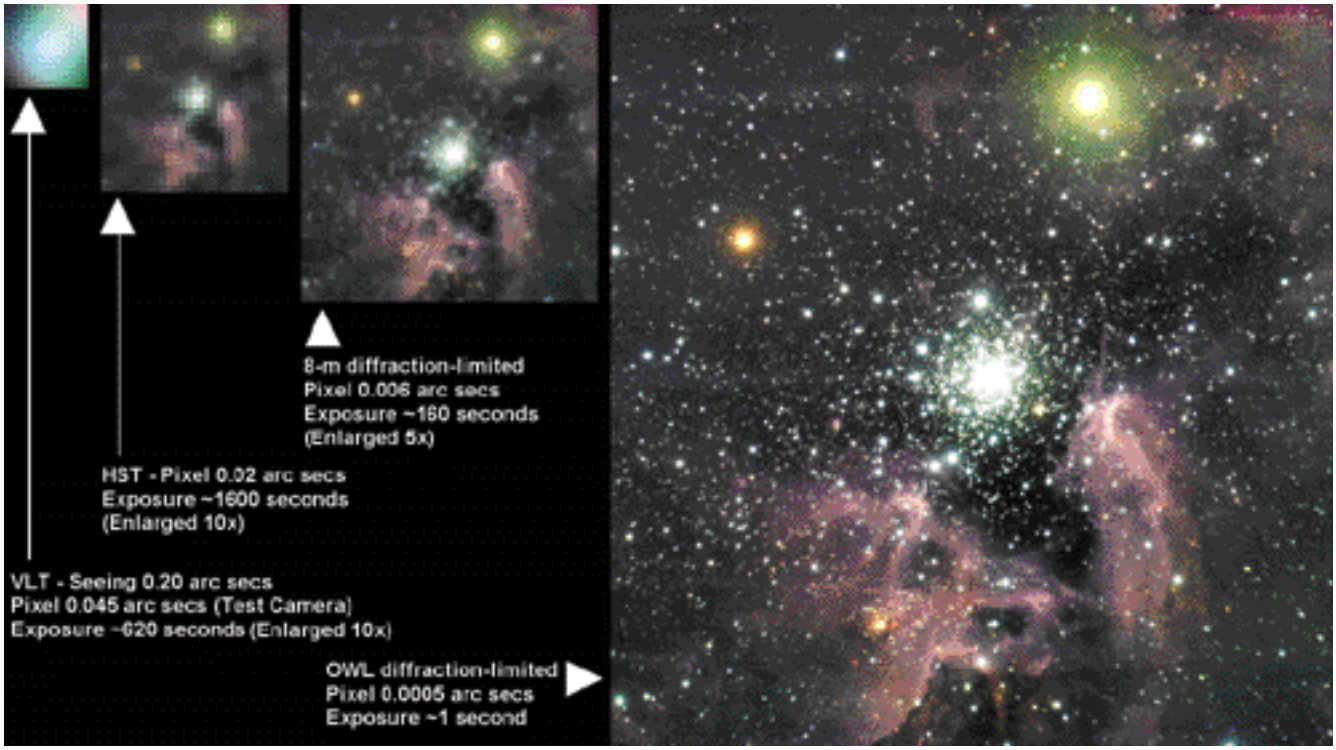

Figure 3: Resolution, from 0.2 arcseconds seeing to diffraction-limited with 100-m. All images 0.6 × 0.6 arc seconds [2].

(active control), the cost estimates range nowadays between $0.3 to $1 billion (respectively 30-m CELT and 100-m OWL). These costs are large (though not as large as, say, a space experiment), but possibly within what some large international collaboration can achieve.

From the point of view of "astronomical strategy", therefore, all this would also allow perhaps to optimise the space and ground facilities according to their *natural* location (*e.g.* optical/NIR astronomy from the ground, UV or thermal IR astronomy from space, etc), stressing their complementary rather than competitive roles. And this with the possibility of a reduction in "global" costs (the cost of HST would allow to build and operate at least *three* OWLs…)

Why 100 m? The original starting point for the development of the OWL concept (at the time called the WTT, alternatively for Wide Terrestrial Telescope or Wishful Thinking Telescope) was twofold. On one side a preliminary and naive science case (what is the telescope size needed to do spectroscopy of the faintest sources that will be discovered by NGST). On the other side, the interest in exploring the technological limitations in view of the recent advances, especially to what limit one could push angular resolution. In other terms: could the factor-of-two become an order-of-magnitude?

The progress both of the science case and of the design concept since the early days allows us to give some answers (albeit incomplete) to the question:

(i) The HST "lesson" has shown that angular resolution is a key to advance in many areas of astronomy, both in the local and in the far Universe. Achieving the diffraction limit is a key requirement of any design.

(ii) Milliarcsecond resolution will be achieved by interferometry (*e.g.* VLTI) for relatively bright objects and very small fields of view. The science-case (including the original 'complementarity with NGST'one) requirements are now, for the same resolution, field (~ arcminutes) and depth ($\geq 35^{th}$ magnitude), *i.e.* filled aperture diameters $\geq$ 100 m.

(iii) For diffraction-limited performance, the 'detectivity' for point sources goes as D^4 (both flux and contrast gain as D^2). One could say that a 100-m telescope would be able to do in 10 years the science a 50-m would take 100 years to do!

(iv) Last but not least, technology allows it: the current technological limitation on diameter of the (fully scalable) OWL design is ~140 m.

Feasibility issues: do we need an intermediate step? Another question that often arises is whether we need an intermediate step to whatever size we think we should achieve for scientific reasons (in other words, whether we wish to maintain the 'factor-of-two' paradigm even if its technological *raison d'être* has been overcome). The debate has vocal supporters on both sides (we OWLers are obviously for going directly to the maximum size required by the science and allowed by the technology). "Accusations" of respectively excessive conservatism or excessive ambition are exchanged in a friendly way at each meeting about Extremely Large Telescopes (ELTs). The interpretation of where exactly technology stands and how much can be extrapolated is at the core of the issue. We think this (very healthy) debate will go on for some time yet, and will be the main topic of the OWL Phase A study which is underway (goal for completion: early 2003).

Diffraction limit *vs.* seeing limit. Why make the diffraction limit such a strong requirement for ELTs is yet another subject of debate. On this, our position is very strong: we consider a seeing-limited ELT (deprecatingly named a "light bucket") as a goal not worth pursuing. While it is clear that the atmosphere will not always be "AO-friendly" and that, therefore, concepts of instrumentation to be used in such circumstances should be developed, there are scientific as well as technical reasons to justify our position.

Typically the seeing limit designs go together with wide field (here wide is many arcminutes) and/or high spectral resolution ($\geqslant$ 50,000) requirements. Apart from the *overwhelming* role of the background for seeing-limited imaging (sky counts of thousands of photons per second per pixel for a 50-m telescope), source confusion is a major scientific issue. From the technical point of view, building incredibly fast focal reducers, or high-resolution spectrographs with collimators the size of present-day telescopes, may pose technical challenges more extreme than building the telescope itself.

On the opposite side, imagers for diffraction-limited telescopes need very

slow *f*-numbers (50 or so, although admittedly here the challenge is to have enough detector area to cover a reasonable field, and to avoid severe saturation from 'bright' sources). Milliarcsecond(s) slits would make the beam size of a high-resolution spectrograph comparable to that of UVES or HIRES (*i.e.* instrumentation could be considered "comparatively" easy in the diffraction-limited case).

In the seeing-limited case, a spectroscopic telescope (of say 25–30 m and 5,000–20,000 resolution) could occupy an interesting scientific niche. Such a design is being considered as the natural evolution of the HET (Sebring et al.), and is the first one to have actually been called ELT (in other words, we have stolen the generic name from them. Another possibility for generic name is Jerry Nelson's suggestion of calling the future behemoths Giant Optical Devices or GODs. The hint about *hubris* is quite clear…).

Resolution, resolutely. Angular resolution and sensitivity are the highest-priority requirements. They are also closely intertwined, as high resolution implies high energy concentration in the core of the Point Spread Function (it is not a coincidence that the Strehl Ratio is called *Resolution* by optical physicists and engineers).

Figure 3 crudely illustrates the effect of increased resolution by showing the same hypothetical 0.6 × 0.6 arcsecond^2 field, as seen by a seeing-limited telescope under best conditions (FWHM ~ 0.2 arcsecs), by HST, by an 8-m diffraction-limited telescope and by OWL, respectively. Assuming the pixel size in the rightmost (OWL) image to be ~ 0.5 mas, the left frames have been convolved with the theoretical Point Spread Functions associated to each case. For the diffraction-limited image the exposure times have been adjusted to provide roughly the same total integrated intensity, taking into account collecting area. A corrective factor has been applied to the seeing-limited image to provide comparable peak intensity (this is due to the oversampling of the seeing-limited image).

Figure 3 also illustrates the fact that field size is a relative concept and should be evaluated in relation to its information content: the 0.6 × 0.6 arcsecond^2 field shown here becomes ~ 1,400,000 pixels when seen by OWL.

OWL's performance. At ten times the combined collecting area of every telescope ever built, a 100-m filled aperture telescope would open completely new horizons in observational astronomy – going from 10 m to 100 m represents a "quantum" jump similar to that of going from the naked eye to Galileo's telescope (see Fig. 2).

We have built a simulator of the performance of the OWL, which can also be used for different-size telescopes (and compared with similar calculations presented at the March 2000 SPIE conference or at the Bäckaskog 1999 Workshop on Extremely Large Telescopes, *e.g.* Mountain et al.). The simulator uses the PSF produced by the most recent optical design iteration, and includes the typical ingredients (diffusion, sky and telescope background, detector properties, and as complete as possible a list of noise sources). The output is a simulated image or spectrum (see Fig. 4).

A magnitude limit for isolated point sources of V = 38 in 10 hours can be achieved assuming diffraction-limited performance (whether there *are* such isolated sources is a different question, see below). Comparing this performance with the predicted one for NGST shows that the two instruments would be highly complementary. The NGST would have unmatched performance in the thermal IR, while a ground-based 100-m would be a better imager at $\lambda < 2.5$ μm and a better spectrograph ($\geq$ 5000) at $\lambda < 5$ μm. Sensitivity-wise, the 100-m would not compete in the thermal IR, although it would have much higher spatial resolution.

In terms of complementarity, OWL would also have a synergetic role with ALMA (*e.g.* in finding and/or studying proto-planets) and with VLBI (the radio astronomers have been waiting for us optical/IR people to catch up in spatial resolution for decades!)

Interferometry. Is interferometry an alternative to filled aperture? The consensus seems to be that this is not the case. Interferometry has a clearly separate scientific niche – for similar baselines its field of view (few arcseconds) and (bright) magnitude limits are definitely not competitive with the predicted performance of a filled aperture telescope. On the other side, baselines of hundreds of metres, if not of kilometres (in space even hundreds of km, as in the NASA plans), might well be the future of interferometry. Looking for the details of comparatively bright objects at the micro-arcsecond level, looking for and discovering earth-like planets, studying the surface of stars even further away are a domain where interferometry will always be first. In a sense, it is a "brighter object" precursor for any filled aperture telescope of the same size that may come in the future.

Items for the Science Case

The science case for the extremely large telescopes of the future is not fully developed yet. Some meetings have taken place on the subject, and more are planned (there will be at least one Workshop on this in 2000). However, it is difficult to think of a branch of astronomy that would not be deeply affected by the availability of a 50- or 100-m telescope with the characteristics outlined earlier.

In any event, there are a number of questions that the Science Case should pose, and find answers to, which will affect the final set of requirements for telescopes like the OWL. Do we need the angular resolution? Is 1 milliarcsecond too much, too little, enough? Is investing in AO research justified? Could we live with seeing limited? Can we not? Do we need 100 m? Are 50 m enough? Are 30 m? Are 20 m? Should we push even further? What is a sensible magnitude limit? Is interferometry a better alternative or a precursor? Do we need the optical and its tighter design tolerances and extremely more complex AO (especially since the faint/far Universe is very redshifted)? Do we have a compelling science case? Is "spectroscopy of the faintest NGST sources" enough? Is "unmatched potential for new discoveries" relevant? Is "search for biospheres" too public-oriented? Indeed, do we need an ELT?

In the following we will discuss some areas where OWL could give unprecedented contributions. This is by no means supposed to be a complete panorama, but rather reflects some personal biases.

Confusion about confusion. There is a widespread concern that ELTs may hit the confusion limit, thereby voiding their very *raison d'être.* Much of this concern is tied to observations obtained in the past, either from the ground or from space, with instrumentation whose angular resolution was very limited (*e.g.* the first X-ray satellites or the very deep optical images in 2″ seeing of the '80s). Recent developments have shown that whenever a better resolution is achieved, what looked like the confusion limit resolves itself in individual objects (*e.g.* the X-ray background, now known to consist mostly of resolved sources, or the HDF images, which show more empty space than objects).

Admittedly, there *may* be a confusion limit somewhere. However, the back-of-

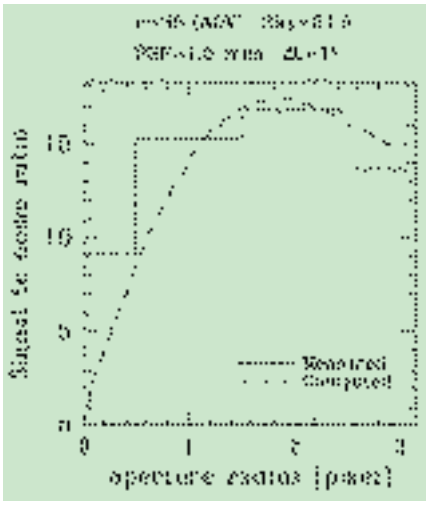

Figure 4: Output from the simulator. S/N for a 35th-magniture star in a 1-hour exposure measured on simulated image.

the-envelope argument that "all far galaxies are 1″ across, there are about 10^{11} galaxies and 10^{11} arcseconds, therefore, there must be a point where everything overlaps" fails when one resolves a square arcsecond in $>10^6$ pixels (crowding may still be an issue, though). The topic, however, is fascinating (and tightly connected with Olbers'paradox), and will be the subject of a future paper. For the purpose of this discussion, however, the only thing confusing about confusion is whether it is an issue or not. There is a clear tendency in the community to think that it is not.

Star-formation history of the Universe. This is an example of a possible science case which shows very well what the potentiality of a 100-m telescope could be, although by the time we may have one, the scientific problem will most likely have been already solved.

The history of stellar formation in the Universe is today one of the 'hot topics' in astrophysics. Its goal is to determine which kind of evolution has taken place from the epoch of formation of the first stars to today. To do so, "measurements" of star-formation rates are obtained in objects at a variety of look back times, and used to determine a global trend. These measurements are usually obtained by comparing some observed integral quantities of unresolved objects (typically an emission-line flux) with predictions made by evolution models. Although the method is crude, results are being obtained and a comprehensive picture is starting to emerge.

With a telescope like OWL, what are today "unresolved objects" would be resolved in their stellar components. For example, one could see O stars out to a redshift $z \sim 2$, detect individual HII regions at $z \sim 3$, measure SNe out to $z \sim 10$ (see below). Determining the star-formation rates in individual galaxies would go from relying on the assumptions of theoretical models and their comparison with integrated measurements, to the study of individual stellar components, much in the way it is done for the "nearby" Universe.

Symbiosis with NGST. This was the "original" science case for a 100-m telescope, and runs much in the same vein as the case made by Matt Mountain[1] for a 50-m telescope to observe the faintest galaxies in the HDFs. The symbiosis with NGST would however not only be of the "finder/spectrometer" variety (though much science would be obtained in this way), but as explained above also in terms of complementarity in the space of parameters (wavelength coverage, angular resolution, spectral resolution, sensitivity, etc). The feeling is that a science case to complement the NGST is a strong one, but cannot be the main case for a 100-m telescope.

Measure of H. Cepheids could be measured with OWL out to a distance modulus ($m - M$) ~ 43 (*i.e.* $z \sim 0.8$). This would allow the measurement of H and its dependence on redshift (*not* H_0) unencumbered by local effects (*e.g.* the exact distance to Virgo). In fact, the distance to Virgo, and the value of H_0, would be determined as "plot intercept" at $t = 0$! There is an interesting parallel to be done here with HST to get a "feeling" of what crowding problems we could have. Crowding would start affecting the photometry of individual Cepheids at about this distance in much the same way it does for HST images of Virgo galaxies. In fact, we would be about 100 times further than Virgo with a resolution about 100 times better than HST (Cepheids are observed with HST mainly in the undersampled Wide Field chips).

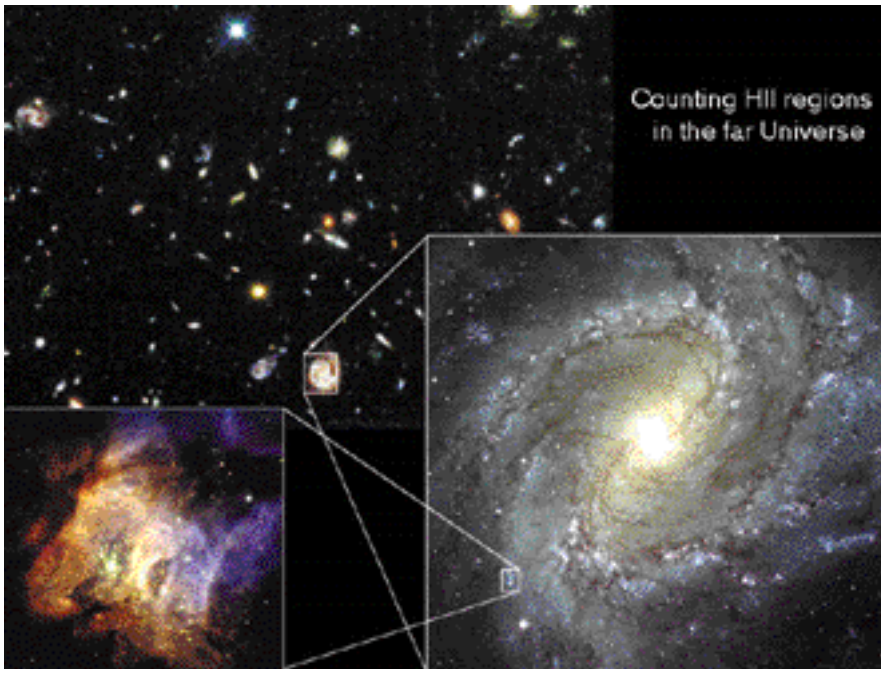

Figure 5: OWL's view of a galaxy in the HDF.

Supernovae at $z \sim 10$. An "isolated", *underluminous* Type II supernova like SN 1987A would be visible at ($m - M$) ~ 53. Assuming that crowding and/or increased background would bring the limit to 50 (*i.e.* $z \sim 10$, the exact value depending on one's favourite cosmology), we would still be able to detect *any* SN ever exploded out to that redshift (!).

Figure 6 shows model calculations of supernova rates assuming a 10^{12} $M_\odot$ elliptical galaxy beginning star formation at $z = 10$. The rates are several dozen per year (*i.e.* ~ 0.3 per day!). Even for much less massive galaxies the rates are a few per year. This means that any deep exposure in a field ≤ 1 arcmin^2 will contain *several* new supernovae.

Since these SNe will be at high redshift, the observed light-curves will be in the rest UV. This actually makes their identification easier, since Type-II light-curves last typically 12 to 24 hours in the UV: time dilation will lengthen the curves by $(1 + z)$ making them ideal to discover. (Note that the optical light-curves, intrinsically some months long, would last years due to dilation).

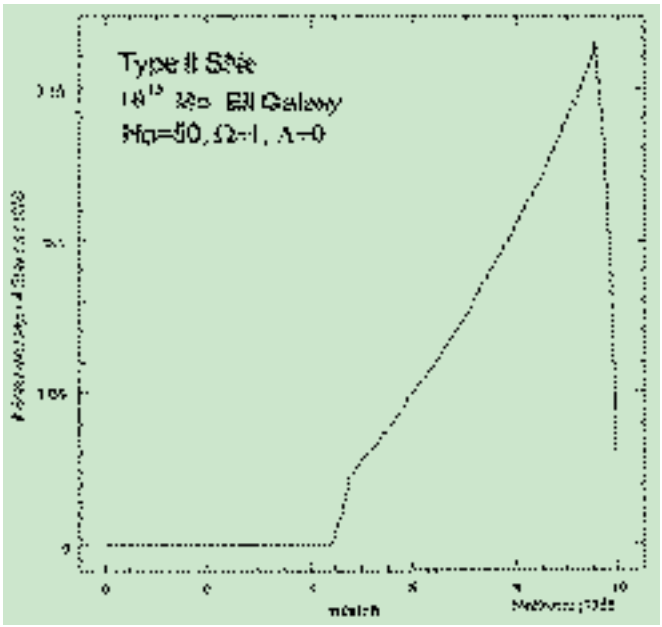

Figure 6: Type-II SN rate at high redshift for a 10^{12} $M_\odot$ elliptical galaxy (Matteucci 1998).

Figure 7: Simulation of the Solar System at 10 parsecs. Jupiter can be seen on the right. Saturn would also be detected, about 10 cm on the right of this page.

The study of SNe out to $z \sim 10$ (if indeed stars started forming at or before that redshift, which is not certain by any means) would allow to access ~ 30% of the co-moving volume (*i.e.* mass) of the Universe (at present, through SNe we can access less than 3%). Star formation rates at such early ages would be a natural by-product of these studies. Nearer SNe would be bright enough to provide "light bulbs" to study the intergalactic medium on many more lines of sight than those provided by other bright but less common objects, *e.g.* QSOs. And of course, although with lower rates and at "nearer" distances (their rate peaks at $z_I \sim z_{II} - 2.5$), the brighter Type-I SNe will also contribute to the study.

Other high-redshift Universe studies. A telescope with the resolution and sensitivity of OWL's would find some of the most important applications in the study of the furthest and faintest objects in the Universe. Among many others, studies of the proto-galactic building blocks and the dynamics of their merging into higher hierarchical structures. The possibility of probing even higher redshifts with Gamma-Ray Bursts (if they exist at earlier epochs) is also very exciting, as they are intrinsically orders of magnitude brighter than even SNe.

High-frequency phenomena. Rapid variability is an area where the improvements brought by larger collecting areas can be truly enormous. The power spectrum of such phenomena is in fact proportional to the square of the flux, *i.e.* $P \sim D^4$. Dainis Dravins showed at the Bäckaskog Workshop that extremely large telescopes open a window on the study of quantum phenomena in the Universe which were till now only observed in the laboratory.

Nearby Universe. In the nearer Universe we have again a myriad of possible contributions. The detection of brown dwarfs in the Magellanic Clouds would enable us to determine an accurate IMF for those galaxies. It would be possible to observe White Dwarfs in the Andromeda galaxy and solar-like stars in galaxies in the Virgo cluster enabling detailed studies of stellar populations in a large variety of galaxies. The environment of several AGNs would be resolved, and the morphology and dynamics of the inner parts nearest to the central black hole could be tracked and understood. If the rings around SN 1987A are a common phenomenon, they could be detected as far as the Coma cluster. In our own galaxy, we could study regions like Orion at sub-AU scales, determining the interactions between stars being born and the parent gas. We would detect protoplanetary disks and determine whether planets are forming there, and image the surface of hundreds of stars, promoting them from points to objects. Unlike interferometry (which also can image stellar surfaces, but needs many observations along many baselines to reconstruct a "picture") these observations will be very short, allowing the detection of dynamic phenomena on the surfaces of stars other than the Sun.

Extra-solar planets. Finally, a critical contribution will be in the subject of extra-solar planets. Not so much in the discovery of them (we expect that interferometry will be quite successful in this), but rather in their spectroscopic study. Determining their chemical composition, looking for possible biospheres will be one of the great goals of the next generation of ELTs. Figure 7 shows a simulation of an observation of the Solar System at 10 parsecs (based on the PSF of an earlier optical design, and including the effect of microroughness and dust diffusion on the mirror) where Jupiter and Saturn would be detected readily. Several exposures would be necessary to detect the Earth in the glare of the Sun. Sophisticated coronographic techniques would actually make this observation "easier" (or possible at a larger distances).

Operational issues. The sheer size of a project like OWL, or any other ELT project, makes it unlikely that the operational scenario would be similar to that of the current generation of telescopes. We believe that the current (mild) trend towards Large Programmes (where the need for deep – *i.e.* long – exposures is combined with the statistical requirement of a large number of measurements) will evolve towards some sort of "Large Project" approach, similarly to what happens in particle physics. In this sense, maybe even the instrumentation plan could be adapted to such an approach (*e.g.* a Project would develop the "best" instrument for the observation, and when it is over a new Project with possibly new instruments would take over). What we imagine is "seasons" in which OWL (or whatever) will image the surface of all 'imageable' stars, or study 10^5 SNe, or follow the dynamics of the disruption of a star by an AGN's black hole. In other words, a series of self-contained programmes which tackle (and hopefully solve!) well defined problems, one at a time.

SCALABILITY – Why Not?

The last two decades of the 20th century have seen the design and completion of a new generation of large telescopes with diameters on the order of 8 to 10 metres. To various degrees, concepts developed on this occasion have concentrated on the feasibility of the optics, controlled optical performance, cost reduction, and have been quite successful in their endeavours.

The achievements of recent projects could hardly be summarised in a few lines, but we emphasise three major breakthroughs:

- Optical segmentation (Keck).
- Cost-effective optical and mechanical solutions (Hobby-Eberly)
- Active optical control (NTT, VLT, Gemini and Subaru).

The lessons learned from these projects are, to some extent, already being implemented in a series of projects (e.g. GTC, SALT), but future concepts may quite naturally rely on a broad integration of positive features of each approach. Perhaps the most far-reaching innovations have been brought by the Keck, with virtually unlimited scalability of the telescope primary optics, and by the VLT, with highly reliable and performance-effective functionality (active optics, field stabilisation). Scalability was traditionally limited by the difficulty to cast large, homogeneous glass substrates, and progress over the last century has been relatively slow. Indeed, even the relatively modest size increase achieved by the most recent telescopes with monolithic primary mirrors would have been impossible without innovative system approaches (e.g. active optics) which relaxed constraints on substrate fabrication.

Optical scalability having been solved, other limitations will inevitably apply. Taking only feasibility criteria into account, and modern telescopes being essentially actively controlled opto-mechanical systems, these new limitations may arise either in the area of structural design, control, or a combination of both. Our perception is that the fundamental limitations will be set by structural design, an area where predictability is far higher than with optical fabrication. However, it should be observed that, despite the fact that control technologies are rapidly evolving towards very complex systems, those technologies are also crucial when it comes to ensuring that performance requirements are efficiently and reliably met. Reliability will indeed be a major issue for extremely large telescopes, which will incorporate about one order of magnitude more active degrees of freedom (e.g. position actuators). In this respect, however, the Keck and VLT performances are encouraging.

Although there is still major effort to be accomplished in order to come to a consolidated design, it appears already

that OWL is most likely feasible within currently available technologies and industrial capacity. Actually, the successive iterations of the opto-mechanical design indicate that OWL diameter is quite probably below the current feasibility limit for a steerable optical telescope, which we estimate to be in the 130–150-metre range.

Adaptive optics set aside, OWL's actual limitation seems to be cost, which we constrain to 1,000 million Euros, capital investment, including contingency. Such budget is within a scale comparable to that of space-based projects and spread over a longer time scale. Additionally, it can reasonably be argued that progress in ground-based telescopes is broadly beneficial in terms of cost and efficiency as it allows space-based projects to concentrate on, and be optimised for, specific applications which cannot be undertaken from the ground – because of physical rather than technological reasons.

It is obviously essential that the concept allows a competitive schedule, which should be the case as the telescope could, according to tentative estimates, deliver unmatched resolution and collecting power well before full completion.

Telescope Conceptual Design

Top level requirements

The requirements for OWL correspond to diffraction-limited resolution over a field of 30 arc seconds in the visible and 2 arc minutes in the infrared ($\lambda \sim 2$ µm), with goals of 1 and 3 arc minutes, respectively. The telescope must be optimised for visible and near-infrared wave bands, although the high resolution still allows some competitive science applications in the thermal infrared[14]. Collecting power is set to ~ 6000 m^2, with a goal of 7000.

The optical quality requirement is set to *Strehl Ratio > 20%* (goal ≥ 40%) at $\lambda = 500$ nm and above, over the entire science field of view and after adaptive correction of atmospheric turbulence with a seeing angle of 0.5 arcseconds or better. We tentatively split this requirement into telescope and atmospheric contributions:

Strehl Ratio associated with all error sources except atmospheric turbulence ≥ 50% (goal ≥ 70%);

Strehl Ratio associated with the correction of atmospheric turbulence ≥ 40% (goal ≥ 60%).

It is not yet entirely clear what the field limitations of multi-conjugate adaptive optics are; preliminary analysis show that under representative conditions, a 3-adaptive-mirrors system would provide an isoplanatic field of ~ 20 arcseconds in the visible; larger fields may require more complex adaptive systems.

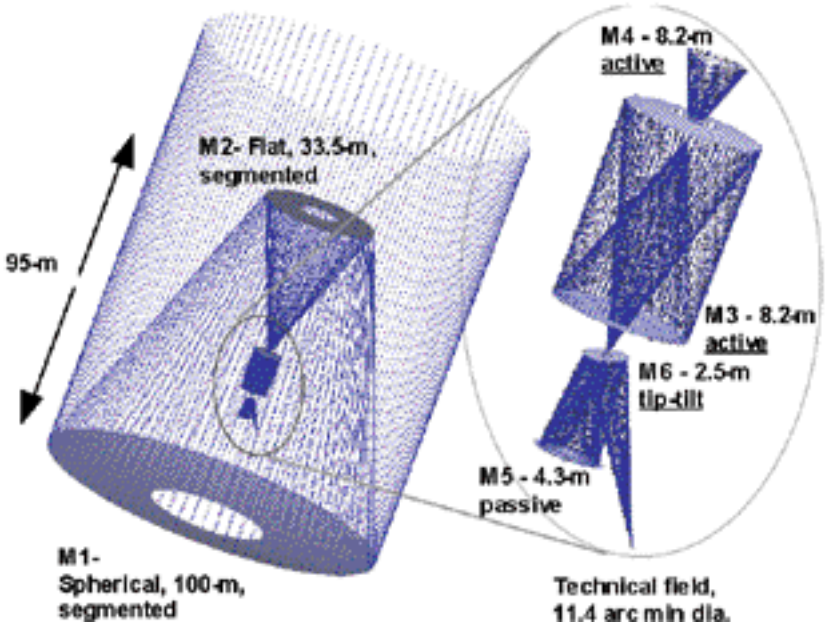

Figure 8: Layout of the optical design, 6-mirror solution.

Design considerations

We consider that the essential function of the system is to reliably deliver a minimally disturbed – in terms of amplitude and phase – wavefront to the science detector, over a specified field of view. As disturbances inevitably occur – atmospheric turbulence, telescope optics, tracking, etc. –, those must be either minimised or corrected, or both.

It is quite logical to distinguish between atmospheric and telescope disturbances for their very different spatial and dynamic properties, the former being arguably the most difficult to compensate. Therefore, we incorporate into the telescope concept dedicated adaptive modules, to be designed and optimised for correction of atmospheric turbulence at specified wave bands, and we request that the telescope contribution to the wavefront error delivered to the adaptive module(s) be small with respect to the wavefront error associated with atmospheric turbulence. In brief, we request the telescope itself to be seeing-limited. It should be noted that, in purely seeing-limited mode where the relevant wavefront quality parameter is slope, the aperture size implies that fairly large wavefront amplitudes can be tolerated. For example, a wavefront tilt of 0.1 arcseconds over the total aperture corresponds to a wavefront amplitude of 48 microns peak-to-valley with OWL whereas it would correspond to 3.9 microns with the 8-m VLT.

Taking into account the telescope size and some implied technology solutions (e.g. optical segmentation), we come to the unsurprising conclusion that the telescope itself should provide the following functions: phasing, field stabilisation, and active optics, including active alignment. The case for field stabilisation is very strong, as a "closed" co-rotating enclosure would be very costly and anyway inefficient in protecting the telescope from wind.

As pointed out earlier, we consider modern telescopes to be controlled opto-mechanical assemblies. The sheer size of OWLonly emphasises the need for a coherent system approach, with rational trade-offs and compromises between different areas, e.g. optical and structural designs. It is also essential that from the earliest stages the design incorporates integration, maintenance and operation considerations. Besides cost, the two essential reasons are construction schedule and operational reliability, the latter playing a critical role when it comes to telescope efficiency.

Optics

Several designs have been explored, from classical Ritchey-Chrétien to siderostat solutions. The shape of the primary mirror is the focus of a hot discussion in the community. Proponents of aspheric designs invoke the lower number of surfaces an aspheric primary-mirror design would imply, and progress of optical fabrication allowing cost-effective production of off-axis aspheric surfaces.

It does however not appear possible to provide the necessary telescope functions with two optical surfaces; field stabilisation, in particular, would require a relatively small, low inertia secondary mirror (in the 2- to 3-m range for effective correction with typical wind frequency spectra) and therefore imply horrendous sensitivity to decentres. In order to minimise structure height, a small secondary also implies a very fast primary mirror design, thereby exacerbating fabrication and centring issues,

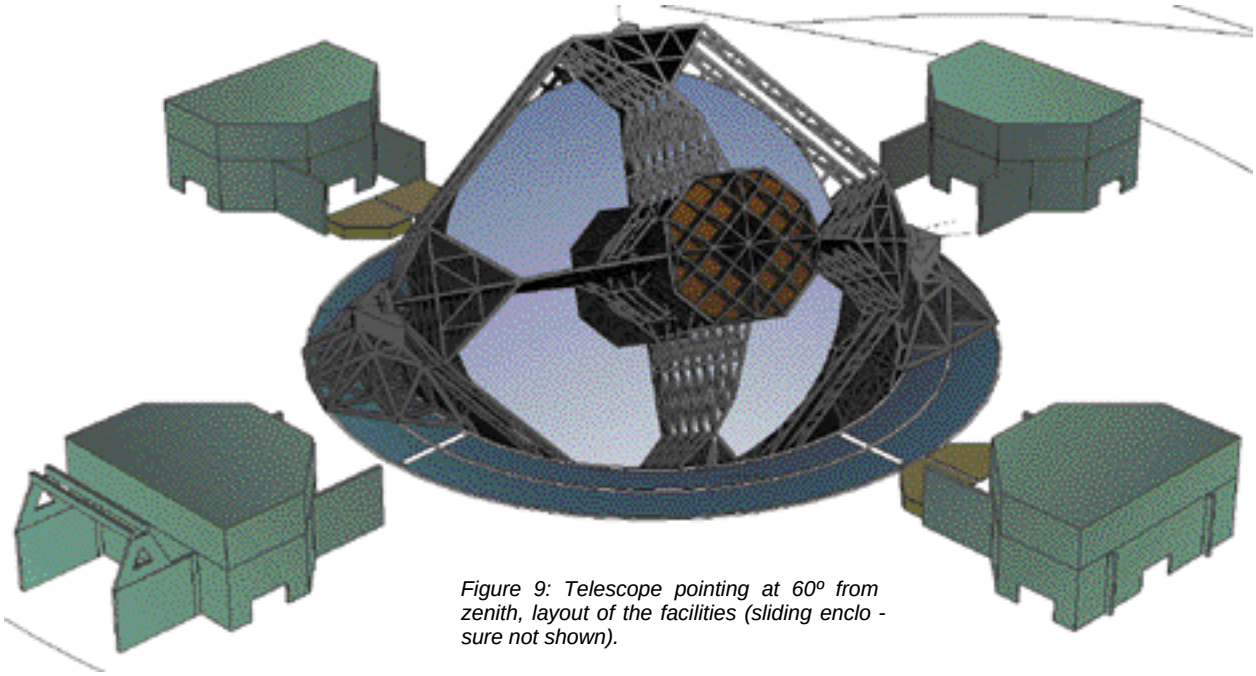

Figure 9: Telescope pointing at 60º from zenith, layout of the facilities (sliding enclo - sure not shown).

and increasing field aberrations. A possible way around these constraints would be to allow a large secondary mirror and to re-image the pupil of the telescope to perform field stabilisation with a conveniently sized surface. Unless the secondary mirror would be concave – which implies a longer telescope structure – such solution, however, raises considerable concerns as to the feasibility of this mirror. It also implies a larger number of surfaces, thereby eliminating the prime argument in favour of an aspheric primary mirror design.

The cost argument is particularly interesting, as it shows how much progress has been realised in optical fabrication over the last decade. There is rather consistent agreement that current technology – polishing of warped segments on planetary machines combined with ion-beam finishing – could lead to an increase of polishing costs for aspheric segments by about 50% – down from 300 to 500% – with respect to all-identical, spherical segments. This figure is however incomplete, as it does not take into account more stringent requirements on substrate homogeneity and residual stresses, which would lead to a cost overshoot far exceeding that of the pure figuring activities. Additionally, polishing of warped segments is intrinsically less deterministic hence less adapted to mass-production, and this solution leads to undesirable schedule risks.

Any trade-off must also incorporate mechanical constraints, and in particular the inevitable difficulty to provide high structural rigidity at the level of the secondary mirror. As will become evident later, this aspect has played a crucial role in the selection of the OWL baseline design.

The considerations outlined above point towards spherical primary and secondary mirror solutions. It should be noted that the trade-off is dependent on telescope diameter; cost considerations set aside, aspheric solutions are probably still superior as long as field stabilisation does not require pupil re-imaging. The limit is probably in the 20 to 30 metre range, possibly more with active mechanics and suitable shielding from wind, but certainly well below 100 m.

We have selected a 6-mirror configuration[11,17], with spherical primary and flat secondary mirrors (Fig. 8). Spherical and field aberrations are compensated by a 4-mirror corrector, which includes two 8-m-class active, aspheric mirrors, a focusing 4.3-m aspheric mirror and a flat tip-tilt conveniently located for field stabilisation. Primary-secondary mirror separation is 95 m, down from 136 m of the first design iteration.

The diffraction-limited (Strehl Ratio $\geq$ 80%) field of view in the visible is close to 3 arcminutes and the total field is ~ 11 arcminutes. The latter, called *technical field*, provides for guide stars for tracking, active optics, and possibly phasing and adaptive correction with natural guide stars. A laser guide star solution would require a smaller technical field of view (~ 6–7 arcminutes) and lead to some design simplification.

It should be noted that the optical configuration is quite favourable with respect to mechanical design, as the secondary mirror is flat (hence insensitive to lateral decentres) and as the position and design space for the corrector mechanics permit high structural stiffness at this location. A sensitivity analysis has shown[17] that with a fairly simple internal metrology system the telescope could be kept in a configuration where residual alignment errors would be well corrected by active optics.

The primary mirror would be made of ~ 1600 hexagonal segments, ~ 2.0-m flat-to-flat i.e. about the maximum size allowed for cost-effective transport in standard containers. No extensive trade-off has been made so far but we rule out very large segments as those would lead to unacceptably high material, figuring, and transport costs and require substantial investment in production facilities in order to comply with a reasonable schedule. There are, indeed, strong engineering arguments in favour of relatively small segments, such as the 1-m ones proposed by Nelson et al. at the March 2000 SPIE conference in Munich. A certain relaxation is however possible with spherical segments, as the added complexity implied by the aspheric deviation – which increases quadratically with the aspheric segment size – disappears. Handling and maintenance would also benefit from a reduced segment size, although auxiliary equipment for automated procedures will be mandatory anyway.

The baseline solution for the mirror substrate is glass-ceramics and, according to suppliers, production within 6–8 years would only require duplication of existing production facilities[12]. A very promising alternative is Silicon Carbide, which would allow a ~ 75% mass reduction for the primary mirror with a conservatively simple lightweight design, and a mass saving of ~ 4,000 tons for the telescope structure. This technology is, however, not (yet?) demonstrated for mass-production; further studies will have to take place prior to final selection of the mirror technology.

Figuring would require three to four 8-m-class polishing (planetary) machines, complemented with one or two 2-m-class ion-beam finishing machines. It should be noted that 1-m-class, diffraction-limited laser amplifier windows are currently produced[13,15] at

a rate fully comparable to that needed for OWL.

Phasing of the primary and secondary mirrors relies conservatively on the same solution as the Keck one, i.e. position sensing combined with sensor calibration. An extensive summary of the mirror phasing techniques applied to the Keck telescopes is presented by Chanan[19]. Calibration is however more complex with OWL as the primary and secondary mirrors must be phased separately. In the worst-case scenario, daytime calibration of one of the two mirrors would be required – in practice, interferometric measurements performed on the flat secondary mirror – while the other of the two would be phased on the sky according the scheme described by Chanan. We are also exploring on-sky closed-loop phasing techniques, which should provide a more efficient control of phasing errors. Quite a number of on-sky phasing methods have been proposed in the recent past; most are based on curvature sensing or interferometric measurements of one kind or another. These methods are generally sensitive to atmospheric turbulence and require either short exposure or sub-apertures smaller than the atmospheric coherence length, thereby implying use of relatively bright stars – or closing the adaptive loop before the phasing one. The actual limitations are, however, still to be assessed. A particularly attractive method, which should allow to differentiate primary and secondary mirror phasing errors, is the one proposed by Cuevas et al[20].

Adaptive optics

Attaining diffraction-limited resolution over a field of view largely exceeding that allowed by conventional adaptive optics is a top priority requirement for OWL. Conservative estimates[21] indicate that multi-conjugate adaptive optics[22] (MCAO) should allow for a corrected field of view of at least 20 arcseconds in the visible, assuming a set of three adaptive mirrors conjugated to optimised altitudes. There is ongoing debate on the respective merits of a tomographic-oriented correction strategy, followed by the Gemini team, and a layer-oriented one, proposed by Ragazzoni et al. A European Research and Training Network (RTN) has recently been set up, on ESO's initiative, to address the general issue of adaptive optics for extremely large telescopes.

In the visible, the implied characteristics of adaptive modules (about 500,000 active elements on a 100-m telescope, a corresponding wavefront sampling and commensurate computing power) leaves no doubt as to the technological challenge. Novel ideas about wavefront sensing (e.g. pyramidic wavefront sensors) and spectacularly fast progress in cost-effective technologies which could potentially be applied to adaptive mirrors (MEMs or MOEMs), together with the strong pressure to achieve MCAO correction on existing 8-m-class telescopes in a very near future, leaves room for cautious optimism. Prototypes are under development – the Observatory of Marseille, in particular, is working towards a ~ 5000 active elements to be tested by 2003–2004 and based on a scalable technology.

Extensive discussions of adaptive optics aspects for OWL and extremely large telescopes are presented elsewhere[13, 21, 22, 23, 24]. Proposals for MCAO demonstrators or even functional instruments to be installed within a fairly short time frame on the VLT and Gemini, respectively, have been made. However promising such developments could be, it is impossible, at this stage, to make any substantiated statement as to their outcomes. Therefore, the telescope design incorporates the most conservative assumptions regarding the eventual technology solutions, which implies, in particular, large field of view for reasonable sky coverage with natural guide star. All attempts are made to avoid constraints on the design and correction range of the adaptive modules, which implies that the telescope be able to deliver seeing-limited performance comparable to that of existing large telescopes without relying on adaptive correction.

Mechanics

Several mount solutions have been explored, including de-coupled geometries[12] based on fully separate structures for the primary and secondary mirrors. As was – to some extent – expected, the best compromise in terms of cost, performance, and feasibility in a broad sense (i.e. including assembly, integration and maintenance aspects) seems to be an alt-az concept.

As in the case of the main optics, the mechanical design[26] relies heavily on standardised modules and parts, allowing cost reduction factors which are normally not attainable with classical telescope designs. Manufactured or pre-assembled parts are constrained to having dimensions compatible with cost-effective transport in standard 40-ft containers. It should be pointed out that, in view of the structure dimensions, the standardisation does not necessarily impair performance. Particular attention is given to assembly and integration constraints as well as to suitability for maintenance[26].

The all-steel structure has a moving mass of the order of 13,500 tons (including mirrors) and does not rely on advanced materials. Iso-static and hyper-static configurations are being evaluated, the former yielding lower dynamic performance and the latter slightly higher mass, complexity, and cost. First locked rotor frequency is 1.5 Hz for the iso-static and 2.4 Hz for the hyper-static configurations, respectively. Static deformations require the decentres of the secondary mirror and of the corrector to be compensated, but the relevant tolerances, which are set to guarantee that the on-sky correction loop by active optics can be closed, are not particularly stringent[17].

There is no provision for a co-rotating enclosure, the advantage of which being anyway dubious in view of the enormous opening such enclosure would have. Protection against adverse environmental conditions and excessive day-time heating would be ensured by a sliding hangar, whose dimensions may be unusual in astronomy but actually comparable to, or lower than, those of large movable enclosures built for a variety of applications[25]. Air conditioning would lead to prohibitive costs and is not foreseen; open air operation and unobstructed air circulation within beams and nodes seem sufficient to guarantee that the structure reaches thermal equilibrium within an acceptably short time. In this respect, it should be noted that OWL structure is, in proportion to size, more than an order of magnitude less massive than that of the VLT.

Open-air operation is evidently a major issue with respect to tracking and, as mentioned before, full protection from the effect of wind is not a realistic option. Hence the need for field stabilisation. The latter is provided by a 2.5-m-class flat mirror located in a pupil image, and there is reasonable confidence that a bandwidth of 5–7 Hz could be achieved with available mirror technology. It should also be noted that active and passive damping systems have not yet been incorporated into the design.

The kinematics of the structure is comparable to that of the VLT telescopes: 3 minutes for 90º elevation range, 12 minutes for 360º azimuth range, maximum centrifugal acceleration not exceeding 0.1 g at any location of the structure, and 1 degree zenithal blind angle. The number of motor segments would be on the order of 200 for elevation and 400 for azimuth. These figures are based on VLT technology and appear very conservative.

The telescope can point towards horizon, which allows to reduce the dimensions of the sliding enclosure and facilitates maintenance of the secondary mirror unit and extraction of the corrector unit along the axis of the telescope. Mirror covers are foreseen; they would consist of four quadrants sliding into the structure when the telescope is pointing towards zenith. One of these covers would be equipped with segments handling systems and *in situ* cleaning facilities allowing periodic cleaning of the primary mirror. Figure 9 shows the telescope pointing towards 60º zenithal distance, mirror covers re-

tracted. The sliding enclosure is not figured.

Conclusions

Progress of OWL conceptual design does not reveal any obvious show-stopper. Underlying the feasibility of a 100-m-class telescope is the fact that traditional scalability issues, such as the feasibility of the optics, have shifted to entirely new areas, namely mechanics and control. These last are evidently more predictable, and their limitations inevitably exceed those so far applying to conventional telescope design – a size increase by a factor 2 per generation.

A preliminary cost model has been assembled and, to some extent, consolidated. The total capital investment remains within the target maximum of 1,000 million Euros, including contingency. It should be pointed out, however, that some of the most determinant cost positions correspond to subsystems involving mass production (primary optics, structure), an area traditionally *terra incognita* to telescope designers. The full implication of mass-production of the primary optics, of actuators and sensors, and of the structure may be underestimated. Our cost estimate should therefore be consolidated by industrial studies. Our perception is that current estimates are probably conservative.

There is strong indication that a competitive schedule is possible; the critical path is set by the mechanics, and, in contrast to the situation which prevailed at the time the last generation of 8- to 10-m-class telescopes was designed, long-lead items such as the main optics do not require time-consuming technology developments. Whereby achieving technical first light within 8–9 years after project go-ahead would be a challenging objective, flexibility in the subsequent integration phases should allow a start of partial science operation at full resolution within 11 and 12 years in the infrared and in the visible, respectively.

The current schedule calls for a completion of phase A, including demonstration of the principle of multi-conjugate adaptive optics on the VLT, by 2003. As ambitious as such objective may seem, it should be recalled that the design of the OWL observatory relies extensively on proven technologies, bar adaptive optics – an approach which has also been adopted for the CELT project. In this respect, it should be pointed out that technology development for long-lead items (primary mirrors) played a determinant role with the current generation of 8–10-m-class telescopes. These specific, highly time-consuming technology developments being largely unnecessary for extremely large telescopes such as CELT and OWL, tighter scheduling may become possible.

Further information and publications about the OWL study are available at http://www.eso.org/owl

Acknowledgements

The concept presented in this article is the result of the work of several people. The authors wish to thank, in particular, Bernard Delabre, Enzo Brunetto, Marco Quattri, Franz Koch, Guy Monnet, Norbert Hubin, Miska Le Louarn, Elise Viard and Andrei Tokovinin for their valuable input.

References

[1]M. Mountain, What is beyond the current generation of ground-based 8-m to 10-m class telescopes and the VLT-I ?, SPIE 2871, pp. 597–606, 1996.

[2]B. Meinel, An overview of the Technological Possibilities of Future Telescopes, 1978, ESO Conf. Proc. **23**, 13.

[3]L. D. Barr, Factors Influencing Selection of a Next Generation Telescope Concept, 1979, Proc. SPIE Vol. **172**, 8.

[4]A. Ardeberg, T. Andersen, B. Lindberg, M. Owner-Petersen, T. Korhonen, P. Søndergård, Breaking the 8-m Barrier – One Approach for a 25m Class Optical Telescope, ESO Conf. and Workshop Proc. No. **42**, pp. 75–78, 1992.

[5]T. Andersen, A. Ardeberg, J. Beckers, R. Flicker, A. Gontcharov, N. C. Jessen, E. Mannery, M. Owner-Pertersen, H. Riewaldt, The proposed 50 m Swedish Extremely Large Telescope, 2000, Bäckaskog Workshop on Extremely Large Telescopes, ESO Conf. and Workshop Proc. No. **57**, p. 72.

[6]T. Sebring, F. Bash, F. Ray, L. Ramsey, The Extremely Large Telescope: Further Adventures in Feasibility, SPIE Proc. 3352, p. 792, 1998.

[7]T. Sebring, G. Moretto, F. Bash, F. Ray, L. Ramsey, The Extremely Large Telescope (ELT), A Scientific Opportunity; An Engineering Certainty; 2000, Bäckaskog Workshop on Extremely Large Telescopes, ESO Conf. and Workshop Proc. No. **57**, p. 53.

[8]J. E. Nelson, Design concepts for the California extremely large telescope (CELT); 2000, SPIE 4004.

[9]R. Gilmozzi, B. Delabre, P. Dierickx, N. Hubin , F. Koch, G. Monnet, M. Quattri, F. Rigaut, R.N. Wilson, The Future of Filled Aperture Telescopes: is a 100m Feasible?; 1998, Advanced Technology Optical/IR Telescopes VI, SPIE 3352, 778.

[10]P. Dierickx, R. Gilmozzi, OWL Concept Overview; 2000, Bäckaskog Workshop on Extremely Large Telescopes, ESO Conf. and Workshop Proc. No. **57**, p. 43.

[11]P. Dierickx, J. Beletic, B. Delabre, M. Ferrari, R. Gilmozzi, N. Hubin, The Optics of the OWL 100-M Adaptive Telescope; 2000, Bäckaskog Workshop on Extremely Large Telescopes, ESO Conf. and Workshop Proc. No. **57**, p. 97.

[12]E. Brunetto, F. Koch, M. Quattri, OWL: first steps towards designing the mechanical structure; 2000, Bäckaskog Workshop on Extremely Large Telescopes, ESO Conf. and Workshop Proc. No. **57**, p. 109.

[13]N. Hubin, M. Le Louarn, New Challenges for Adaptive Optics: The OWL Project; 2000, Bäckaskog Workshop on Extremely Large Telescopes, ESO Conf. and Workshop Proc. No. **57**, p. 202.

[14]H. U. Käufl, G. Monnet, From ISAAC to GOLIATH, or better not!? Infrared instrumentation concepts for 100m class telescopes; 2000, Bäckaskog Workshop on Extremely Large Telescopes, ESO Conf. and Workshop Proc. No. **57**, p. 282.

[15]H. F. Morian, Segmented mirrors from SCHOTT GLAS for the ELTs; 2000, Bäckaskog Workshop on Extremely Large Telescopes, ESO Conf. and Workshop Proc. No. **57**, p. 249.

[16]R. Geyl, M. Cayrel, Extremely large telescopes – a manufacturer point of view; 2000, Bäckaskog Workshop on Extremely Large Telescopes, ESO Conf. and Workshop Proc. No. **57**, p. 237.

[17]P. Dierickx, B. Delabre, L. Noethe, OWL Optical Design, Active Optics and Error Budget, 2000, SPIE 4003.

[18]R. Geyl, M. Cayrel, REOSC approach to ELTs and segmented optics; 2000, SPIE 4003.

[19]G. Chanan, Phasing the primary mirror segments of the Keck telescopes: a comparison of different techniques, 2000, SPIE 4003.

[20]S. Cuevas Cardona, V. G. Orlov, F. Garfias, V. V. Voitsekovich, L. Sanchez, Curvature equation for segmented telescopes, 2000, SPIE 4003.

[21]N. Hubin, M. le Louarn, M. Sarazin, A. Tokovinin, New challenges for adaptive optics: the OWL 100 m telescope, 2000, SPIE 4007.

[22]F. Rigaut, R. Ragazzoni, M. Chun, M. Mountain, Adaptive Optics Challenges for the ELT ; 2000, Bäckaskog Workshop on Extremely Large Telescopes, ESO Conf. and Workshop Proc. No. **57**, p. 168.

[23]R. Ragazzoni, J. Farinato, E. Marchetti, Adaptive optics for 100 m class telescopes: new challenges require new solutions, 2000, SPIE 4007.

[24]R. Ragazzoni, Adaptive optics for giant telescopes: NGS vs. LGS, ; 2000, Bäckaskog Workshop on Extremely Large Telescopes, ESO Conf. and Workshop Proc. No. **57**, p. 175.

[25]M. Quattri, F. Koch, Analyzing the requirements of the enclosure and infrastructures for OWL and elaborating on possible solutions; 2000, SPIE 4004.

[26]E. Brunetto, F. Koch, M. Quattri, OWL: further steps in designing the telescope and in assessing its performances; 2000, SPIE 4004.

Paranal Impressions

KUEYEN is tilted towards the hori - zontal position during a test expo - sure sequence. (Photo obtained on March 23, 2000). ▶

Photographs by H.-H. Heyer

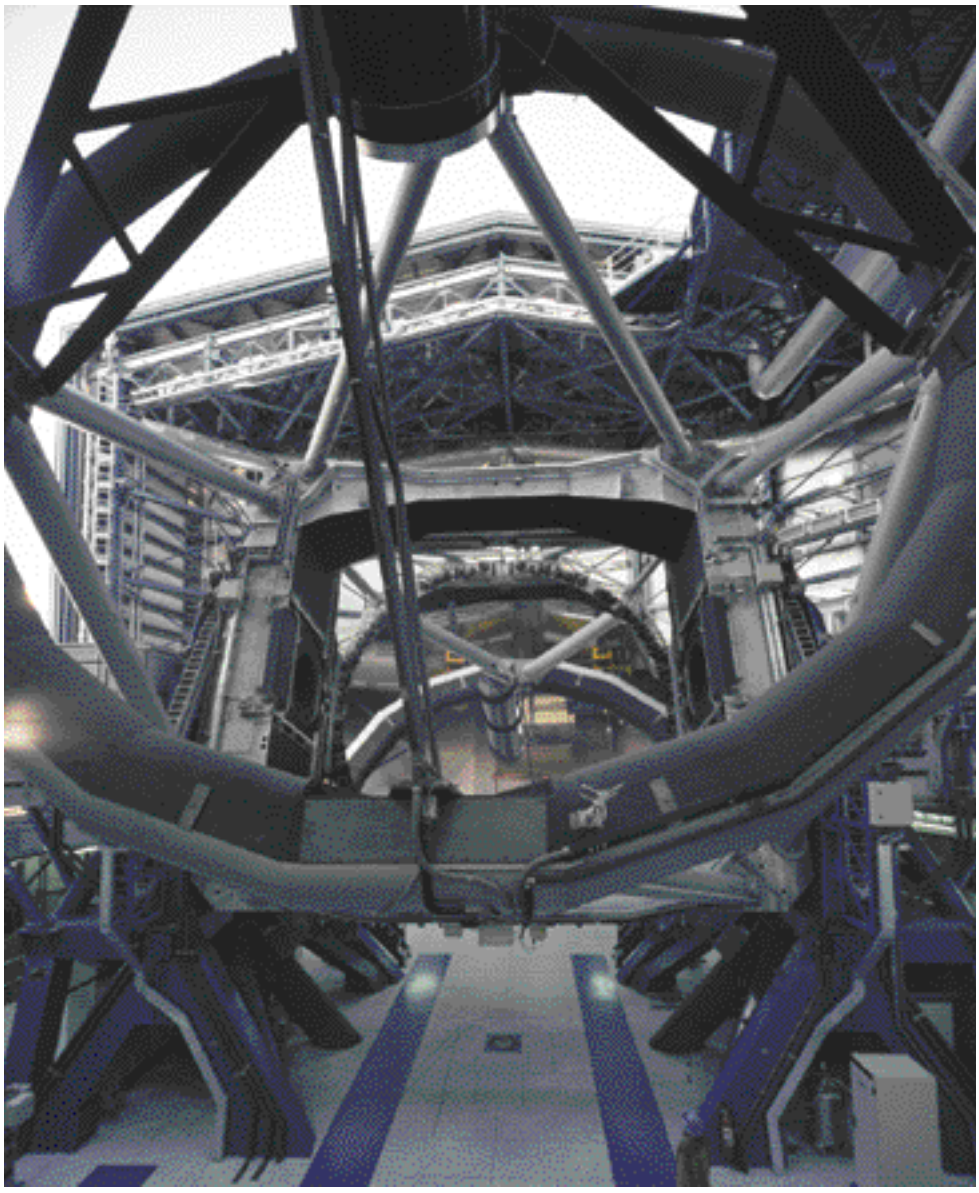

Daytime routine work in the control room at the observing modules for ANTU (right) and KUEYEN (left). (Photo obtained on March 20, 2000). ▼

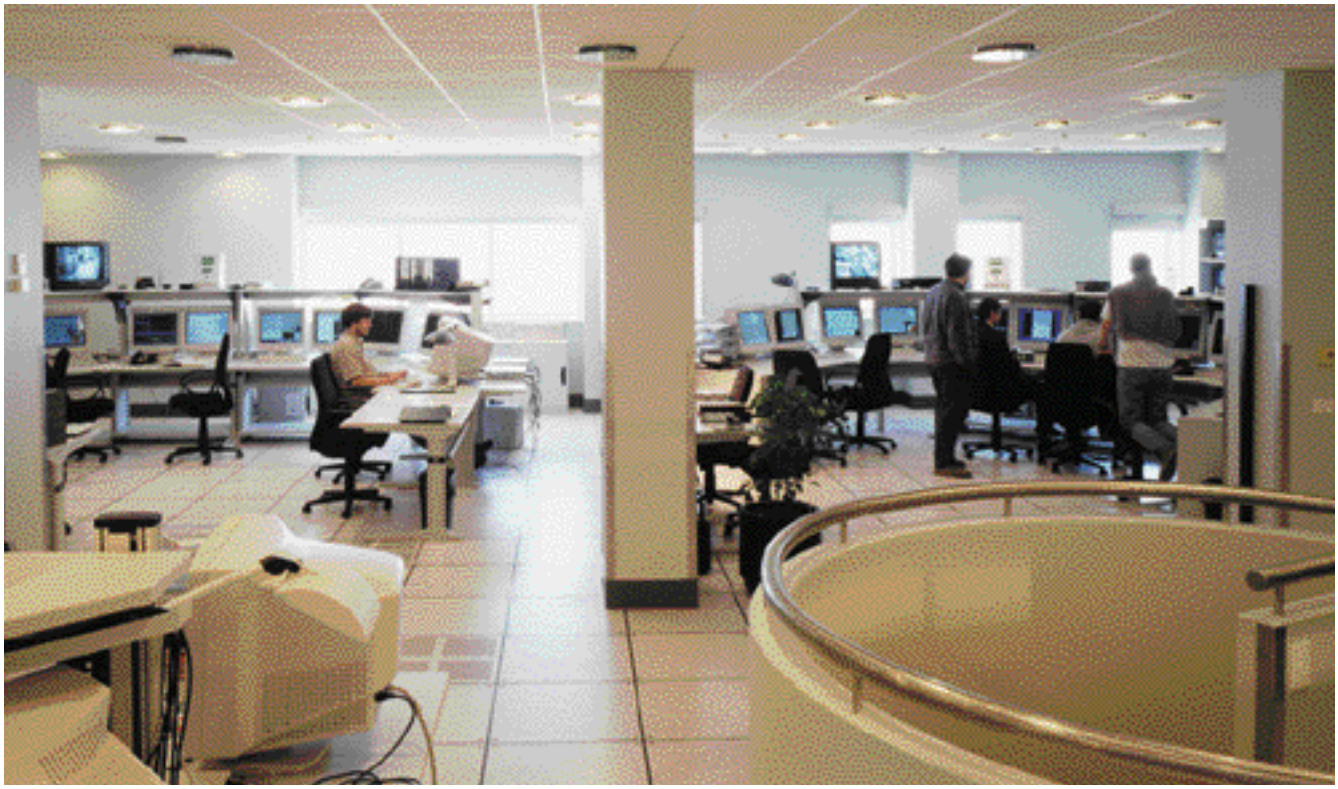

The ESO Photometric and Astrometric Analysis Programme for Adaptive Optics

D. CURRIE[a], D. BONACCINI[a]
E. DIOLAITI[b], S. TORDO[a], K. NAESGARDE[a], J. LIWING[a],
O. BENDINELLI[b], G. PARMEGGIANI[c], L. CLOSE[a]

Contact E-mail: dcurrie@eso.org
[a]European Southern Observatory, Garching bei München, Germany
[b]Università di Bologna – Dipartimento di Astronomia, Bologna, Italy
[c]Osservatorio Astronomico di Bologna, Italy

Abstract

The European Southern Observatory is currently developing an array of software analysis packages to perform Photometry and Astrometry (P&A) on both stellar and diffuse objects observed with Adaptive Optics (AO) Systems[1, 2]. As they are completed, the component programmes of ESO-PAPAO will be made available to AO observers using ADONIS on the 3.6-metre telescope at La Silla and later, to those observers using the various AO systems being developed for the 8.2-metre VLT telescopes at Paranal, such as NAOS-CONICA and MACAO-SINFONI.

The performances of the ESO-PAPAO package are being extensively quantified; both to support their use in astrophysical analysis and as a guide for the definition of AO observing programmes. The algorithms are being developed in IDL. A user interface programme (ION) allows immediate access to the ESO-PAPAO by observers not familiar with IDL. We will describe the objectives of the ESO-PAPAO, the calibrated ADONIS data sets that have been collected for distribution to contributors to the ESO-PAPAO programme, and the methods and results of numerical tests of photometric precision in comparing the various different analysis packages. In particular, the STARFINDER[3,4,5] (see this issue, p. 23) programme, developed at the University of Bologna in a collaborative effort with ESO, has been applied to data from ADONIS at La Silla, UHAO at Mauna Kea, and HST. Results from the analysis of this astronomical AO data will be presented, i.e. photometric precision of 0.01 to 0.05 magnitudes and astrometric precision of ~ 0.1 pixel in crowded fields with strong isoplanatic effects. The structure of PAPAO is illustrated in the chart on page 21.

1. Introduction

Over the past decade, the operation of Adaptive Optics Systems, led by the COME-ON > COME-ON+ > ADONIS systems on ESO's 3.6-metre telescope at La Silla, Chile[6, 7], have demonstrated the effectiveness of this technology in the field of high-resolution astronomy.

The optimal extraction of scientifically valid results from AO data can be a difficult operation. The challenges in AO Data Reduction were initially reviewed in 1995–1997 by the AO Data Reduction Working Group, organised by N. Hubin[8]. In 1997–1998, D. Bonaccini and J. Christou installed IDAC, an implementation of myopic deconvolution specially suited to AO data, tested it with real AO data, and made it available to ESO users[9,10]. Today the new IDAC 2.7 is kindly supported by Keith Hege at the University of Arizona, and linked at http://www.ls.eso.org/lasilla/Telescopes/360cat/adonis/html/datared.html . The use of IDAC has been encouraged for AO users with tutorials and performance test procedures, linked at the same Web site. Users are encouraged to provide feedback. However, with the development and imminent deployment of VLT instruments using Adaptive Optics, it has become necessary to provide AO support in photometry, astrometry, and deconvolution for the general observer using these ESO systems. To address this issue, the Photometry and Astrometry Programme for Adaptive Optics (PAPAO) was initiated in September of 1998[1, 2] by D. Currie, D. Bonaccini and F. Rigaut. This recognised the need for specific AO data-reduction algorithms and their software implementations, and for the quantitative comparison of the performance of these packages. The latter will allow the selection of the appropriate package for a specific scientific objective, and the quantification of the precision of the resulting scientific analysis. It is the PAPAO that will be addressed in this paper.

1.1 Classes of Adaptive Optics Data

The primary application of AO to date has been in broad-band imaging, followed by narrow-band imaging (this includes 89% of all referred AO publications[11]). This will be the topic of the current presentation. However, there are a large variety of data types that must be addressed in a similar manner in the near future, that are reviewed elsewhere[1].

2. Motivation and Objectives of PAPAO

The primary objectives of the ESO Photometry and Astrometry Programme for Adaptive Optics (PAPAO) are to provide the tools to define appropriate observational procedures, to reduce the AO data obtained specifically in support of this programme, and to evaluate the precision and accuracy of the results obtained with these new methods of data reduction. These tools will address the general ESO observer, using the ESO AO systems, that is, ADONIS[6, 7], CONICA/NAOS[12], and the AO systems that will be implemented at Paranal in the next few years (e.g. SINFONI). These tools will be publicly available at the Web Sites at ESO and at the PAPAO collaborating institutes as a contribution to AO observers in general.

2.1 Motivation of PAPAO

The observational imaging data obtained from the Adaptive Optics systems have many features that make the extraction of valid scientific results much more challenging than the analysis of images obtained from conventional low-resolution telescope imaging. The Point Spread Function (PSF) has extended wings (similar to the PSF of the Hubble Space telescope prior to the repair mission, due to optical errors in the primary mirror). In addition, the structure of the AO PSF changes over the field of view, and it is not constant in time, neither within a single observation nor from one observation to another (i.e. as one changes filters, maps an area in the sky, or observes a PSF calibration star at a later time).

Starting in October 2001, the CONICA/NAOS system, incorporating a 196-element Shack-Hartmann AO System and a 1–5 micron camera on the VLT (UT3), will start to be used by general astronomers of the ESO community. As an example of the need and motivation for an ESO AO ToolKit, we may look at the history of the publications from the ADONIS system over the past four years of facility operation[11]. In our opinion, up to now, these data-processing problems have reduced the scientific output favouring those with detailed experience, i.e., those who have built the instrument or belong to the institutes that built it.

In order to assure the effective use of CONICA/NAOS and future AO instruments, ESO created the PAPAO programme within the AO Group of the Instrumentation Division to provide a ToolKit of software packages, adapted to the AO systems on the ESO telescopes. In principle, such a package should address a wide range of science aspects, for both photometry and astrometry, and for both stellar and diffuse or nebular objects. It should apply to data obtained with both high and low Strehl ratios and images that are both well-sampled and under-sampled.

2.2 Programme Structure of the PAPAO

The PAPAO programme at ESO consists of three primary components. The first is the collection of algorithms to perform photometry and astrometry which are to be available in a public form, and which are documented for a general observer. The second component, the major current effort, consists of the collection of AO data, both a focused set of observations using ADONIS on the ESO 3.6-metre telescope at La Silla, and the identification and collection of data contributed by astronomers operating on other telescopes with other Adaptive Optics systems. The third component has two parts. The first part is the evaluation of the performance of the candidate software packages for the ESO ToolKit using real telescope data. The second part is the identification of those algorithms, programmes, and elements of programmes, that are particularly effective in photometry and astrometry and which should be developed for inclusion in future versions of the ESO ToolKit.

2.3 Scope and Objectives of PAPAO

The software has a widget interface so that the astronomer does not require a knowledge of any specific programming language. The first element of the ESO ToolKit is STARFINDER[3,4,5], a software programme for stellar photometry being developed in a collaboration between the University of Bologna and ESO. In support of the AO astronomer (but not as part of the PAPAO) are a number of the other software programmes that are available within the ESO System, that is, eclipse (for preprocessing ADONIS and future data from other AO systems in a pipeline manner), IDAC (for myopic deconvolution, and of course the large general packages of MIDAS, IDL and IRAF.

A quantitative evaluation of the performance of the ToolKit packages on real telescope data from AO systems will be provided on the ESO Web Site for PAPAO. The results of this evaluation are a part of the Algorithm Testing portion of the PAPAO programme discussed below.

2.3.1 Relative versus Absolute Photometry

The primary consideration in this discussion will be relative photometry, that is, the relative magnitude of different stars or the relative brightness of components of extended structures within a given frame or image. Of course, this does not address all of the features of a photometric reduction. The procedures connected with the selection, observation and reduction of photometric standard stars is an essential part of the procedure. However, our early tests within the PAPAO indicated that the photometric errors in relative photometry were essentially as large as the published errors in absolute photometry, so we have initially concentrated on the consideration of relative photometry in this programme.

2.3.2 Astronomer interface and programming language

The ToolKit has been developed in the IDL language, from Research Systems, Inc. The TookKit packages operate with a widget user interface. This means that the astronomer does not need to have knowledge of IDL or any other processing language. All of the options and procedures are presented in the form of buttons, with on-line help files available for detailed explanations. The IDL code will be available on the PAPAO Web Site. Concerning the IDL licensing issue, one technically feasible approach for the licensing could be for ESO to operate the ION interface to IDL on the ESO computers. This would allow the remote user to use his own computer and Web Browser to operate these ToolKit programmes on the ESO computer and license. Thus he/she could run the elements of the ToolKit on the ESO computers without a local IDL license, using a browser on his/her PC or workstation at his/her own institution. A demonstration and evaluation of this mode of operation will be conducted in June-July 2000, to evaluate the feasibility and identify any problems. If you are interested in participating in this test to evaluate STARFINDER and the remote operation capabilities of ION, please contact dcurrie@eso.org.

2.4 The Challenge to PAPAO

There are two primary challenges to achieving improvements in photometry and astrometry that parallel the very significant advances in the hardware side of adaptive optics. The first is the complexity and variability of the PSF. In the small patches of Figure 2, we can see the complexity of the wings of PSFs. Although these images have been enhanced to show the fainter stars, the accurate inclusion of the light in these wings is necessary to obtain good photometric accuracy. Comparison of the successive images of the PSF show both the super-speckles that are stable enough that they do not decrease as the square root of N, and the shorter-term effects of the atmosphere. The super-speckles usually remain stable for successive exposures on the target, but can significantly change when going across the sky to a new PSF calibration star. The shorter-term difference can be seen by comparing the differences in the patches that were taken over a few minutes. This is a significant effect in a programme to obtain 1% photometry. In Figure 3, we can see the difference in the PSF at different parts of a single image (the an-isoplanatic effect). Thus a star near the guide star has a near diffraction-limited structure, while an image at the edge of the field of view is highly elongated toward the guide star. Again, this requires extreme care and a good knowledge of the variable PSF to obtain high precision on the photometry of both of those stars. Finally, for the infrared observations addressed in this paper, the proper flat fielding of the images is a major challenge with the current generation of infrared arrays. Even a very well studied system (SOFI at La Silla) achieving 1% flat-fielding is a very large challenge.

Like the situation after the launch of the Hubble Space Telescope, a giant leap in instrumentation has provided a large advance in resolution. However, for WFPC to realise the full measure of science from the improved resolution in the presence of an imperfect PSF required an intense study of the proper role of deconvolution. Neither the spherical aberration of Hubble could, nor the AO data processing challenge can be addressed with quick, short-term solutions.

3. Role and Contents of the ESO ToolKit

In this section, we consider the current and planned elements of the ESO ToolKit. We also discuss the current status of each of these elements.

3.1 STARFINDER – SI – for Spatially Invariant Data

This package of programmes addresses photometric and astrometric measurements of well-sampled stellar sources (i.e. unresolved objects). The interface to the user is a widget-based GUI. This software programme has been developed by Emiliano Diolaiti of the Osservatorio Astronomico di Bologna[3,4,5] in collaboration with ESO. This package of programmes is currently in final testing to assure the proper operation with different versions of IDL, different versions of the astron 19 library and different computer systems. This software package will be distributed on the PAPAO Web Site and from a Web Site at the Osservatorio Astronomico di Bologna. It will also be available in the remote operation test in July-August 2000.

3.2 Astrometric Motion of Nebular Clumps

This programme addresses astrometric measurements of nebular (i.e. extended or diffuse) targets, and was originally developed by Dan Dowling[13, 14, 15] for the analysis of the motion of the clumps of dust and gas in the homunculus of η Carinae. This programme used data from the WFPC prior to the repair mission as well as post-repair data from WFPC2. Thus it has addressed the issues of highly accurate astrometry (at the 5 mas level), both for PSFs with strong and negligible wings (i.e. equivalent to high and low Strehl ratios in AO). The programme has been modified for use with AO in the environment of the ESO ToolKit and tested for astrometric accuracy on real telescope data by Katrin Naesgarde[16] and Johan Liwing[17]. However, it still needs to be packaged for the ToolKit, and the widget interface has not been developed at this time.

3.3 STARFINDER – SV – for Spatially Variant AO Data

This package of programmes addresses AO data in which the an-isoplanatism causes significant changes in the shape of the PSF (and thus in the photometric and astrometric measurements), as a function of the distance to the guide star. This is illustrated in Figure 3. Properly handling anisoplanatism effects in AO data is a much required and original contribution. The proper handling of an-isoplanatic effects in AO data is an essential requirement and this work is a unique contribution. The initial version of this programme has been implemented and tested on real telescope data by Diolaiti et al.[3,4,5]. Discussion of its effectiveness for processing data with very significant an-isoplanatism has been investigated. The code is in the process of being finalised and made into a user programme with a widget interface at the University of Bologna (Italy).

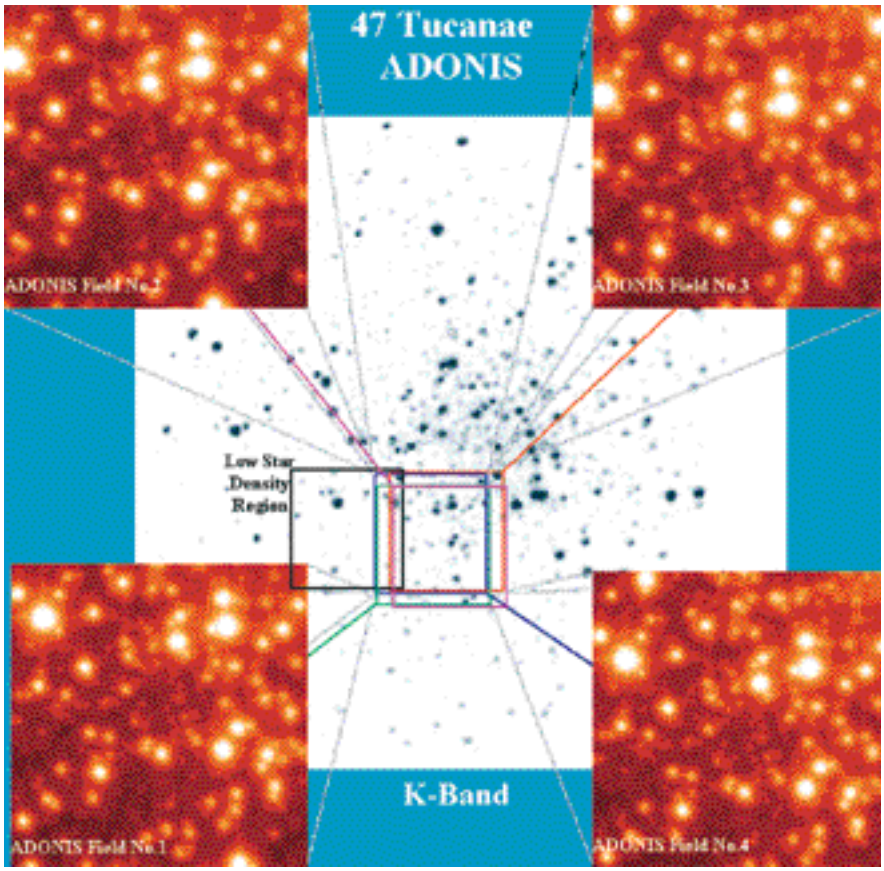

Figure 1 illustrates the type of data that has been collected on ADONIS. This shows the images for the four overlapping pointings obtained by re-pointing the telescope (or more accurately, moving an internal mirror in the ADONIS system). The background is a ground-based K-band image of the centre of the globular cluster 47 TUC. The area in common is delineated by a solid white line. The area observed with each pointing is indicated by the solid thin and dashed lines. Thus going from the lower left, we have field #1, which is shown with a thin green line, and clockwise around the square we have fields #2, #3 and #4.

3.4 DAOPHOT

A version of DAOPHOT (i.e., from the IDL version developed by W. Landsman[18]) will also be made available for the convenience of ESO ToolKit users. It has been automated and can be more effective than STARFINDER for the analysis of under-sampled images[16,17]. However, this has not yet been made into a facility programme and the widget interface has not been developed. However, a standard facility version is installed in the standard IRAF NOAO digiphot package that runs under any installation of IRAF.

3.5 Deconvolution and Spatially Dependant Regularisation of the PSF

Deconvolution is required for the accurate analysis of AO data on diffuse or nebular objects. Various existing algorithms are generally available to the user. For example, different implementations of the Lucy-Richardson algorithm are available for MIDAS, IRAF, STSDAS and IDL. Myopic deconvolution algorithms are also available (e.g. IDAC). However, for targets that have a significant extension or are not very close to the axis defined by the guide star (on average on average at the level of ten arcseconds in K-band in K-band), the PSF will change significantly (as seenn in Figure 3) and a Spatially Variant Deconvolution (SVD) is required. The simplest method is the patch approach to SVD, in which the complete image is considered as a family of small regions, where one tries to find a PSF star (and perhaps a photometric star) in each small patch. These calibration references, if available in each patch, would then be used for a Spatially Invariant Deconvolution (SID).

To our knowledge, there are no SVD packages currently available that properly handle the spatially variant PSF. In this discussion, we will consider a two-step approach, although a software package might very well combine them into a single programme. The first step is to homogenise or regularise the PSF so that it has the same form over the entire field of view. This requires first

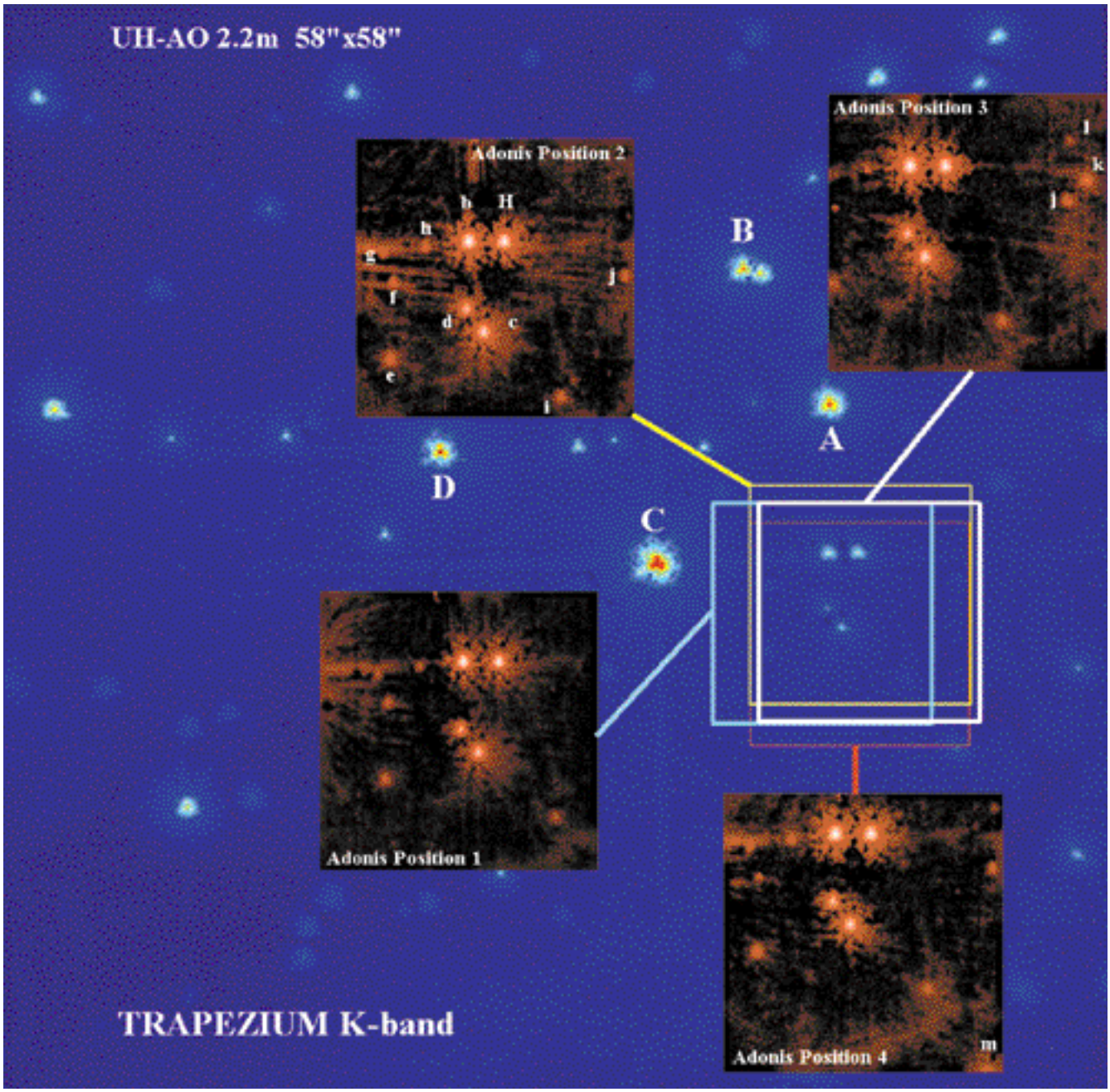

Figure 2: These images illustrate the High Strehl Stellar Observations conducted in the Trapezium in Orion. The large image (in blue) has been obtained in K-band on the 2.2 metre telescope[20] using the 13-elements UHAO[21] and the 1024 × 1024 QUIRC camera. Within this, we indicate the bright stars selected for guide stars for the observations. This entire cluster is named Θ[1] The square boxes indicate the position of the separate ADONIS FoVs obtained by Currie with 50 mas pixels to critically sample the core (2.5 pixels across the FWHM). The red im - ages are the bad pixel corrected, de-biased, flat fielded sky subtracted and averaged ADONIS SHARPII 256 x 256 images for each of the four pointings. Each box is 12.5 by 12.5 arcseconds.

calibrating the parameters that describe the an-isoplanatism. Then one would create the continuously variable PSF in a (currently not available) programme to make the PSF uniform. The second step is to apply one of the SIV algorithms to the homogeneous-PSF frame. Thus the key issue is the homogenisation algorithm. These issues are of paramount importance in the consideration of continuous distributions (nebular or galaxies) which might be at the edge of the isoplanatic patch so the evaluation of their photometric and astrometric properties are compromised by the PSF variation.

3.5.1 Spatially Dependent Homogenisation/Deconvolution

The development of a spatially dependent homogenisation/deconvolution has been a project of the University of Bologna and ESO. This programme would transform the image with a variable PSF, using a continuously parameterised model of the spatial variation of the PSF, into an image that has a uniform PSF. This procedure can be followed by a spatially invariant deconvolution of a conventional type (i.e., the Lucy-Richardson or PLUCYpackage, IDAC[9, 10], or other methods more adapted to the specific science objectives at hand).

3.5.2 Spatially Dependent Regularisation by Warping

This procedure corrects for the spatial variable PSF across the image, using a simple model of the variation of the PSF due to isoplanatic effects, i.e. the incorporation of the Gaussian elongation and broadening of the stellar images that has been demonstrated to be the dominant effect. This procedure has been demonstrated on AO data using an IDL implementation package[19]. These procedures have not been converted into a facility package at this time, nor have they have been widgetised.

3.6 Availability and Access to the ESO ToolKit

As these programmes are completed, they will be available to be downloaded from a Web page at ESO located at http://www.eso.org/science/papao/programs. IDAC is available at www.eso.org/aot, in the Adonis pages. The STARFINDER series will also be available on a mirrored Web Site at the University of Bologna. These programmes will also be offered as elements of the package for the standard distribution of IDL routines in the astron package[18]. For participation in the remote operation test in July-August 2000, contact dcurrie@eso.org.

4. Data Collection for the PAPAO

Without quantitative comparative evaluations, one cannot reliably select the proper software package for a particular science objective. Quantitative results from the comparison of the packages, using well-calibrated telescope data, are needed to select the proper software tool, and quantify the random and systematic errors of the science products. Thus, the data collection component of the PAPAO programme was designed to provide well-calibrated sets of data, that address the many parameters that were, and are, expected to significantly affect the procedures and accuracy of the AO data analysis. The uniformity of data collection procedures and the calibration procedures are extremely important to provide meaningful intercomparison of different observing conditions and different software packages. The primary body of data has been collected using the ADONIS system on ESO's 3.6-metre telescope at La Silla. In addition, we have received contributions of data from other observers using other AO systems. These external contributions are not calibrated in the manner discussed below. However, these external data frequently fill gaps, that is, data that cannot, or have not yet, been collected on ADONIS at La Silla.

4.1 ADONIS Data

In general, we have collected data sets with extensive calibration. Access to different data sets, with extensive calibration data is necessary to isolate, identify and quantify the different effects that have an impact on the photometric and astrometric accuracy. The identification of the optimal calibration data set and the attendant collection and analysis procedures is an evolving process. Some of the current procedures are discussed below. Here we describe the sources, standardised processing procedure, and output for specific data sets.

4.2 47 TUC Data Set from Adonis

In this discussion, we shall explicitly consider a few of the data sets obtained on the ADONIS System. The initial data set was collected in December 1998, consisting of images of the inner region of the globular cluster 47 TUC (NGC 104). These data, as well as all other data from ADONIS, were obtained by D. Currie.

4.2.1 The Central Crowded Region

This field, shown in Figure 1, for the evaluation of software performance, is near, but not exactly centred on the core of the cluster. The exact location was selected to overlap with observations that have been conducted using NICMOS with HST as well as observations by F. Ferraro. This field (as well as a series of overlapping fields) is shown in Figure 1. For the ADONIS system, we used the camera optics providing 100 mas pixels and a 25 arcsecond Field of View (FoV) with the Ks or K' filter. Thus, the PSF would have been badly under-sampled, if the Strehl ratio had been high (this data happened to have a relatively low Strehl ratio). These observations provide a set of unresolved objects of various intensities with relatively low background. The data consisted of four pointings obtained within an hour, where the pointing for each group was offset by a couple of arc-seconds. There are 10 images for each group, with an individual exposure time of 0.6 seconds. The bad pixels were removed, the images flat-fielded, the sky and dark frames subtracted, and then the ten successive images were combined using a median filter acting on each pixel. The images denoted T0 and T1 were then combined (with appropriate translation) to form T01. The same procedure was performed using the groups T2 and T3 to form T23. The PSF was independently obtained for each image (i.e. for T01 and T23) by the method defined by whatever Photometry Programme was being tested and the photometry was performed separately for each of T01 and T23. Analysis of this type was performed on this data set by several individuals at ESO and at Bologna. Some of these results are described below. This procedure was in general performed for each of the sets of results listed in the table. This 47 TUC data set was also distributed to the ten international groups in the AO data-processing community in November 1999, and is available to be downloaded at http://www.eso.org/science/papao/data/47tuc/.

4.2.2 The Outer, Less Crowded Region

At the same time that the above observations were recorded, observations were made of an adjoining region of the cluster, i.e. the region indicated by the black square in Figure 1. There were three purposes in observing this second field. The first purpose is to provide a less crowded region that will allow the application of the same algorithm to two regions with different degrees of crowding observed at the same time with the same atmospheric and AO system parameters. This test can evaluate the effects of crowding on different photometry and astrometry algorithms. This second less crowded region also allows a cleaner extraction of a (non-simultaneous) PSF, and gives a better estimation of the sky background.

4.3 ADONIS Data on the Trapezium

The two primary objectives of the Trapezium series was (1) to obtain well-calibrated data sets using ADONIS that have the high Strehl ratio that is representative of the expected Strehl ratios for CONICA/NAOS and (2) to obtain data sets to test the accuracy of software programmes that provide for the correction for the effects of an-isoplanatism.

4.3.1 High Strehl Data

We wish to obtain a well-calibrated and redundant data set that can be used for independent internal intercomparisons of the photometry and astrometry. The redundancy means that the data is recorded in a manner to provide a quantitative evaluation of the precision of the P&A. To achieve this with ADONIS observations we need a region with an acceptable number of stars for statistical security (ten or more stars in the FoV of the high-resolution camera mode, i.e., a region of 10 by 10 arc-seconds), and a very bright star, 6th magnitude or brighter, very near-by, to permit the optimal operation of ADONIS, and no star in the FoV that will saturate the detector. Such a region has been found in the Trapezium, and is indicated by the boxes in Figure 3. As shown in the figure, we point to four, highly overlapped regions. Thus in each of these four regions or patches, we can independently determine an internally defined PSF for that frame, and use that PSF to reduce the data in that frame. Thus we have four independent sets of the stellar magnitudes of the stars for which the stars obviously have the same magnitudes for all of the four pointings. The data were recorded with an exposure time such that the two stars H and b (~ 11th magnitude in K-band) are somewhat over-exposed in order to collect precise data on the wings or halos of the PSF. The stars c and d are well-exposed with the peak at 0.6 and 0.3 saturation. Finally, there is a cluster of ten fainter stars, the brightest of which is five magnitudes fainter than Ha.

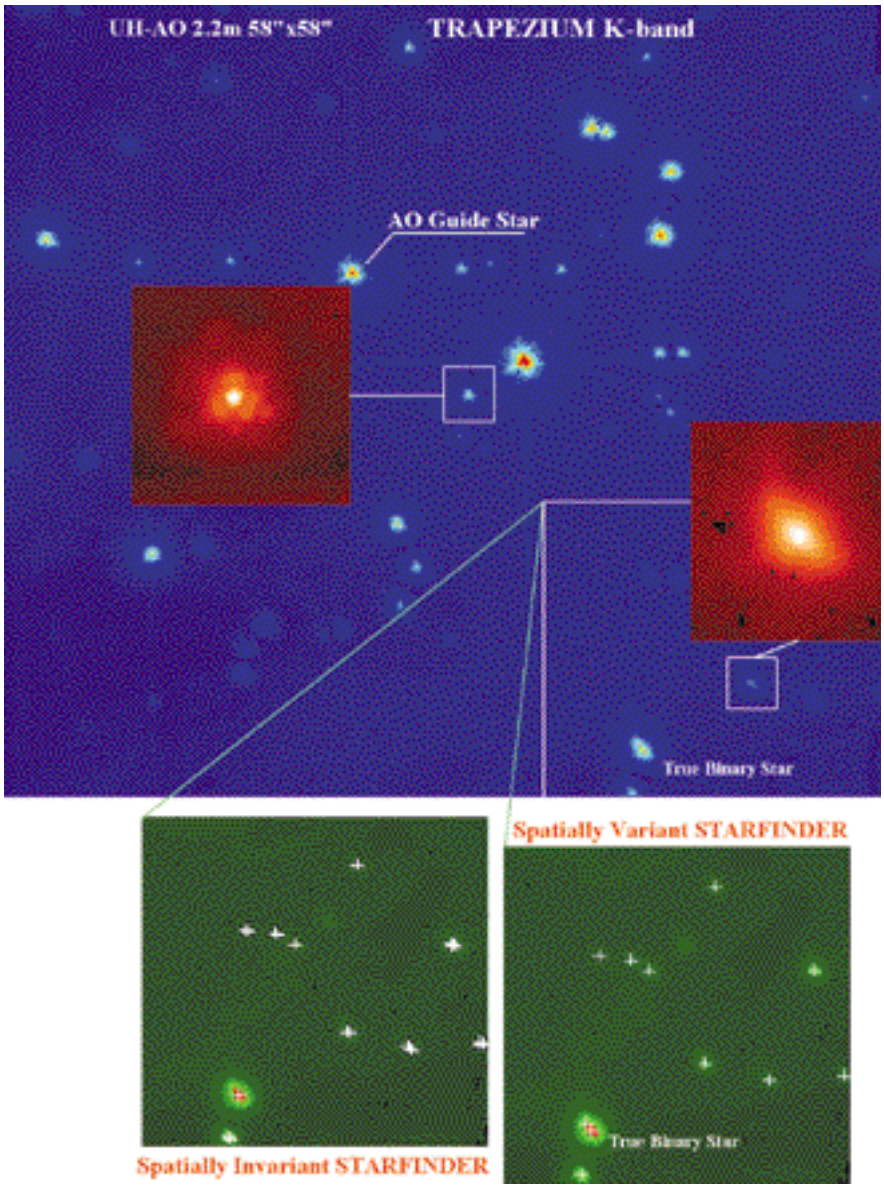

Figure 3: In the image of the Trapezium, we can see the effects of an-isoplanatism, that is, the change in the PSF in different parts of the image. At the bottom, we see the effects (on the left) of processing with a constant PSF(SI). We see in the left bottom panel that this soft - ware detected each of the distorted stars as a star with multiple components. On the right is the result of our continually parameterised model of the variable PSF that was used in the Spatially Variant Version of STARFINDER. Now all the distorted stars are identified as single stars (with the exception of the brightest star, which is actually the only true binary star in the field).

Finally, to permit the evaluation of the precision of the blind and myopic deconvolution algorithms, for each of the four pointings, a cube of short-exposure data was recorded. Thus the performance of myopic and/or blind deconvolution implementations can be tested. The photometric and astrometric precision can then be determined by inter-comparing the four independent myopic deconvolutions on the four independent cubes. The proximity of the bright stars allows the ADONIS data to be taken with a high Strehl ratio (32%). With the inter-comparison of the myopic deconvolution followed by the photometry and astrometry of the four patches in hand, one may then compare this precision with the precision obtained by the more conventional processing of the averaged cube of the same data. These data sets, bad-pixel corrected, flat-fielded, and sky subtracted, can be downloaded from http://www.eso.org/science/papao/data/trap

4.3.3 An-Isoplanatism Data Sets

A separate goal of PAPAO is to address the effects of an-isoplanatism, the variation of the PSF across the field of view as a function of the distance to the guide star. This effect is caused by the fact that the target star passes through a somewhat different sample of atmosphere than the atmosphere that is sensed and corrected by the AO systems which is locked on the guide star. An ideal data set could have been obtained in the manner of the UHAO image (background image in Figures 3 and 4). This entire region could be observed using different guide stars. This single 1024 × 1024 QUIRC image would then have contained the guide stars, and a large number of stars recorded simultaneously (with the same space variant PSF and the same an-isoplanatic parameters). However, the UHAO data was taken with certain science objectives, rather than the technical objectives of PAPAO. With the smaller 256 by 256 array of ADONIS, we must consider a different strategy. For this, we need to find an interesting field for which there are three or four bright stars at the edge of the isoplanatic patch, that is, within 25 arc-seconds of the centre of our Region of Interest (RoI). Preferably, these stars should be very bright, since the an-isoplanatic effects can be measured more easily with high Strehl images. While such fields are rare, the region discussed above (see Fig. 2) in the Trapezium satisfies all of these criteria. Thus we can collect data satisfying both the high Strehl ratio objectives and the an-isoplanatism objectives at the same time. This means that we can observe the same RoI (the RoI indicated in Figure 2) with up to four different guide stars. Since we have the four different pointings or patches for each guide star, we can determine the internal error structure, and thus cleanly isolate the effects of the an-isoplanatic errors and corrections. A proper programme to correct for the an-isoplanatic effects should result in good agreement for the data taken with A, C, and D used as guide stars. Most of the Trapezium data sets have been collected in the following manner. We observe the Region of Interest (RoI) using the first star (#1 C) as the Natural Guide Star. Four overlapping regions contained in the RoI (similar to the discussion of the observations of 47 TUC) are obtained. Then we start a similar procedure with the next Natural Guide Star, ((#1 D). We again observe four slightly overlapping images of the same RoI that was observed with ((#1 C as the guide star. Finally, we go to the third Natural Guide Star ((#1 A) and again collect four overlapping images.

4.4 ADONIS Data on η Carinae (the Homunculus)

We now address a quite different class of objects. In this case, we are interested in obtaining data sets to address the performance of deconvolution algorithms. These deconvolution algorithms are intended to improve the photometric SNR, and to remove artifacts for nebular or galactic objects, i.e., diffuse or continuous targets. In particular, this set of data should allow us to address the precision or accuracy of the recovery of the high-frequency components in the image.

4.4.1 Spatially Invariant Analysis

To this end, we are then interested in a quantitative evaluation of the accuracy and artifact introduction of spatially invariant deconvolution procedures. To address this, we need to select an object which extends over a major part of the ADONIS field of view, has a considerable amount of fine detail, an object for which we have other data that indicates the reality of the details of the structure, and finally, an object bright enough to allow a sequence of short exposures to test blind and myopic deconvolution algorithms and implementations. For this we have selected a portion of the Homunculus of η Carinae, perhaps the unique object which simultaneously satisfies all these criteria. We have previously produced astrometrically rectified images for the studies of the motion of the clumps in the homunculus[13, 22, 23]. There is a range of brightness, and very short exposures are adequate to obtain a good signal-to-noise ratio, even with a 50 milli-arc-second resolution. η Carinae itself is bright enough to be an excellent guide star, sufficient to get good Strehl ratios for the Homunculus images. This data has been bad-pixel corrected, flat-fielded, and sky and dark subtracted. The resultant images for two overlapping regions observed in K-band with 50 mas/pixel are shown in Figure 4, where they can be compared to our image from the WFPC in Hα. These images have been analysed at ESO, in particular, applying the Lucy-Richardson algorithm and myopic deconvolution in the implementation of IDAC. The results of these deconvolutions have been analysed on a pixel-by-pixel evaluation to address the performance of the algorithms, using various figures of merit. In the future, we plan to address this behaviour in terms of the spatial frequency, that is, averages over small blocks of pixels in order to separate the high frequency performance from the lower frequency performance.

4.4.2 Data for An-Isoplanatic Effects in Continuous Targets

However, even with the new NGS AO systems that are being developed and installed on the 8-metre-class telescopes, the lack of guide stars in the very immediate vicinity of the target will results in strong an-isoplanatic distortion of the targets shape and brightness distribution, as indicated in Figure 3. For this reason, we wish to explore the post-detection software methods that correct for the influence of a PSF that changes its shape over the field of view. In particular, we wish to determine the effectiveness of the very few spatially variant deconvolution algorithms to remove the effects of the an-isoplanatic variation of the PSF across the observed field of view. Since we do not have the God's Truth, we need to again develop a procedure of observing with multiple Natural Guide Stars and look for internal consistency. In this type of analysis, we will determine the photometric structure of the object, as determined independently from each of the data sets. The P&A from a properly operating software deconvolution programme, or more precisely the spatial frequency components of the P&A should agree, even though they have used guide stars that are at different distances and different orientations with respect to the RoI. However, to perform these observations in a reasonable amount of telescope time, we need a very bright nebular object that has, within tens of arcseconds, at least three stars bright enough to be natural guide stars for ADONIS. In the selection of a portion of the homunculus of η Carinae, we have three guide stars within 15 arcseconds, and a total of five guide stars within 25 arcseconds of the centre of the region of interest as shown in Figure 5. All five of these stars are brighter than 11th magnitude, quite acceptable as guide stars for ADONIS. Thus we have a rather ideal configuration to test the continuous distribution.

The relatively bright guide stars are at distances of 6 arcsecond (mv = 6), 8″ at 10th, 8″ at 10th, 12″ at 12th and 25″ at 11th. This makes it a unique object for the performance of these tests. In addition, we have an extensive set of WFPC data for comparison of the small linear features. To allow the precise comparison, we took two views of the RoI, slightly translated. In addition, we observed the four stars at a greater distance from the RoI to obtain the parameters that describe the degree of anisoplanatism.

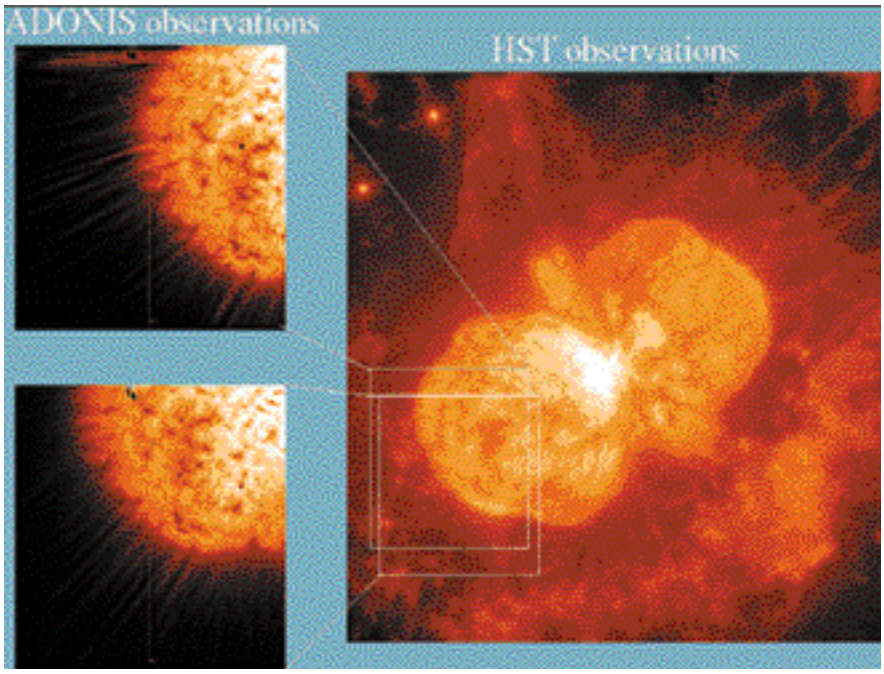

Figure 4 illustrates the data set that has been used for the analysis of nebular objects. The large figure on the right from the Hubble Space Telescope shows the regions selected for the ADONIS observations (the central part of the SE lobe of the homuculus of η Carinae). This was selected because it is bright at K-band, allowing short exposures even at 50 mas resolution, has a number of relatively bright guide stars near it i.e. at distances of 6 arc second (mv=6), 8" at 10th, 8" at 10th, 12" at 12th) and 25" at 11th.

4.5 Summary of Data Sets for Community Analysis

Table 1 describes some of the data sets that have been obtained using ADONIS and other systems, and are being prepared for use, internally and externally over the next year. Well-calibrated data, obtained under a variety of conditions with the same calibration procedures, are necessary to separate the various parameters that affect the accuracy of the data analysis by various software programmes. They are in various states of pre-processing, calibration and validation. All are in K-band unless otherwise stated. There are various criteria that describe the parameters that will affect the collection and analysis of AO data. We give rough indications of the domain in which each of the data sets falls. The average density of stars per arcsecond roughly indicates the number of stars that may be expected to be found in the wings of adjacent stars. This of course depends upon the seeing at the time, but this column gives an estimate of the density in the most critical region for the AO correction. An indication of the Strehl ratio is given. A precise definition is difficult in these crowded fields, and the use of the Strehl ratio of a calibration star must be checked for the stability. Data sets that are currently available are indicated by a "+" and are indexed at http://www.eso.org/science/papao/data/47tuc/

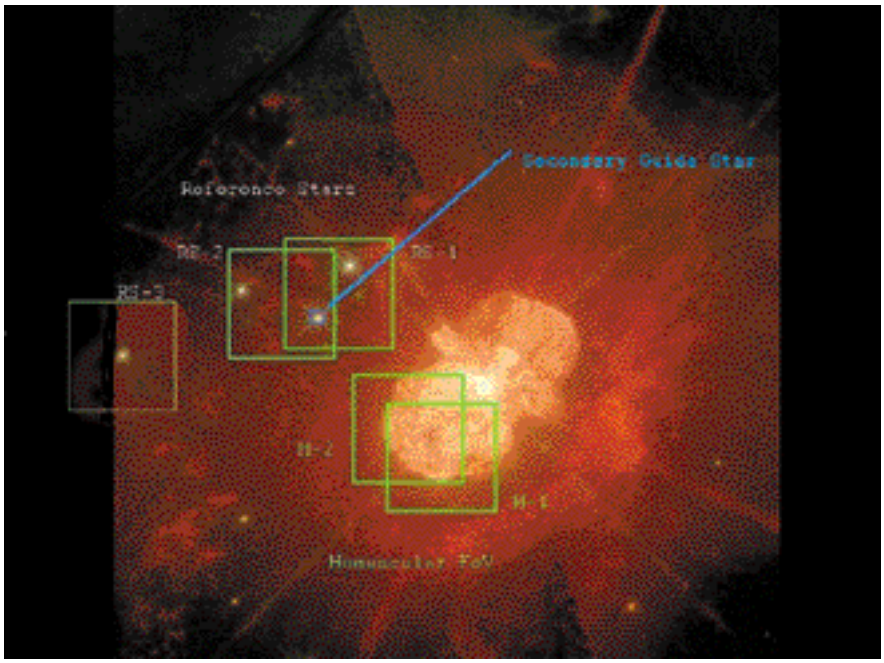

Figure 5: This uses our HST image to illustrate the ADONIS data sets obtained by Currie to address the deconvolution procedures with an-isoplanatic effects for nebular objects. The first two regions (H-1 and H-2) were selected for analysis (these are the regions shown in Figure 4). They are the central part of the SE lobe of the Homunculus. The other three regions (RS-1, RS-2, and RS-3) were selected to evaluate the an-isoplanatic parameters when the central star was being used for the guide star. We later looked at the same five patches but using first one then another of the outer stars as the natural guide star. For scale, each of the green boxes is 12.5 arcseconds on a side. We have an extensive set of WFPC data for compari - son of the small linear features.

The fourth column indicates the sampling, the first number being the number of pixels in the theoretical diffraction-limited core. This addresses issues in obtaining and translating the core of the PSF. The fifth column is the (linear) number of pixels in the wings caused by the atmospheric effects. This indicates the area in which the photometry is strongly affected by the variability of the lower levels of the PSF. The remaining data sets will be placed upon the PA-PAO Web Site as the pre-processing and calibration isare completed.

5. Algorithm Testing Component of the PAPAO

The portion of the PAPAO programme concerning the testing of the various photometry and astrometry algorithms divides into two parts. The first part is to develop numerical simulated data to evaluate performance of each of the packages of software programmes. The results of this analysis will be provided on the web page. This will illustrate the science performance of the software programmes in the ESO ToolKit, results at the level that might be obtained by a general observer, that is, an individual who is not an expert in AO. Some of the initial results of this analysis will be presented below, as an example of the type of analysis that will be developed. A second part of the algorithm testing programme involves the distribution of selected field-data sets to be processed by those individuals who have developed the code for various photometry and astrometry software packages that are of interest for AO data. The main objective of this second partcomponent is to identify and select the best programmes and/or algorithms to develop, test, and implement the next generation of the ESO ToolKit. The second objective in this second portion of the algorithm testing part is to discover better procedures for the use of the publicly available software.

Table 1.

Target/ DataSet	Star Density	Strehl Ratio	Samples/ # pixels FWHM in wings		Description and Comments
47 TUC_A +	0.8	low	1.5	6	This data set is composed of 25″ by 26″ images described in the previous section, and it was distributed to ten groups for external testing by experts in November 1999
47 TUC_A_2 +	0.8	low	1.5	6	This data set was obtained at approximately the same time as 47 TUC_A, but it has a lower stellar density. It will thus be used to compare the relation between the crowding and the photometric and astrometric precision when the atmospheric conditions and AO system parameters are similar.
T Cluster 25.0	high	high	3.0	6	This is an ADONIS data set augmented with synthetic stars each of which has the proper noise and PSF (both in shape and in an-isoplanatic variation obtained for actual observation). This serves as a set of absolute calibrators at high crowding.
47 TUC_B +	0.8	med	1.5	6	This data set contains 100 frame sets especially obtained for testing blind and myopic deconvolution programmes
47 TUC_B_2 +	0.8	med	1.5	6	This data set contains 100 frame sets, especially obtained for testing various blind and myopic deconvolution programmes. It has a lower density of stars than 47 TUC B.
Homunculus +	—	med	3.0	12	These are 100 frame sets to test various implementations of blind and myopic deconvolution on a continuous (or nebular) object that has both a large dynamic range and many very fine features.
Trapezium +	low	32%	3.0	12	This data set addressed the an-isoplanatic effects for unresolved objects with relatively high Strehl ratios. The low stellar density allows the isolation of the crowding versus an-isoplanatism (although having fewer stars causes some statistical problems).
Homunculus +	—	high	3.0	12	This is an H-band data set for an extended target. Multiple exposures are taken to investigate and quantify the an-isoplanatic effects (see paragraph on an-isoplanatic data sets for homuncular images)

Table 2.

Programme	Analyst	# Stars Analysed	Dynamic Range	RMS Magnitude 14 stars 3.9 mag Stdev	error	65 stars 4.4 mag Stdev	error
SF-9905	Tordo	120	7.14	0.055	0.010	0.033	0.003
SF-9905	Tordo	127	7.14	0.059	0.011		
SF-9905	Tordo	175	7.37	0.087	0.016		
DAOPHOT	Tordo	73	4.75	0.056	0.011	0.040	0.004
SF-9905	Naesgarde	23	2.1	0.0253	0.005		
DAOPHOT	Naesgarde	23	2.1	0.0144	0.003		
SF-9909	Diolaiti	266	9.0	0.040	0.008	0.023	0.002

** This analysis excludes three out-liers, since the edge of the field was not excluded from the comparison calculation.
• Two versions of STARFINDER have been used. SF-9905 was installed by E. Diolaiti on the ESO computer system in May 1999 and has been available for evaluation in Garching. SF-9909 was a later version used by E. Diolaiti for some of his tests conducted at Bologna Observatory.

5.1 Results of the Algorithm Testing Component of the PAPAO

In Table 2 we list the comparative results obtained by using the various different software programmes. In each case, we compare the magnitudes (and positions) obtained for each different pointing or patch. Then the magnitudes or positions of a given star obtained in each of the patches are compared. The mean magnitude or position over the entire frame is zeroed, and the residuals are plotted as a function of magnitude. The dependence of the size of the errors on the stellar magnitude gives an indication as to the source of the error: photon noise, read noise, PSF noise or flat-fielding errors. Clearly we are not addressing all the possible errors, but the starting point is here. Then we can consider the effect of significantly different atmospheric conditions, different optimisations of the AO system, as well as methods of correcting the saturation and extraction of the PSF.

We first consider a set of 20 bright (and some fainter) stars, then a set of the brightest 60 stars, and then a set of the brightest 120 stars. Stars at the edge of the field and other anomalies have been eliminated from the numbers for all of the groups (thus each run uses the same set of stars). The RMS Magnitude indicates the differences between the measured magnitude of a star in T01 and the measured magnitude of a star in T23. The average value of all the stars over the field is set to zero, so we are evaluating the differences a given software programme measures for the same stars, and not including the zero point issue. In general, we see that the range of the internal errors in the measurements is between 0.088 and 0.014 magnitudes, that is, between 8.4 and 1.3 per cent.

The set of 14 stars analysed in the right panel of Table 2 was selected in order to have a common set among all analysts (who had analysed this data set within different research objectives). For the case of 14 stars the purely statistical error bars are about the values of the standard deviation found in the table. Therefore, the difference between the P&A programmes which were tested is not statistically significant (two sigma) for this small set of stars. However, it is clear that the performance is about a factor of thirty worse than the theoretical performance, that is, the photometric noise is much worse than the noise to be computed from the photon statistics, the sky noise, and the readout noise. On the other hand, this may be contributed by the problems of flat fielding that have not been explicitly quantified on this data. For the case of 65 stars, the purely statistical error bars are listed. The differences are marginally significant. Note that earlier tests of the ROMAFOT programme (several analyses based upon a data set obtained on NGC 1850) indicates that it obtained precision at about the same level. Similar results, with precision at the level of between 5 and 20 mas, have been obtained for the astrometric measurements of the same image of 47 TUC. These statistical aspects indicate another area where a careful integrated plan of data collection and data analysis is essential for obtaining statistically significant comparisons.

Note that the errors found in these ESO analyses are smaller (better accuracy) than those found in the literature. On the other hand, we have not included the absolute errors in the photometry. However, the errors found are still more then ten times the magnitude of the expected errors computed from the photon noise (which is dominant in this domain), readout noise and sky noise.

5.2 Flat-Fielding Effects in AO

Another source of errors for precise photometry is errors of various types in the flat-fielding procedure. In principle, we may expect the accuracy of the flat-fielding to be of the order of 0.3 to 1%. This is the experience of SOFI, where these procedures have been checked in detail. However, these results would be the end product of an extensive investigation that has not yet been carried out on the ADONIS SHARPII camera. One must address the problems of reproducibility as well as the difference between a flat field produced by a continuous distribution (the sky) and that produced by points of light, i.e. the shading or illumination corrections. These have not yet been checked independently, so there is an unknown component in the photometric results presented here that is due to the flat fielding problems. A study of such flat-fielding effect is important for high-accuracy AO photometry. It will also require the collection of test data from the telescope addressing higher dynamics range. Such observations are difficult on the SHARP II camera, since operating with the brightest object in saturation is not acceptable for this array. Thus the noise must be reduced by repeated observations, so improvements go at the square-root of the time, requiring significant telescope time.

5.3 Effectiveness of Prior Deconvolution

Traditionally, it has been presumed that one could improve the photometry and astrometry that could be obtained from AO data by performing a deconvolution on the image before measuring the intensities and position of the stars. In this section, we address the results of performing a Lucy-Richardson or a myopic deconvolution before performing the photometry. In this case, we have used our 47 TUC image, and performed the photometry. Then the image was deconvolved, using the Lucy-Richardson algorithm and IDAC programme. For each of the deconvo-

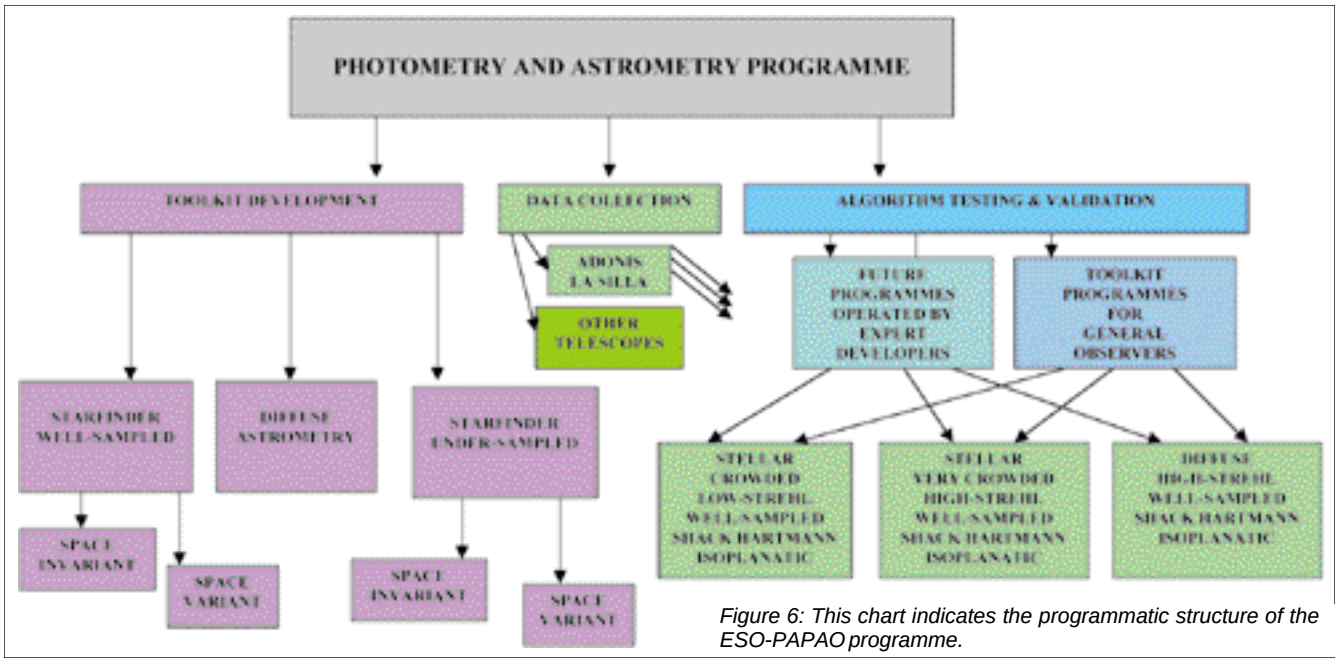

Figure 6: This chart indicates the programmatic structure of the ESO-PAPAO programme.

lution algorithms, tests were performed with both 500 and 2500 cycles. This was followed by the use of DAOPHOT and/or STARFINDER for the photometry.

The last column in Table 3 directly compares the photometric precision when using deconvolution referenced to the photometric precision obtained on the image with no deconvolution. Thus we see that the use of deconvolution degrades the photometric accuracy. More precisely, this expresses the differences between the magnitudes determined for the two patches (T01 and T23) when using STARFINDER before and after deconvolution. Thus it indicates the precision obtained with a given photometry software programme applied to the patches with different pointings before and after various deconvolution procedures. For example, after 2,500 iterations of IDAC, the photometric errors in the RMS Magnitude sense were larger by a factor of three than if the photometry had been performed with no deconvolution. These deconvolutions were done with the standard rules or default procedures for the use of the deconvolution algorithms. It may be that these results could be improved by the expert use of the deconvolution algorithms. If this is the case, we would hope to be able to incorporate these improvements into the procedures that would be distributed in the ToolKit. Thus, if there is better performance available with expert intervention we wish to define the operating rules that allow a non-expert to achieve the same results. However, these results by K. Naesgarde and J. Liwing using IDAC 2.4 on a stellar cluster agree almost completely with an analysis of a binary system performed by J. Christou and D. Bonaccini[24].

5.4 Role of Under-Sampled Images

The issue of the degree of sampling has been critically important on the ADONIS system, and will remain important on the 8–10-metre telescopes. In principle, we should always critically sample the data, that is, have more than two pixels in the diffraction-limited core of the image. Practically, this is normally feasible (depending upon the relation between read noise and target brightness) for single objects, but for targets like stellar clusters, we need a statistically significant sample of stars. This is a force toward less than critical sampling (presuming the AO camera system allows the astronomer the choice of different spatial sampling rates). As we go to the visible, it will also be important in terms of read noise. However, there is no information available at present as to the dependence of the feasible photometric accuracy as a function of sampling rate to guide the astronomer. Initial studies have been conducted under the PAPAO programme. Similar analysis of under-sampled images showed a reversed effect, the DAOPHOT performed about a factor of two better than STARFINDER. In order to obtain a set of under-sampled images with all of the required properties for the astrometric studies in a reasonable time scale, we have used data obtained from our observations with WFPC and WFPC2 of the HST[25,22,23]. The results indicated that DAOPHOT did significantly better than the STARFINDER (to be expected on the basis of the algorithm structure of STARFINDER). This appears to be due to the procedure in DAOPHOT for determining the PSF. It starts with an analytically defined initial guess and looks for corrections from the data. This has the advantage that the analytic core can be translated more precisely than the estimate obtained directly from the data as in STARFINDER. However, on the version of DAOPHOT we have used (in the astron library of IDL), we must use a double Gaussian version, and cannot insert and fit the best analytic model that we expect from the physics of the AO process.

Table 3.

Deconvolution Method	# Iterations	Standard Deviation	Relative Photometric Accuracy
None		0.0144	1.00
Lucy-Richardson	500	0.0157	0.83
Lucy-Richardson	2,500	0.0485	0.33
IDAC	500	0.0661	0.25
IDAC	2,500	0.0463	0.31

6. Current Status of PAPAO Programme

6.1 Preliminary Conclusions

6.1.1 Numerical Results on Stellar Clusters (i.e. Unresolved Targets)

We have three primary conclusions at this time. These are based upon analysis at ESO, that is, the analysis in the spirit of the General ESO observer, rather than by the developers of the codes. We still await the expert analysis results.

(1) For Well-Sampled Images with relatively low Strehl ratios, and relatively low levels of nebulosity, the three photometry and astrometry programmes that we have tested, i.e. STARFINDER, DAOPHOT and ROMAFOT give similar accuracy. While there are statistically significant differences, in general, they are relatively fine points.

(2) When more similar PSF characterise the data, in a manner that also reduced the flat-fielding errors, the photometric and astrometric errors are reduced. STARFINDER does significantly better, when the deleterious effects of PSF variation and flat-fielding are reduced.

(3) For Under-Sampled HSTImages, DAOPHOTperforms significantly better than STARFINDER. This may be due to the DAOPHOT assumption of a functional representation for the PSF that is reasonably correct, and which can be analytically translated to the centre of another star. This helps both in the formation of an averaged PSF and for the star that is being measured.

(4) For stellar photometry, the prior use of deconvolution (at least in the forms of Lucy-Richardson and myopic deconvolution) does not improve the precision of the photometry. Of course the primary use of such algorithms is for morphology and astrometry. Preliminary results on the photometry of continuous distributions are inconclusive.

Finally, a large improvement is required in order that the AO photometry and astrometry may reach the desired levels of accuracy, although a large part of this may be due to the flat fielding that also affects non-AO infrared photometry.

6.1.2 Current Programmatic Issues

The initial domains of performance have been identified for several software packages. We have seen that the procedures for the determination of the PSF must be investigated more completely. The widget-based Spatially Invariant STARFINDER will be available in July of 2000. The first set of data (well-resolved low Strehl stellar clusters) have been distributed to the community. A second set (well-resolved, high Strehl stellar clusters with calibrators) is available on the PAPAO Web Site at http://www.eso.org/science/papao/

6.2 Invitation to ESO Community

We invite and strongly encourage all interested to participate in the PAPAO programme. This participation may take a number of different forms. This may consist of applying your favourite photometry and/or astrometry algorithm to some of the calibrated PAPAO data sets. It may also consist of contributing your algorithms for testing by the broader community, or the contribution of your data sets to be used in PAPAO.

FREE TEST OF STARFINDER for ESO COMMUNITY

ESO is supporting a test of STARFINDER and the RSI software package ION. This test will occur from mid-June through mid-August. This will permit remote users to test STARFINDER on some of the data sets discussed in the article. We would be very interested in reports of the results, both concerning the software, and concerning the numerical results. Please contact the author at dcurrie@eso.org for the appropriate procedures to cross the ESO firewall.

Data sets with a single frame FoV that are significantly larger than the isoplanatic patch, and that are recorded for two or more guide stars that are separated by approximately 10 arc seconds, would be particularly valuable. Finally, we are interested in working with beta testers of the programmes to be released within the ESO ToolKit. In July and August, we will be testing the software package ION that allows remote participants to use STARFINDER on the ESO computers and IDLlicense. If you are interested in participating in these tests, please contact dcurrie@eso.org

7. Acknowledgements

We would like to acknowledge the generous allocation of ESO telescope time to the AO data reduction programme PAPAO, and the support of the members of the 3.6-metre team at La Silla. We would also like to acknowledge the contribution of data, for our engineering purposes, by L. Close[20], F. Rigaut, and S. Hippler.

References

[1]Currie, D.E., Diolaiti, D., Bonaccini, S., Tordo, K., Naesgarde, J., Liwing, O., Bendinelli, G., Parmeggiani, L. The ESO Photometric and Astrometric Analysis Program for AO: A Programmatic and Numerical Analysis Proc. of SPIE Vol. 4007 Adaptive Optical Systems Technology Editor: P. Wizinowich, #4007–72 1–12 (in press) (2000).

[2]Currie, D.G., E. Diolaiti; S. Tordo; K. Naesgarde, J. Liwing, O. Bendinelli; G. Parmeggiani, L. Close, D. Bonaccini. (1999) ESO Photometric and Astrometric Analysis Program for Adaptive Optics ADASS-IX 1999.

[3]Diolaiti, D., Bendinelli O., Bonaccini D., Parmeggiani G., & Rigaut F. STARFINDER: an IDL GUI based code to Analyze Crowded Fields with Isoplanatic Correcting PSF Fitting (1998) in ESO/OSA - Topical Meeting on Astronomy with Adaptive Optics., ed. D. Bonaccini (Garching b. Meunchen, ESO), p.175).

[4]Diolaiti, E. et. al. Proc. of SPIE Vol. 4007 Adaptive Optical Systems Technology Editor: P. Wizinowich, #4007–74 1–12 (in press) (2000).

[5]Diolaiti, E., D. Currie, O. Bendinelli, G. Parmeggiani, L. Close, D. Bonaccini (1999) Astronomical Data Analysis Software and Systems – IX 1999.

[6]Bonaccini, D., Prieto, E., Corporon, P., Christou, J., Le Mignan, D., Prado, P., Gredel, R., and Hubin, N., (1997) "Performance of the ESO AO system ADONIS, at La Silla 3.6m telescope, SPIE Proceedings Vol 3126, "Adaptive Optics and Applications", Tyson and Fugate Eds.

[7]http://www.ls.eso.org/lasilla/Telescopes/360cat/adonis/

[8]http://www.eso.org/projects/aot/aowg

[9]Christou, J.C., Bonaccini, D. et. al (1999) "Myopic Deconvolution of Adaptive Optics Images" *The Messenger*, No. 97, p. 14–22, http://www.eso.org/gen-fac/pubs/messenger/

[10]Christou, J.C., Ellerbroek, B., Fugate, B.Q., Bonaccini, D. and Stanga, R. (1995), Rayleigh Beacon Adaptive Optics Imaging of ADS 9781: Measurements of the Isoplanatic Field of View, *ApJ*, 450, 869–879.

[11]Close, L. M. (2000) SPIE 4007 "A Review of Published Galactic and Solar System Science: A Bright Future for Adaptive Optics Science".

[12]http://www.eso.org/instruments/naos/index.html

[13]Currie, D.G. and D.M. Dowling. (1999) "Astrometric Motion and Doppler Velocity" Eta Carinae at the Millennium, ASP Conference Series, Vol. 179 J.A. Morse, R.M. Humphries, and A. Damineli, eds.

[14]Dowling, D.M. (1996) "The Astrometric Expansion and 3-D Structure of eta Carinae" University of Maryland, Ph. D. Thesis.

[15]Currie, D.G., Dowling, D.M., Shaya, E.J., Hester, J., Scowen, P., Groth, E.J.; Lynds, R., O'Neil, E.J., Jr.; Wide Field/Planetary Camera Instrument Definition Team "Astrometric Analysis of the Homunculus of eta Carinae With the Hubble Space Telescope" 1996, AJ, 112, 1115.

[16]Naesgarde, K. (1999) "Accuracy in Differential Photometry – STARFINDER vs. DAOPHOT" Master's Thesis TRITA-FYS #XXX, Stockholm.

[17]Liwing, (1999) "Accuracy of Different Methods for Differential Astrometry" Master's Thesis TRITA-FYS #XXX, Stockholm.

[18]Landsman, W.B. (1995) "The IDL Astronomy User's Library" Astronomical Data Analysis Software and Systems IV, ASP Conference Series, Vol. 77, 1995, R.A. Shaw, H.E. Payne, and J.J.E. Hayes, eds., p. 437.

[19]Avizonis, P. V.(1997) Ph. D. Thesis University of Maryland.

[20]Simon, M., Close, L.M., Beck, T.L. "Adaptive Optics Imaging of the Orion Trapezium Cluster" (1999) *AJ*, **117** 1375–1386.

[21]Roddier, F., Northcott, M., Graves, J.E., "A simple low-order adaptive optics system for near-infrared applications" 1991 *PASP* **103** 131–149.

[22]Currie, D.G., D.M. Dowling, E. Shaya, J.J. Hester, HSTWFPC IDTand HSTWFPC2 IDT "3-D Structure of the Bipolar Dust Shell of eta Carinae" (1996) "Role of Dust in the Formation of Stars, Garching bei Muenchen, Federal Republic of Germany, 11–14 September 1995, Proceedings of

the ESO Workshop, Käufl, H.U. and Siebenmorgen, R. (Ed.) Springer-Verlag, 89–94.
[23]Currie, D., D. Le Mignant, B. Svensson, E. Diolaiti, S. Tordo, K. Naesgarde, J. Liwing, O. Bendinelli, G. Parmeggiani, D. Bonaccini "Hyper-Velocity Jets and Homuncular Motion in eta Carinae: an Application of the Fabry-Perot, ADONIS and AO Software" SPIE Vol. 4007 AO Systems Technology Editor: P. Wizinowich, # 4007–75, 1–12 (in press) (2000a)+
[24]Christou, J. and Bonaccini, D. "An Analysis of ADONIS Data, tau Canis majoris – Deconvolution".
http://www.ls.eso.org/lasilla/Telescopes/360cat/adonis/html/datared.html#idac
[25]Hester, J.J.; Light, R.M., Westphal, J.A., Currie, D.G., Groth, E.J.; Holtzmann, J.A., Lauer, T.R., O'Neil, E.J., Jr. "Hubble Space Telescope imaging of Eta Carinae" 1991 *AJ* **102**, 654–657.

STARFINDER: a Code to Analyse Isoplanatic High-Resolution Stellar Fields

E. DIOLAITI[1], O. BENDINELLI[1], D. BONACCINI[2], L. CLOSE[2], D. CURRIE[2], G. PARMEGGIANI[3]

[1]Università di Bologna – Dipartimento di Astronomia; [2]ESO; [3]Osservatorio Astronomico di Bologna

1. Introduction

StarFinder is a code designed to analyse Adaptive Optics images of very crowded fields. A typical AO observation has a well-sampled and complex-shape PSF, showing a sharp peak, one or more fragmented diffraction rings and an extended irregular halo. The approach followed in StarFinder (Diolaiti et al., 1999a, 1999b, 2000) is to analyse the stellar field with a digital image of the PSF, without any analytic approximation.

Under the assumptions of isoplanatism and well-sampling, StarFinder models the observed stellar field as a superposition of shifted scaled replicas of the PSF lying on a smooth background due to faint undetected stars, possible faint diffuse objects and noise.

The procedure derives first a PSF digital template from the brightest isolated field stars; then a catalogue of presumed objects is formed, searching for the relative intensity maxima in the CCD frame.

In the following step the images of the suspected stars are analysed in order of decreasing luminosity; each suspected object is accepted on the basis of its correlation coefficient with the PSF template; the relative astrometry and photometry of the source are determined by means of a fit, taking into account the contribution of the local non-uniform background and of the already detected stars.

At the end of the analysis it is possible to remove the contribution of all the stars detected up to this point and perform a new search for previously lost objects (e.g. secondary components of close binaries).

StarFinder is not a general-purpose algorithm for object recognition: it should be intended as a tool to obtain high-precision astrometry and photometry in adequately sampled high-resolution images of crowded stellar fields. In practice it can be applied not only to high-Strehl AO observations, but also to low-Strehl images. The code versatility has been also proved by an application to a set of HST NICMOS images (Section 3.3); in Aloisi et al. (2000) there is a comparison between our results and those obtained by DAOPHOT.

Much more intriguing and difficult to solve is the case of a field with space variant PSF, due to anisoplanatic effects in AO observations. In general the analysis of an anisoplanatic field requires the knowledge of the local PSF. The extension of StarFinder to the space variant case is in progress. Preliminary results have been presented at the ESO/SPIE meeting Astronomical Telescopes and Instrumentation 2000 (Diolaiti et al., 2000).

2. Analysis Procedure

2.1 PSF determination

The PSF is treated as a template for all the stars in the isoplanatic patch, so its knowledge is of basic importance for a reliable analysis.

The PSF extraction procedure included in StarFinder is based on the median average of a set of suitable stars selected by the user. Before being combined they are cleaned from the most contaminating sources, background-subtracted, centred with sub-pixel accuracy and normalised. The centring is performed by an iterative shift of the stellar image in order to cancel the sub-pixel offset of its centroid. The halo of the retrieved PSF is then smoothed, applying a variable box-size median filtering technique.

The PSF extraction procedure is able to reconstruct approximately the core of

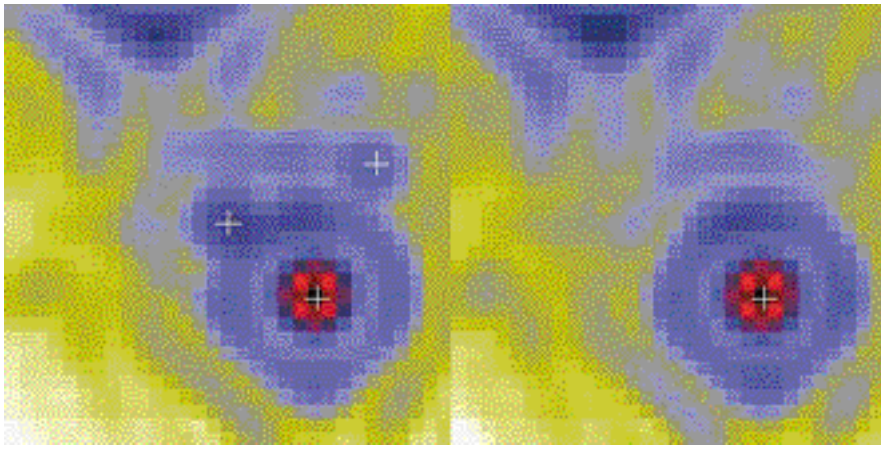

Figure 1: Left: sub-image extracted from a (simulated) stellar field, including the central star to be analysed, a brighter source which is already known, a fainter one, which will be examined later, and the PSF feature of a much brighter star, represented by the structure in the upper-left part of the sub-image. Right: corresponding sub-region extracted from the stellar field model, containing one replica of the PSF for each star detected so far.

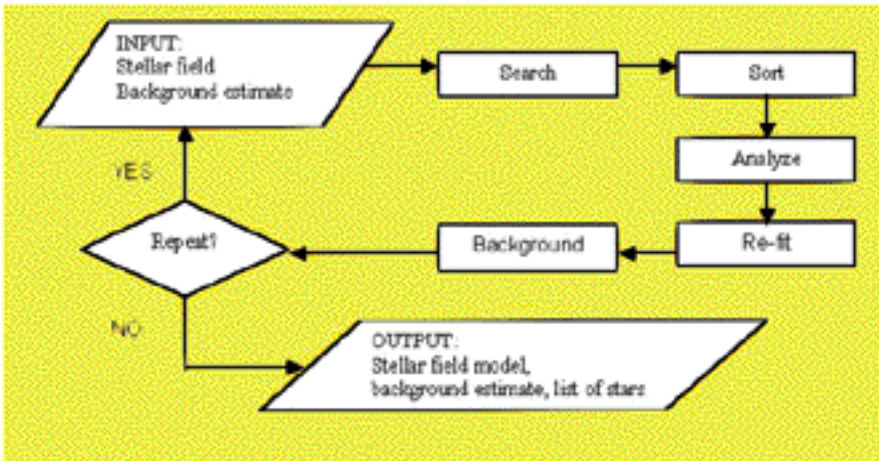

Figure 2. Flow-chart of the algorithm for star detection and analysis.

saturated stars, replacing the corrupted pixels with the central part of a preliminary estimate of the PSF: accurate positioning is accomplished by means of a cross-correlation technique, whereas the scaling factor is determined with a least squares fit to the wings of the star that is analysed.

2.2 Standard analysis of the stellar field

The starting point is a list of presumed stars, including the relative maxima which fulfil the detection condition

$$i(x, y) > b(x, y) + t, \qquad (1)$$

where $i(x, y)$ is the observed intensity, $b(x, y)$ the background emission and t a detection threshold, which may be chosen as a function of the noise standard deviation. Preliminary image smoothing reduces the incidence of noise spikes.

The presumed stars are listed by decreasing intensity and analysed one by one. In order to illustrate a generic step of the algorithm, we assume that the first n objects have already been examined and that a suitably scaled and positioned replica of the PSF has been put in a 'synthetic stellar field' for each star detected up to this point. We consider now the *(n+1)-th* object in the list. First of all, a small sub-image of fixed size is extracted around the object (Fig.1, left). Notice that the actual box size is comparable to the diameter of the first diffraction ring of the PSF, then smaller than shown in Figure 1; the only purpose of this picture is to illustrate a typical situation occurring in the analysis of a stellar field.

This region of interest may contain brighter stars already analysed, fainter objects neglected in the current step and PSF features of other stars lying both within or outside the sub-image support. The information on the brighter sources is recorded in a synthetic stellar field model (Fig. 1, right), defined as the sum of two terms: a superposition of PSF replicas, one for each star detected up to this point, and an estimate of the background emission, assumed to be non uniform in general.

The complexity of the PSF features might lead to spurious detections: to assess the reliability of the object of interest (the relative maximum at the centre of the left panel in Figure 1), we subtract the contribution of the background and of the brighter stars, derived from the synthetic field (Fig.1, right).

If a statistically significant residual can still be identified, it is compared to the PSF with a correlation check, as an objective measure of similarity. The correlation coefficient is computed on the core of the PSF: typically the central spike of the diffraction pattern is considered, out to the first dark ring. A correlation threshold (e.g. 0.7–0.8) must be fixed in order to discriminate and reject unlikely detections. The correlation coefficient represents also an effective tool to select, among the detected stars, the ones with the highest photometric reliability, since a very high correlation value is generally associated to resolved single sources.

The object in hand is accepted only if the correlation coefficient is greater than the selected level, and its position and flux are obtained by means of a local fit. Taking into account the contribution of the bright stars outside the fitting region known from the synthetic field, a slanting plane representing the local background and a sum of shifted weighted replicas of the local PSF, one for each point-source identified in the fitting region. Sub-pixel astrometric accuracy is achieved by a non-linear optimization of the star positions, which is based on the interpolation of the given PSF array. If the fit is acceptable the star field catalogue and the related syntethic image are upgraded by the new entry.

The basic step described above (detection of the suspected stars and analysis) may be repeated: a new list of presumed stars is formed after subtracting the previously detected ones and the analysis is started again on the original image. This iteration is very useful to detect stars in crowded groups, down to separations comparable to the Rayleigh limit for the detection of close binaries.

An optional deblending mode is available. All the objects somewhat more extended than the PSF are considered blends. The measurement of the area is based on thresholding the object at a pre-fixed level below the peak, after subtracting the local background and the other known stars around. The deblending strategy consists of an iterative search for residuals around the object and subsequent fitting; the iteration stops when no more residual is found or the fit of the last residual was not successful.

The flow-chart in Figure 2 represents the main loop of the algorithm, which can be iterated any number of times. In practice after 2–3 iterations the number of detected stars approaches a stable value.

2.3 PSF enhancement

At the end of the overall analysis, it is possible to run again the PSF extraction procedure, exploiting the upgraded estimates of the image background and of the contaminating sources around the PSF stars: this should allow a better determination of the PSF. Then a more accurate analysis can be performed.

2.4 Fitting procedure

The fitting technique treats the PSF as a template which may be scaled and translated. A sub-image centred on the star of interest is extracted and approximated with the model

$$h(x,y) = s_0(x,y) + \sum_{n=1}^{Ns} f_n\, p(x-x_n, y-y_n) + b_0 + b_1 x + b_2 y, \qquad (2)$$

where $s_0(x, y)$ is the fixed contribution of known stars outside the sub-image support, N_s is the number of point sources within the sub-image, x_n, y_n, f_n are the position and flux of the $n-th$ source, $p(x, y)$ is the PSF and b_0, b_1, b_2 are the coefficients of a slanting plane representing the local background.

The optimisation of the parameters is performed by minimising the least squares error between the data and the model, with an iterative Newton-Gauss technique, which requires the computation of the model derivatives. For this purpose the Fourier shift theorem is applied to the PSF:

$$p(x - y_n, y - y_n) = FT^{-1}\left\{ FT\{p(x,y)\}\, e^{-i2\pi(ux_n + vy_n)/N} \right\} \qquad (3)$$

where FT is the discrete Fourier transform, N is the sub-image size and u, v are spatial frequencies. The derivative with respect to x_n is

$$\frac{\partial p(x-x_n, y-y_n)}{\partial x_n} = FT^{-1}\left[FT[p(x,y)] \exp\left[-i2\pi(ux_n + vy_n)/N\right]\left(-i\frac{2\pi u}{N}\right)\right] =$$
$$FT^{-1}\left[\left(-i\frac{2\pi u}{N}\right) FT[p(x-x_n, y-y_n)]\right]$$

and requires in practice an interpolation of the PSF to compute $p(x - y_n, y - y_n)$. This operation may be performed, for instance, with the cubic convolution interpolation implemented in the IDL function *interpolate*. A similar algorithm has been described by Véran *et al.* (1998).

In principle this method can only be applied to well-sampled images, even though tests on under-sampled data are producing encouraging results.

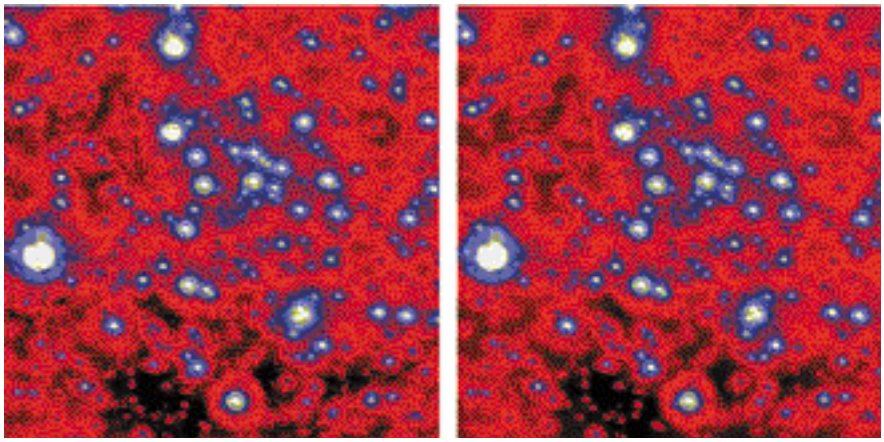

Figure 3: Left: PUEO image of the Galactic centre. Right: reconstructed image, given by the sum of about 1000 detected stars, and the estimated background. The display stretch is square root.

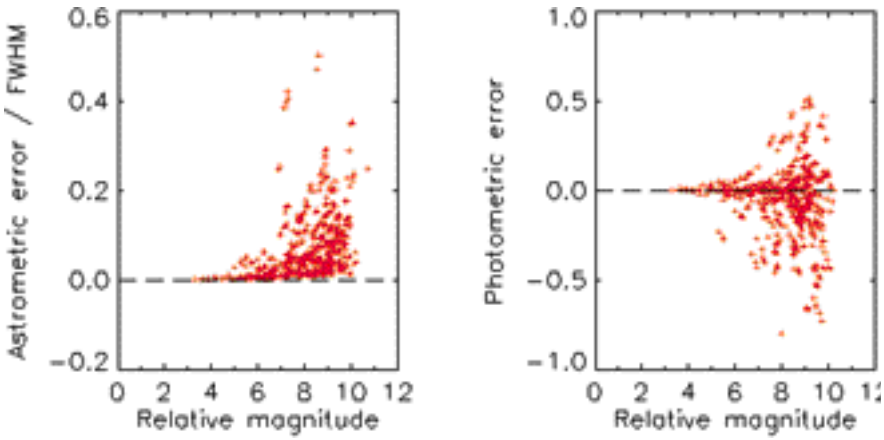

Figure 5: Left: plot of astrometric errors vs. relative magnitude of detected synthetic stars; the errors are quoted in FWHM units (1 FWHM ~ 4 pixels) and represent the distance between the true and the calculated position. Right: plot of photometric errors. A tolerance of 1 PSF FWHM has been used to match each detected star with its true counterpart.

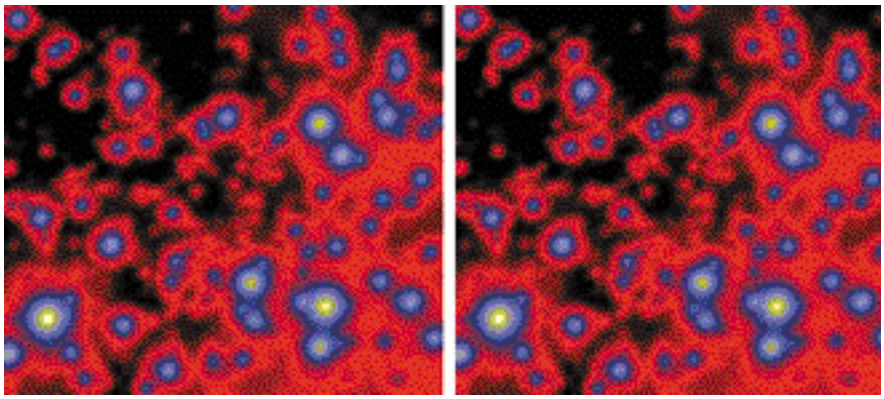

Figure 6: Left: 47 Tuc observed image. Right: reconstructed image. The display stretch is logarithmic.

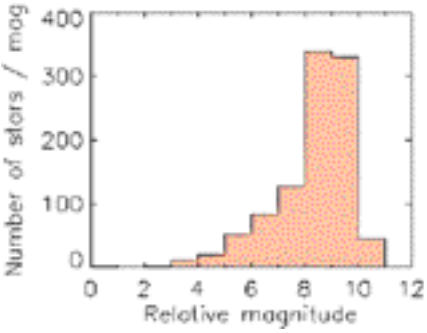

Figure 4. Galactic centre: estimated luminosity function.

3. Applications

3.1 High Strehl case

The code has been run on a K-band PUEO image of the Galactic centre (Fig. 3, left), kindly provided by François Rigaut. This image is an example of a well-sampled high-Strehl AO observation of a stellar field.

The total field of view is about 13 × 13 arcsec^2 and the pixel size 0.035 arcsec. The PSF is stable across the image, apart from some minor features especially on the shape of the first diffraction ring. We will show that assuming a constant PSF it is possible to obtain accurate results.

About 1000 stars have been detected, with a correlation coefficient of at least 0.7; the reconstructed image is shown in Figure 3, right.

We have evaluated the astrometric and photometric accuracy of the code by means of an experiment with synthetic stars: for each magnitude bin in the retrieved luminosity function (Fig. 4), a total of 10% synthetic stars at random position have been added to the image. In practice, 10 frames have been created with this procedure and analysed separately.

The catalogues of detected artificial stars for each frame have been merged together; then the astrometric and photometric errors have been computed and plotted as a function of the true magnitude (Fig. 5).

The plots show accurate astrometry and photometry and there is no apparent photometric bias.

3.2 Low Strehl case

A low-Strehl example is represented by the H-band image of the globular cluster 47 Tuc, observed at the ESO 3.6-m telescope with the ADONIS AO system (Fig. 6). The image is very well sampled with a FWHM of ~ 6 pixels (1 pixel = 0.1 arcsec).

As in the previous high-Strehl case, we have evaluated the accuracy of the algorithm by means of an experiment

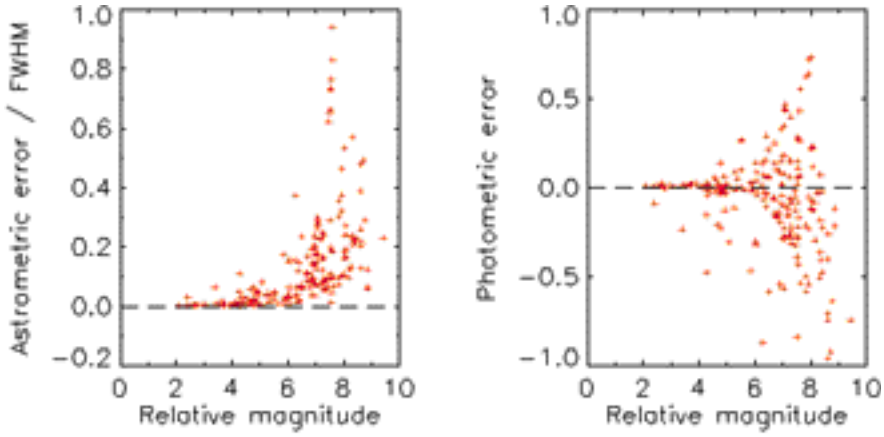

Figure 7: Left: plot of astrometric errors vs. relative magnitude of detected synthetic stars; the errors are quoted in FWHM units (1FWHM ~ 6 pixels) and represent the distance between the true and the calculated position. Right: plot of photometric errors. A tolerance of 1 PSF FWHM has been used to match each detected star with its true counterpart.

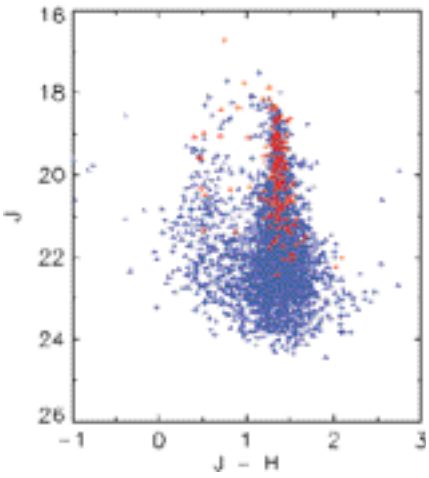

Figure 9. The NGC 1569 CMD diagram. Blue and red crosses: complete set; red crosses: stars with high correlation coeffi - cient.

with synthetic stars. The astrometric and photometric errors for the detected artificial sources are shown in Figure 7.

3.3 HST image

The last application concerns a HST observation of the starburst galaxy NGC 1569,observed with the NICMOS camera in the F110 W and F160 W filters, roughly corresponding to the standard J and H bands. The originally undersampled dithered frames have been combined with the Drizzle code, obtaining two well-sampled images which have been analysed independently (Aloisi et al., 2000). In the F160 W frame, thanks to the finer sampling of the PSF, it has been possible to apply the de-blending strategy based on the recognition of blends by their larger extension as compared to the PSF. The two images, along with the corresponding reconstruction, are shown in Figure 8.

The lists of the detected stars have been compared by matching the corresponding reference frames and retaining all the objects with a relative offset smaller than 1/2 pixel. A subset of the 3133 retrieved common stars

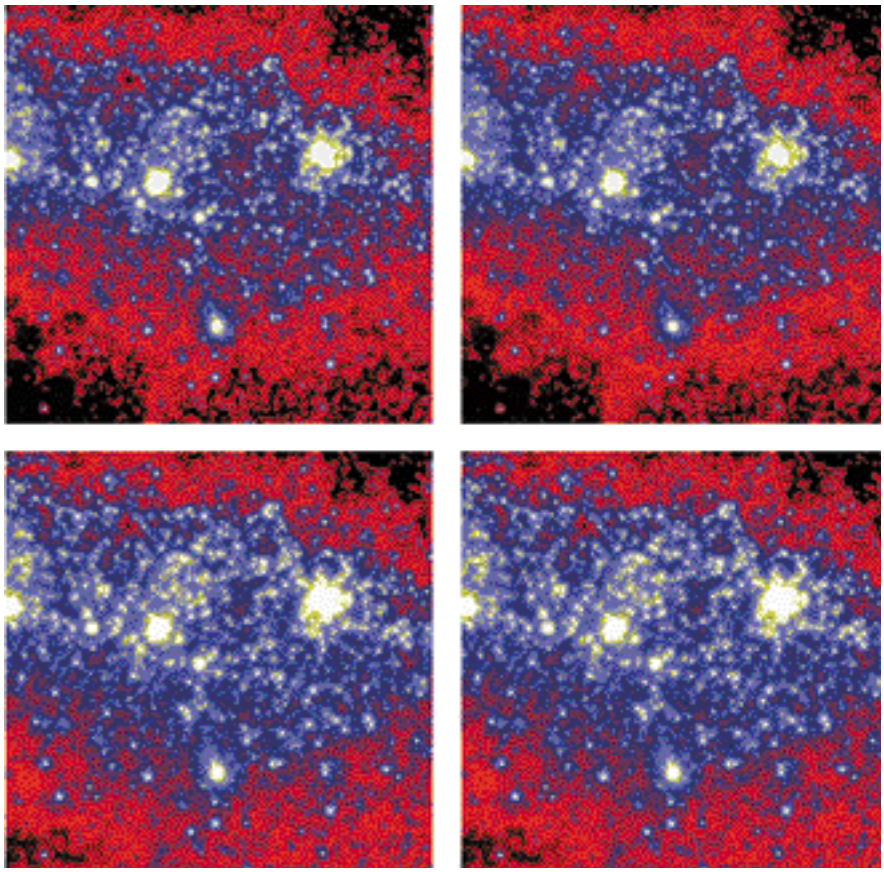

Figure 8: NGC 1569. Top: F110 W band, observed and reconstructed image. Bottom: F160 W band, the same. The display stretch is logarithmic.

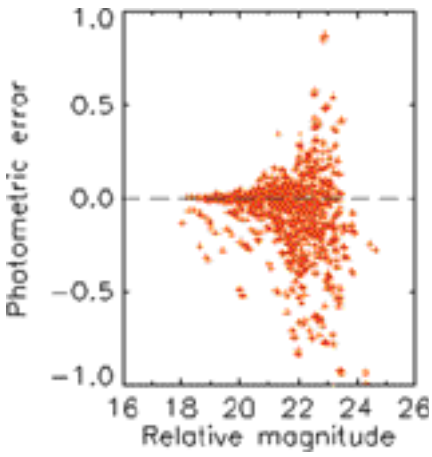

Figure 10: Photometry accuracy plot.

has been created selecting the sources with a very high (more than 0.975) correlation coefficient: high values of this parameter are generally associated to resolved single stars. The complete set of 3133 objects (blue and red crosses) and the selected one including 195 stars (red crosses), are shown in Figure 9.

The photometric accuracy has been evaluated by means of an experiment with synthetic stars, similar to those performed in the previous applications. The photometric errors for the successfully detected synthetic sources in the F110 W filter are plotted in Figure 10; similar results have been obtained for the F160 W frame. The slight bias toward negative errors may be attributed to the extreme crowding of this field: when a synthetic star falls on a fainter source, the latter might be lost whereas the luminosity of the former might be overestimated.

4. The IDL Code

The StarFinder code has been provided with a collection of auxiliary routines for data visualisation and basic

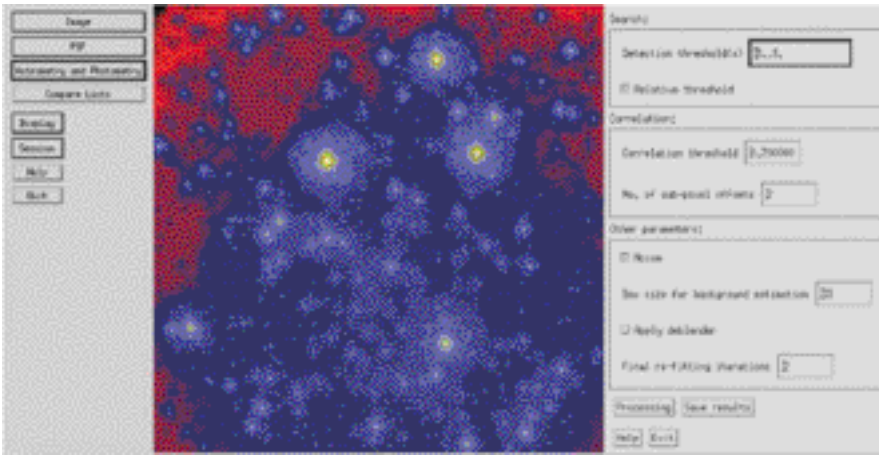

Figure 11: Widget based GUI interface.

image processing, in order to allow the user to analyse a stellar field, produce an output list of objects and compare different lists, e.g. referred to different observations of the same target. The input image is supposed to be just calibrated. The code is entirely written in the IDL language and has been tested on Windows and Unix platforms supporting IDL v. 5.0 or later. A widget-based graphical user interface has been created (Fig. 11). The main widget appearing on the computer screen is an interface to call secondary widget-based applications, in order to perform various operations on the image. The basic documentation about the code can be found in the on-line help pages and in the attached manual. IDL users might wish to run interactively the StarFinder routines, without the widget facilities: complete documentation on each module is available for this purpose. A copy of StarFinder can be obtained in the Web page of the Bologna Observatory (www.bo.astro.it) or by contacting the writer and maintainer of the code (E.D.) at the e-mail address diolaiti@bo.astro.it

5. Conclusions

The elaboration of real and simulated data seems to prove the effectiveness of StarFinder in analysing crowded stellar fields characterised by high Strehl ratio PSFs and correct sampling, reaching in this case the full utilisation of the data information content. The code can be applied also to low Strehl or undersampled data with results comparable to those attainable by other methods. StarFinder is also reasonably fast: the analysis of a field comparable to the Galactic centre image requires between 5 and 10 minutes on a normal PC (Pentium Pro-64 Mb-350 MHz).

The first improvement of StarFinder, available in a near future, will allow to analyse star fields with space variant PSF.

Acknowledgements

François Rigaut is acknowledged for kindly providing the PUEO image of the Galactic centre and for supporting the initial development of this method.

References

Aloisi A. et al., 2000. In preparation.

Diolaiti E. et al., 1999a, "An algorithm for crowded stellar fields analysis", in *Astronomy with Adaptive Optics: present results and future programs*, Sonthofen, ESO Conf. and Workshop Proc. No. 56, p.175.

Diolaiti et al., 1999b, "StarFinder: a code for crowded stellar fields analysis" in *ADASS IX,* Hawaii. In press (astro-ph/9911354).

Diolaiti E. et al., 2000, "StarFinder: an IDL GUI based code to analyze crowded fields with isoplanatic correcting PSF fitting", in *Adaptive Optical System Technology,* Munich. In press (astro-ph/0004101).

Véran J.-P. et al., 1997, *J. Opt. Soc. Am. A*, **14** (11), 3057.

Véran J.-P., Rigaut F., 1998, Proc. SPIE **3353**, 426.

VLT Laser Guide Star Facility: First Successful Test of the Baseline Laser Scheme

D. BONACCINI[a], W. HACKENBERG[a], R.I. DAVIES[b], S. RABIEN[b], and T. OTT[b]

[a]ESO, Garching; [b]Max-Planck-Institut für Extraterrestrische Physik, Garching

The planned baseline laser for the VLT Laser Guide Star Facility (LGSF) consists of dye laser modules, capable of producing > 6.5 W CW each (1). Two such modules can fit on a 1.5 × 1.5 m optical table. The laser concept was developed in a preliminary LGSF study phase (2) and is a variation of the ALFA laser (3) used in Calar Alto (Spain). It uses two Coherent Inc. all-solid state Compass Verdi 10 W lasers at 532 nm, to pump a modified Coherent model 899-21, continuous-wave (cw) ring-dye laser. The dye is Rhodamine 6G (Rh6G).

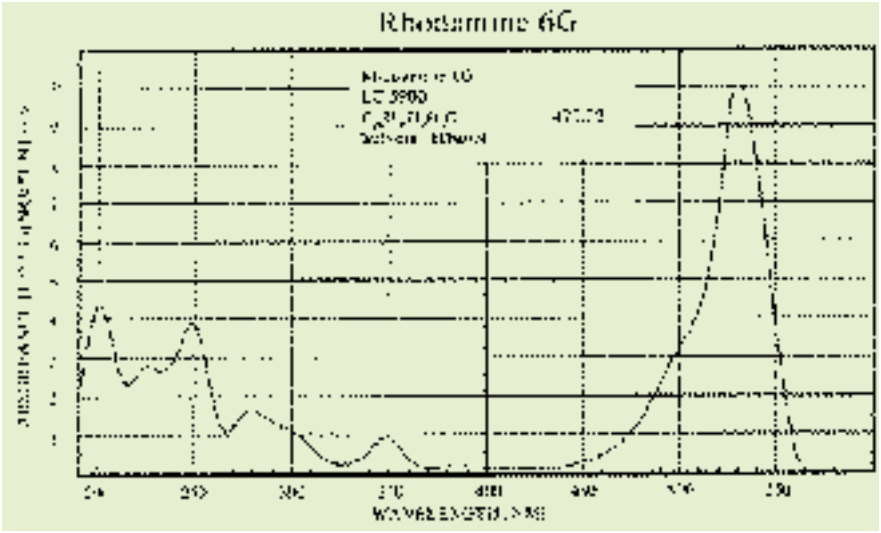

Figure 1: Absorption profile of the laser dye, Rhodamine 6G.

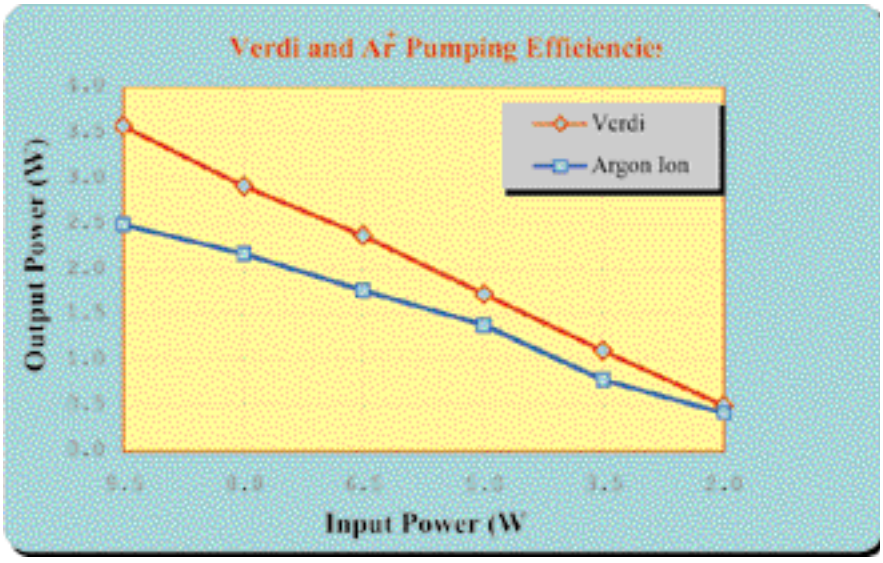

Figure 2: Output powers at 589 nm from the 899-21 ring-dye laser, for different laser-pump powers. The Verdi laser (532 nm) and the Innova Ar⁺ lasers from Coherent Inc. were used. The Verdi pumping gives up to 44% more output, at equivalent pumping powers. The baseline laser module proposed for LGSF will have 20 W pump input power.

We report here the results of testing the LGSF baseline configuration with one 10 W Verdi pump. For this test we pumped the 899-21 ring-dye laser, using alternatively the ALFA Argon-ion pump, or one 10 W CW Verdi. We have used both relatively aged as well as fresh dye solutions. This test is one of a series that has been carried out during the period 13–17 May 2000 in the ALFA laser laboratory at Calar Alto by ESO in collaboration with the team at the Max-Planck-Institut für Extraterrestrische Physik, that is responsible for the ALFA laser system.

Several advantages are obtained with the solid state Verdi as pump laser:

• The pump laser electrical power consumption (for example an equivalent output power of 4.5 W CW) is reduced by a factor ~ 37 from 46 kW to 1.25 kW, allowing the laser system to be installed in the VLT telescope area.

• The Verdi pump wavelength of 532 nm is perfectly matched to the absorption peak of Rh6G, as opposed to the main Ar⁺ wavelength at 514 nm (Fig. 1). The dye-laser output power should, therefore, increase by > 40%.

• The size of the pump laser is reduced by a factor ~ 5, allowing a smaller optical bench to be used.

The Experiment

We have modified the ALFA laser-bench set-up to accommodate flipping between pump lasers. We have limited the experiment to the use of a single Verdi laser, with 9.5 W maximum pump power into the 899-21 dye laser. We varied the pump powers of the Ar⁺ and Verdi lasers, from 2 to 9.5 W, measuring the dye-laser output power and beam quality at 589 nm. At each iteration, we have optimised the 589 nm output power adjusting the condensing optics focus on the dye jet, and the alignment of the ring resonator laser. This was necessary because of the varying thermal load on the resonator optics. The dye-solution circulation pump was set to a pressure of 11 bar.

Using the Verdi laser as pump we observed the following:

• less critical alignment tolerances in the ring-dye laser, compared to the Ar⁺

• lower output power sensitivity to dye aging.

• higher output power, up to 3.6 W CW for 9.5 W pump, with a 44% increase over the Ar⁺ pump efficiency.

Optimisation of the nozzle and an increase of the dye-circulation pump pressure are expected to give a further improvement in output power.

In Figure 2, the single-mode dye-laser output power as a function of the pump power at the 899-21 dye-laser input is shown. The output power reveals a linear dependence on the pump power up to the maximum available input power of 9.5 W. At this pump power, the single-mode output power was measured to be 3.6 W with an extremely good beam quality (M^2 = 1.13). The optical conversion efficiency of 38%, together with the high beam quality, are excellent results for a high-power CW dye-laser system. The free-flowing dye-jet stream was not fully optimised for the 532 nm wavelength. We expect to see further improvements in the conversion efficiency when this is optimised.

Conclusions

We now have experimental evidence that the baseline LGSF laser will meet

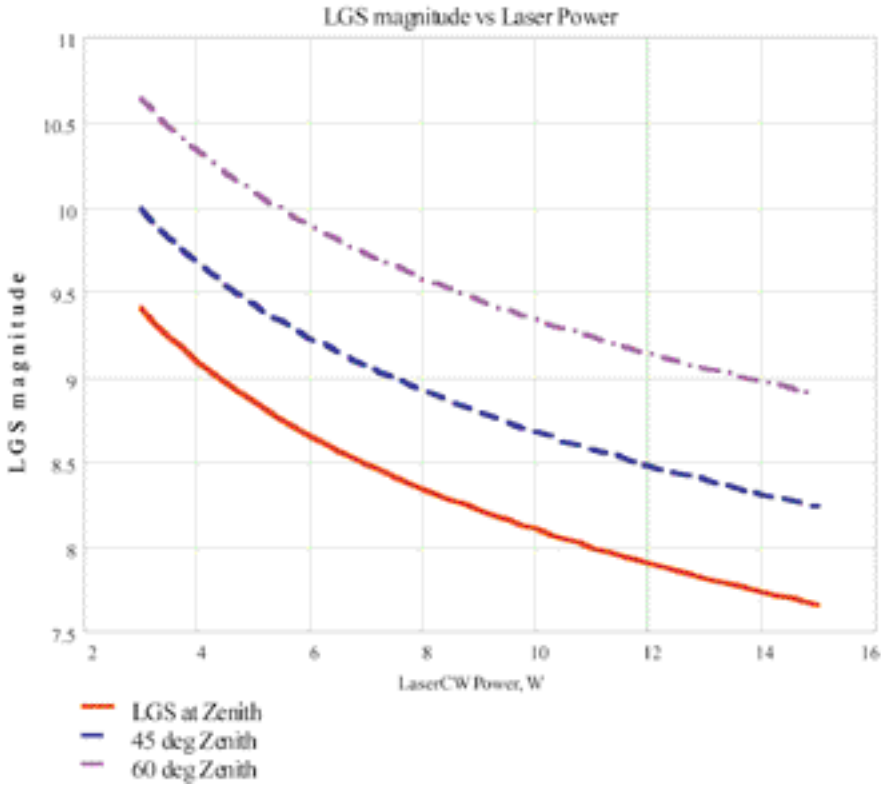

Figure 3: Equivalent V-band magnitude of the LGS, versus sodium laser output power. The one-way transmission assumed for the atmosphere is 0.8 and for the launch optics 0.75, with a sodium column density of 5 × 10^{13} m^{-2}. These are typical average conditions. The three curves represent different LGS zenithal distances.

the optical power requirement, which is to have 589 nm laser modules producing each ≥ 6.5 W CW of narrow-band (10 MHz) laser output power at the sodium D_2 line.

Even without counting potential improvements arising from the dye-nozzle optimisation, we can expect each module to deliver 7.6 W CW at 589 nm, using the 2 × 10 W Verdi pumps. Two complete dye-laser modules will then produce ≥ 13 W CW at 589 nm.

This experiment, together with the former experimental results of the single-mode fibre laser relay[4], completes the feasibility tests for the innovative concepts of the baseline LGSF.

The dye laser tested has proven very stable and reliable. Before freezing the decision on the final laser system for LGSF, we plan to explore further alternatives.

Finally, in Figure 3, we plot the equivalent LGS magnitude in V-band, assuming average sodium column densities, typical atmosphere and launch telescope transmissions for different telescope zenithal distances.

References

(1) Bonaccini, D., Hackenberg, W. and Avila, G: "The Laser Guide Star Facility for the VLT", in Proceedings of the ESO June 23–26 1997 Workshop on 'Laser Technology for Laser Guide Star Adaptive Optics', p. 152–157, N. Hubin ed.

(2) Bonaccini, D., Hackenberg, W., Cullum, M., Quattri, M, Brunetto, E., Quentin, J., Koch, F., Allaert, E. and Van Kesteren, A.: "Laser Guide Star Facility for the ESO VLT", *The Messenger* No. **98**, p.8-13, Dec 1999 – http://www.eso.org/gen-fac/pubs/messenger/

(3) Davies, R.I., Eckart, A., Hackenberg, W., et al., 1998. In: Adaptive Optical System Technologies, Bonaccini, D., Tyson, R.K. (eds.), Proc. SPIE 3353,116.

(4) Hackenberg,W., Bonaccini,D. and Avila,G: "VLT Laser Guide Star Facility Subsystem Design Part I: Fibre Relay Module", *The Messenger* No. 98, p.14–18, Dec 1999 – http://www.eso.org/gen-fac/pubs/messenger/

For information on the Compass Verdi V-10 laser, see www.cohr.com

The La Silla News Page

The editors of the La Silla News Page would like to welcome readers of the fifteenth edition of a page devoted to reporting on technical up - dates and observational achievements at La Silla. We would like this page to inform the astronomical community of changes made to tele - scopes, instruments, operations, and of instrumental performances that cannot be reported conveniently elsewhere. Contributions and inquiries to this page from the community are most welcome.

2p2 Team News

H. JONES

The 2p2 Team continued towards the implementation at the 2.2-m of the same BOB (Broker for Observation Blocks) observing interface as seen at other ESO telescopes. This requires an interface to be written between the existing BOB software and the non-VLT compatible control software for the Wide-Field Imager (WFI) and 2.2-m. Cristian Urrutia, Tatiana Paz and Eduardo Robledo are heading its development. With this software in place, observers can use the VLT Phase 2 Proposal Preparation System (P2PP) for definition of their exposures, whether they are for Visitor or Service Mode.

In the longer term, there are plans to upgrade the current WFI archiving operations to become identical to those presently on Paranal. Such a system would readily streamline the amount of data handling during archiving. This would be an important step for an instrument such as the WFI, from which we currently see data volumes of around 200 Gb per week, the ingestion of which by the Science Archive in Garching carries large overheads.

In January we bade farewell to Team Leader Thomas Augusteijn who left ESO for the Isaac Newton Group of Telescopes on the island of La Palma in the Canary Islands. Our new leader will be Rene Mendez from CTIO here in Chile, who has interests in Galactic structure and astrometry. We wish him a warm welcome to ESO. Rene will commence work with the team in September. In the meantime, existing team member Patrick François, currently on secondment to ESO from Observatoire de Paris, has taken over Team Leader duties. In February we welcomed Fernando Selman to the team. Fernando is currently undertaking his PhD on massive star-formation regions in the LMC, under the supervision of Jorge Melnick. Around the same time we farewelled long-time Telescope Operator Pablo Prado to the Gemini Project. Our best wishes accompany him.

During the re-aluminisation of 2.2-m M1 in April, Alain Gilliotte and Gerardo Ihle inspected the mirror cell as part of ongoing efforts to find the cause of astigmatism often seen as a result of large zenith travel. With the help of members from the Mechanics Team, they discovered a problem with one of the fixed mirror supports. Correction of this now sees astigmatism reduced to the range 0.07 and 0.15 arcsec up to 60 degree zenith distance. For many applications, the amounts of astigmatism are negligible. Further room for improvement is foreseen by Alain which we hope to accommodate during the coming months. A dedicated *Messenger* article has more details.

At the ESO 1.52-m there have recently been major efforts on several fronts. In the final week of April, the mirror was re-aluminised and a replacement slit-unit installed in the Boller and Chivens spectrograph. This should allow observers greater precision when selecting slit-widths with this instrument. At the same time, the control room of the ESO 1.52-m has been extensively refurbished, giving it the same modern and comfortable working environment of other ESO telescopes.

New (or even old) observers are reminded that information on all of our telescopes and instruments can be found through the team web pages at http://www.ls.eso.org/lasilla/Telescopes/2p2T/ This information is kept up-to-date with all major new developments.

News from the 3.6-m Telescope

M. STERZIK, M. KÜRSTER, and the 3.6-m Telescope Team, ESO

After completion of the 3.6-m upgrade project (about which was reported in the September 1999 issue of *The Messenger*), we are now in a phase of consolidation, system finetuning, and optimisation. The general operation of telescope and instrumentation has now become very smooth and reliable, and the users are in general very pleased and satisfied with the quality, stability and comfort that is offered to them.

One week of planned technical downtime was required to perform various maintenance actions last March. Over the past four years, M1 has been successfully re-aluminised in a joint effort of our optics and mechanics team in La Silla. We received a "new" mirror, increased in reflectivity from below 83% to about 90.4%, with microroughness variations from 45 Å to 70 Å. On the same occasion, our lateral pad system (which keeps M1 in its mirror cell without movement or optical aberrations) has been thoroughly revised and adjusted. One radial pneumatic valve has been found damaged by water contamination and has been replaced. During the removal of the M1 cell, the new painting of the telescope was finished, it now shines in fresh, blue colours. Useless air-conditioning ducts were also removed from the dome area.

The second instrument at the 3.6-m that is now running under fully VLT-compliant control is the CES. This instrument has seen a large number of improvements during the past months. The coudé room has been refurbished, permitting an improved temperature stability and light tightness. The pre-disperser has received a long-awaited new control mechanism which permits very precise and reproducible positioning. Also, the grating and slit drive mechanisms were changed in order to make them VLT compliant. All this has led to a nightly spectral stability as well as a night-to-night reproducibility of 0.055 px rms, corresponding to 26 ms^{-1} at a wavelength of 5400Å. The new EEV CCD in use with the CES provides excellent cosmetics and an increased wavelength coverage with 4096 pixels in the dispersion direction (e.g. 35.5Å at 5400Å). A new exposure meter has also been integrated into the instrument.

The La Silla detector group is curently testing another EEV CCD which has a better quantum efficiency, especially in the blue (below 4000 Å), and seems to be comparable to the present one in terms of its other properties (cosmetics, read-out noise). The coming weeks will also see the test of a new object fibre which also has an improved blue efficiency. Provided that both tests yield satisfactory results, the future CES blue efficiency might be enhanced by a factor of about 4 altogether.

In the course of writing these lines, the infrared f/35 focus and adapter are being commissioned under VLT-SW control. Although TIMMI2, the new, second-generation mid-infrared multimode instrument is not a generic VLT-compliant instrument, it will nevertheless make elegant use of the features of the new control system. All cryogenic tests of TIMMI2 have been successfully passed, and detector, optomechanics and instrument control software are completed. Instrument integration will take place at La Silla in the premises of our telescope, and it is now expected that the instrument will be offered to the community next September or October.

A new operational astronomer at the 3.6m telescope is Nancy Ageorges. She will concentrate primarily on our IR instrumentation, especially the operational support for TIMMI2. She replaces Pierre Leisy, who has now become integrated into the NTT team. For us, Pierre will continue developing and implementing an EFOSC DFS pipeline. Nancy's experience with ADONIS will also allow her to partially cover the hole that the ADONIS instrument scientist, Olivier Marco, will open when he starts work on Paranal in September this year.

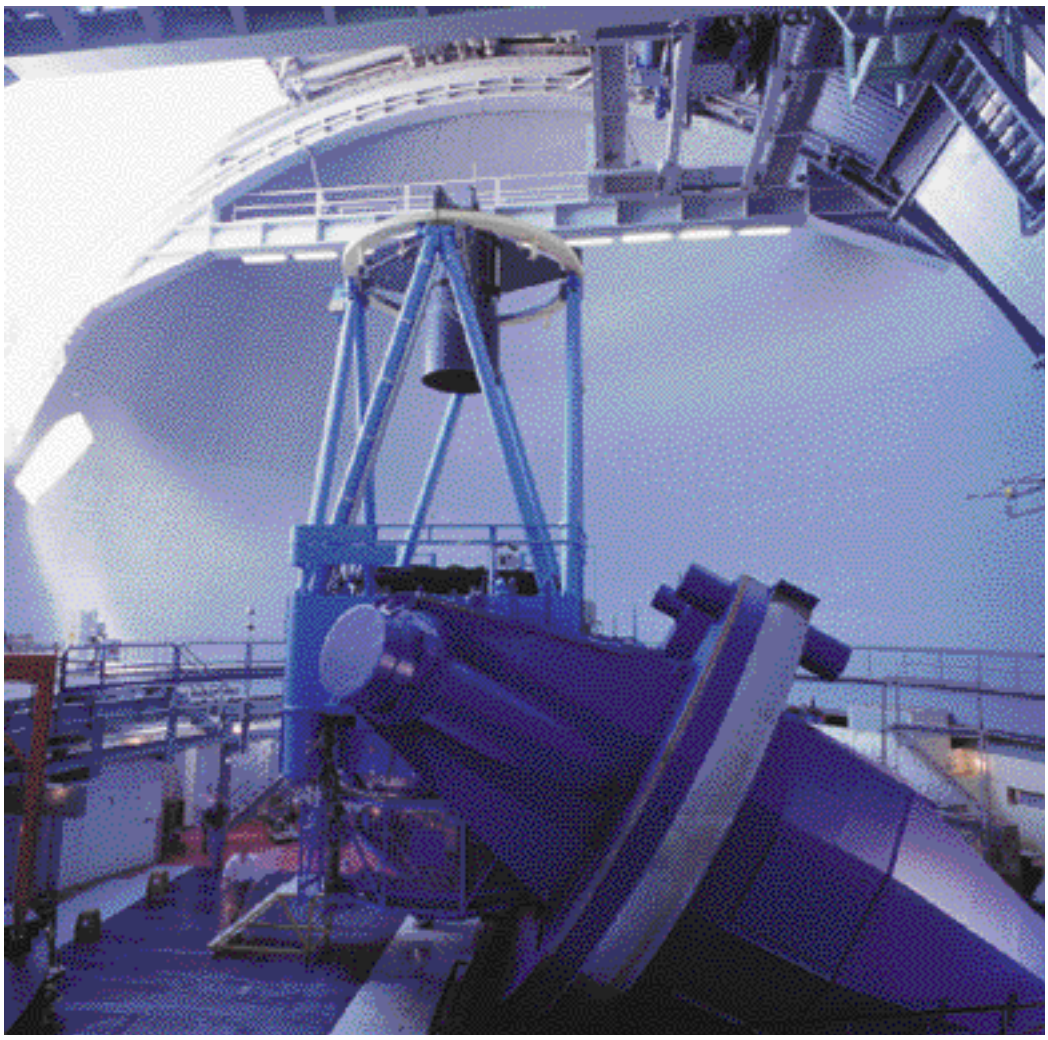

The 3.6-m telescope after installation of the re-aluminised M1. Photographer: H.-H. Heyer

La Silla under the Milky Way. Photographer: H.-H. Heyer

Gamma-Ray Bursts[1] – Pushing Limits with the VLT

H. Pedersen[1a], J.-L. Atteia[2], M. Boer[2], K. Beuermann[3], A.J. Castro-Tirado[4], A. Fruchter[5], J. Greiner[6], R. Hessman[2], J. Hjorth[1b], L. Kaper[7], C. Kouveliotou[7,8], N. Masetti[9], E. Palazzi[9], E. Pian[9], K. Reinsch[2], E. Rol[7], E. van den Heuvel[7], P. Vreeswijk[7], R. Wijers[10]

[1a]Copenhagen University Observatory, holger@astro.ku.dk; [1b]Copenhagen University Observatory; [2]CESR, Toulouse; [3]Universitäts-Sternwarte, Göttingen; [4]LAEFF-INTA, Madrid, and IAA-CSIC, Granada, Spain; [5]Space Telescope Science Institute, Baltimore, USA; [6]Astrophysikalisches Institut Potsdam; [7]Astronomical Institute "Anton Pannekoek", Amsterdam; [8]NASA/USRA, Huntsville, Alabama, USA; [9]Ist. TeSRE, CNR, Bologna; [10]Dept. of Physics and Astronomy, SUNY Stony Brook, USA

1. Introduction

"New kids on the block" – perhaps this is the best way to describe cosmic gamma-ray bursts among the multitude of object types that can be studied by optical telescopes. When they pop up, they give a lot of trouble, and for a while take the attention from all the work in progress. In this report we will describe how ESO observers are making most out of these exciting opportunities, and how the VLT promises to integrate space and ground-based observations in a way never achieved before. But first a few words on the historical background.

2. The Basics

Cosmic gamma-ray bursts (GRB) are studied from spacecraft, since γ-radiation does not penetrate the Earth's atmosphere. The first detection was made in 1967, but the phenomenon became publicly known only in 1973, when 16 events were published, in the *Astrophysical Journal*. This first paper led to a flurry of theoretical works; for several years, the rate with which models were proposed kept pace with the detection of new events. Likewise, on the experimental side, numerous initiatives were taken. To date, more than 60 spacecraft have carried successful gamma-ray burst detectors. The most efficient was BATSE on board the Compton Gamma-Ray Observatory. This instrument has detected about one event every day, on average, since its launch in April 1991.

The hallmark of gamma-ray bursts is diversity: durations can be anything between a few milliseconds and several minutes. Gamma-ray burst 'light-curves' take numerous shapes, from smooth, single peaks to very jagged, multi-peaked graphs. They come from ever new directions, and until recently they could not be associated with any known object population, be it solar-system objects, stars from the Milky Way, distant galaxies, or even quasars. Their γ-ray spectra do not show any obvious emission or absorption lines that could help identify the physical processes responsible for the phenomenon.

Many gamma-ray bursts are surprisingly bright (in γ-rays, 0.1–100 MeV) – for a short moment they easily outshine the sum of all other celestial high-energy sources. Conversely, near the instrumental detection limit there are fewer events than expected from a homogeneous distribution through an Euclidean space. This lack of faint bursts could be explained by either a large Galactic halo population, or a cosmological origin for gamma-ray bursts.

During the early years, it was repeated over and over that optical observations were needed to finally clinch the distance question. Only thereby could one know the total (absolute) amount of energy emitted, and then start discussing in earnest, what is the fundamental physical process in gamma-ray bursts.

3. The BeppoSAX Legacy

In the beginning of 1997, this wish was fulfilled. The previous year, an Italian-Dutch consortium had launched the *Satellite per Astronomia X,* SAX, nicknamed BeppoSAX after the Italian Cosmic-ray and X-ray astronomy pioneer Giuseppe Occhialini.

The satellite was primarily intended to study the 0.1–300 keV spectrum of galactic and extragalactic sources with four Narrow-Field Instruments (NFIs). The scientific payload onboard BeppoSAX also includes a Gamma-Ray Burst Monitor (GRBM, 40–700 keV, all-sky coverage), which is the non-imaging anticoincidence system of the high-energy NFI (the PDS), and two coded-mask Wide-Field Cameras (WFCs, 2–26 keV, 40° × 40° field), pointing at right angles with respect to the NFIs.

Although gamma-ray burst investigation was a secondary task of BeppoSAX, the simultaneous detection of gamma-ray bursts by the GRBM and one of the WFCs proved to be crucial in identification of their counterparts at lower energies thanks to the rapid (4–5 hours) and accurate (~ 3′) localisation afforded by the WFCs.

The good scheduling flexibility of BeppoSAX allows a prompt repointing of the NFIs at the gamma-ray burst error circle and efficient search of the X-ray counterpart. In case of NFI detection of a gamma-ray burst afterglow candidate in X-rays, the error circle is reduced to ~ 50″ in radius. Meanwhile, the rapid dissemination of the error circle centroid co-ordinates makes fast follow-up at ground-based telescopes possible.

The first error circle thus established was for GRB 960720, but came 45 days after trigger and did not result in the finding of a counterpart (in 't Zand et al., 1997). The next, GRB 970111, was announced promptly, and search in the initially large WFC error circle turned up a number of sources, none of which lay in the refined error circle established a few days later[2]. Then, 'third time lucky', came the burst of 28 February 1997, which revolutionised the field. It was detected in the WFC and located to a 3′ error circle. Prompt reorientation of the satellite and activation of the NFIs 10 hours after the burst led to the localisation of a bright, previously unknown X-ray source (Costa et al., 1997).

A second NFI observation 3 days later showed that the source had faded by a factor of 20. Subsequent observations with the ASCA and ROSAT satellites confirmed that the source faded with a power-law, $I \propto (t - t_{GRB})^{\alpha}$ where time is counted in days, and $\alpha \sim -1.3$. This type of decay had indeed been predicted by Mészáros and Rees (1997). In their "fireball" model, a mixture of matter and photons expands at

[1]This year's *Annual Review of Astronomy and Astrophysics* will include a review paper on Gamma-Ray Bursts, authored by Jan van Paradijs, Chryssa Kouveliotou, and Ralph Wijers.

[2]In hindsight, the NFI follow-up observation of this event shows a faint source. This source is consistent with being an afterglow, given what we have learnt of afterglows from later events, but was not recognised as such at the time.

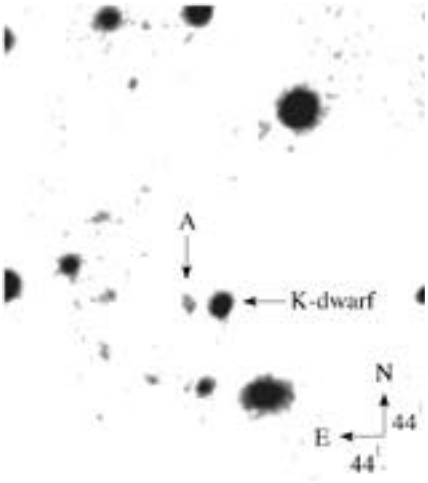

Figure 1: The first optically identified gamma-ray burst, GRB 970228. This image, obtained at the NTT on March 13, 1997, gave the earliest indication that the source was located in a remote galaxy (van Paradijs et al., 1997). "A" marks the combined light of the optical transient and candidate host galaxy, later verified by Hubble Space Telescope observations.

high speed and makes the interstellar medium radiate synchrotron emission when it impacts on it; thus it is exactly like a supernova remnant, except relativistic speeds are involved.

4. The First Optical Transient

The initial 3′ localisation from BeppoSAX's WFC allowed independent ground-based optical observations to start 20.8 hours after the gamma-ray burst. The late Jan van Paradijs, and his two students, Titus Galama and Paul Groot, took this opportunity to make the observation, which forever changed gamma-ray burst astronomy. An exposure from the William Herschel Telescope showed a 21st magnitude object, which had faded by more than 2 magnitudes, when the observation was repeated some days later. Subsequent ESO NTT observations (March 13) showed a fuzzy object at the place where the optical transient (OT) had been (Fig. 1); this was interpreted as a host galaxy (van Paradijs et al., 1997).

This first detection of an optical transient (optical afterglow) sparked an international observing effort, which was unique, except perhaps for SN 1987A. All major ground-based telescopes were used, optical as well as radio. The fading of the optical transient became well documented over a wide wavelength range (Figs. 2a and 2b), and the Hubble Space Telescope confirmed the existence of a host galaxy, which indeed is small and not very conspicuous. The host's distance could not be gauged from the pictures, and remained unknown until 1999, when Keck-II observations placed it at $z = 0.7$ (Djorgovski et al., 1999). At that distance, a supernova would have peaked at magnitude R ~ 25.2; i.e. about 50 times fainter than observed for the OT.

5. A Treasure Hunt of Sorts

It had thus become obvious, that ground-based observers can harvest beautiful and important results, by maintaining close links to the space community.

In this way, observations can start within hours from a gamma-ray burst, perhaps even faster, hence raising the expectation that a counterpart will be encountered brighter than the 21st magnitude found for GRB 970228. Such *targets of opportunity* are now pursued with high priority at many observatories, including La Silla, Paranal and the Hubble Space Telescope.

Key to this process is the distribution via internet of positions derived from SAX, RXTE and from the Interplanetary Network, IPN, (consisting of Ulysses and NEAR, in addition to near-Earth detectors like BATSE, SAX, and Wind). This service is operated by Goddard Space Flight Center (NASA) and has more than 400 clients.[3]

By the time this article goes to press, some 18 low-energy (optical, infrared, radio) counterparts have been identified, worldwide.[4] In a similar but larger number of cases, no optical counterpart

[3]http://gcn.gsfc.nasa.gov

[4]For details, see Jochen Greiner's site http://www.aip.de/~jcg/grb.html The present collaboration plans to establish a web site with information on its activities and results; the URLwill be provided later.

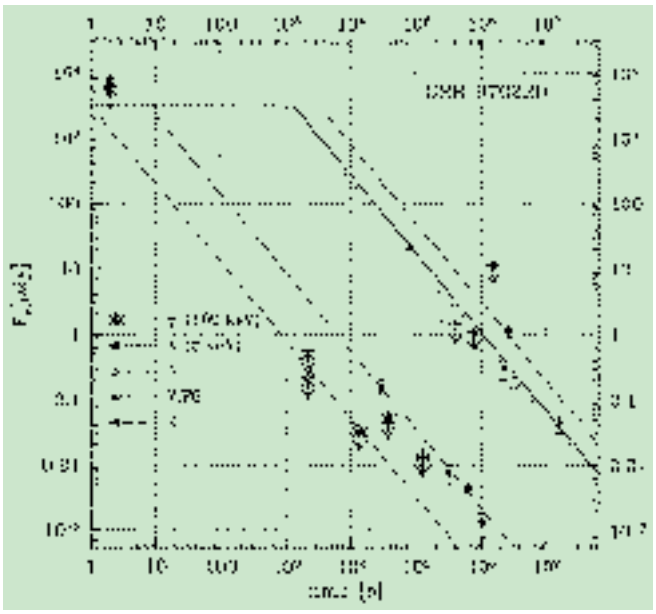

Figure 2a: The afterglow of GRB 970228. The decay of the afterglow emission, over a wide range of energies is shown from γ-rays to the near infrared (K-band). Time is measured in seconds, following the moment of the gamma-ray burst, 1997 February 28.1236 UT. The lines indicate the power-law prediction for a specific blast wave model (from Wijers, Rees, and Mészáros, 1997, with recent data added).

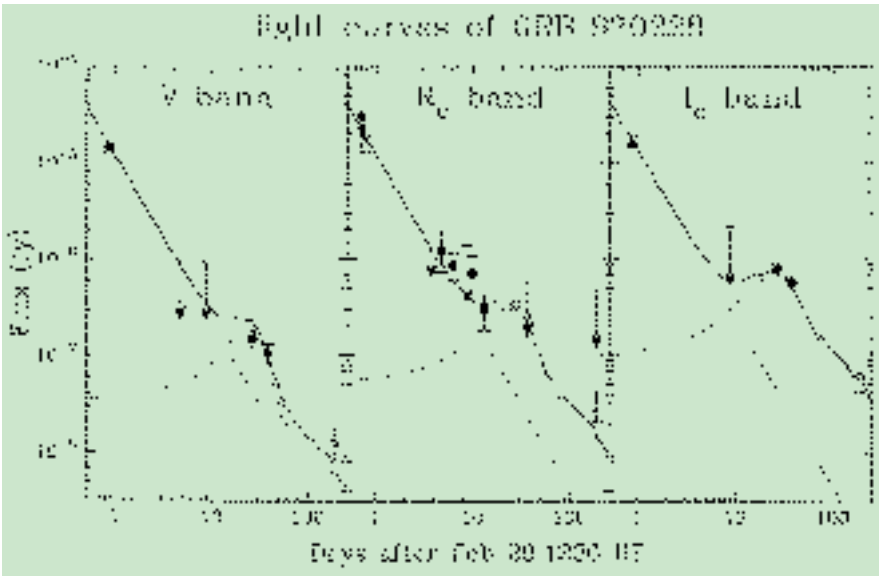

Figure 2b: The light curve of the very first optical transient, OT/GRB 970228, discovered by Jan van Paradijs. The photometric development is documented in three colours, V, R and I. The loss of brightness had already started when optical observations began almost one day after the gamma-ray burst. A hump in the light curve may be caused by a supernova-like component (Galama et al. 2000).

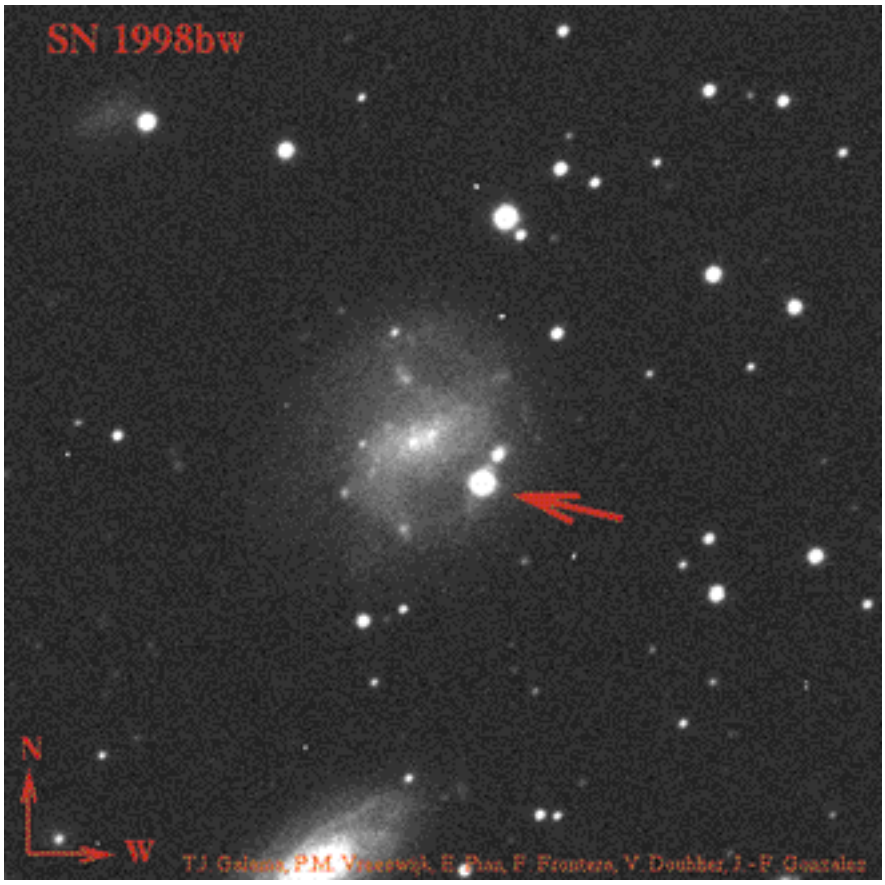

Figure 3: On April 25, 1998, a gamma-ray burst appeared from a location compatible with a highly unusual supernova, SN 1998bw, in the spiral galaxy ESO 184-G82. This picture was obtained at the NTT on May 1, 1998 (Galama et al., 1998). If the association is physical, this implies a much closer distance than observed for several other gamma-ray bursts.

was found. The reason for this is not clear; possibly these searches were not swift nor deep enough, but in two cases (GRB 970828, 000214, and perhaps also 970111) the optical fluxes, predicted from X-ray observations are well above detection limits.

The high redshift found for the GRB 970228 host galaxy turned out not to be anywhere near the record. For GRB 971214, the value z = 3.4 was found (Kulkarni et al., 1998), implying that the burst was emitted 10 billion years ago, equivalent to when the Universe was 11% of its current age.[5] The energetics are equally stunning: assuming isotropic γ-ray emission, this burst must have emitted 3 × 10^{53} erg, equivalent to 16% of the Sun's rest-mass energy.

6. The Supernova Connection

Just as redshifts in the range 0.7–3.4 were about to become accepted, a gamma-ray burst from April 25, 1998, gave reason to rethink the distance scale. The gamma-ray burst itself was not exceptional, but the optical counterpart certainly was. Observations initiated three days later, at the NTT, showed that the error box included a catalogued galaxy, ESO 184–G82. In one of the spiral arms, a 16th magnitude object was noted (Fig. 3); spectroscopy showed this to be a supernova, of type Ic. Could this be a chance alignment? Taking into account the coincidence in both time and place, Jan van Paradijs conservatively calculated the probability as 10^{-4}. This is small, but not entirely convincing. The distance to the galaxy was quickly measured with the Anglo-Australian Telescope to be z = 0.0085, or a mere 130 million light-years. If really the high-energy event was that close, it would mean that gamma-ray bursts span over a very wide, intrinsic luminosity range, at least a factor 10,000 (Galama et al., 1998). Adding to the probability that the two phenomena are indeed related, is the fact that the SN 1998bw in itself is highly unusual, with outflow velocities exceeding 50% of the speed of light (e.g. Leibundgut et al., 2000).

Could there be other supernovae, emitting gamma-ray bursts, or could a SN-like contribution to the light-curve be detected in other optical transients? Naturally, the existing material was scrutinised, and for OT/GRB 970228, the very first OT, a hump, consistent with a high-redshift supernova is indeed noted some 20–30 days after the gamma-ray burst (Fig. 2). Also for GRB 980326, a SN-hump was found (Bloom et al., 1999). In other cases no such SN signature has been observed. It remains uncertain, if there are several classes of cosmological gamma-ray bursts or if all are associated with supernovae, or none.

7. A Spectacular Event in the Northern Sky

On January 23, 1999, a very bright gamma-ray burst occurred in the Northern sky. Its approximate position, derived from BATSE, was distributed over the internet, and within seconds, a robotic telescope at Los Alamos National Laboratories started taking pictures. It caused a sensation in the GRB community, when these data were examined: in its maximum, 47 seconds after the burst trigger and before the γ-ray emission had ceased, the OT had been as bright as 9th magnitude (Akerlof et al., 1999); it could, in principle, have been seen in a pair of binoculars!

The first expectation was that this event was very close. However, a few days later, the redshift z = 1.6 was derived (from Keck-II and the Nordic Optical Telescope). This implies an energy output corresponding to almost two neutron star rest masses. Or in other terms: if GRB 990123 had taken place in the Andromeda Galaxy, the optical flash would have been as bright as the full moon! Such energy output challenges some of the most popular models for the basic energy source, merging pairs of neutron stars. It should also be recalled that no known stellar process will convert mass to electromagnetic energy with 100% efficiency, much is lost in neutrinos. However, if the outflow was directional or jet-like, instead of isotropic, this 'energy crisis' could be lifted.

Unfortunately, it is not the rule that all OTs reach this peak brightness. In at least a dozen of other cases a limit of 14th magnitude was found from robotic CCD observations, and less stringent limits exist from wide-field (all-sky) photographic exposures.

8. Discovery of Polarisation

With the first unit of the VLT (ANTU) in service in April 1999, it was natural to do an all-out effort, as soon as a suitable event occurred. On May 10, members of our team identified the counterpart of a gamma-ray burst, using the Sutherland 1-m in South Africa. When it became night in Chile, everything was prepared, and FORS1 data could be taken already 20 hours after the gamma-ray burst.

This gave one of the first opportunities to try polarimetric observations of a gamma-ray burst counterpart. The splitting of light in orthogonal planes has the potential of revealing information on the

[5]For standard cosmology parameters H_0 = 65 km/s/Mpc, Ω = 0.3, Λ = 0.

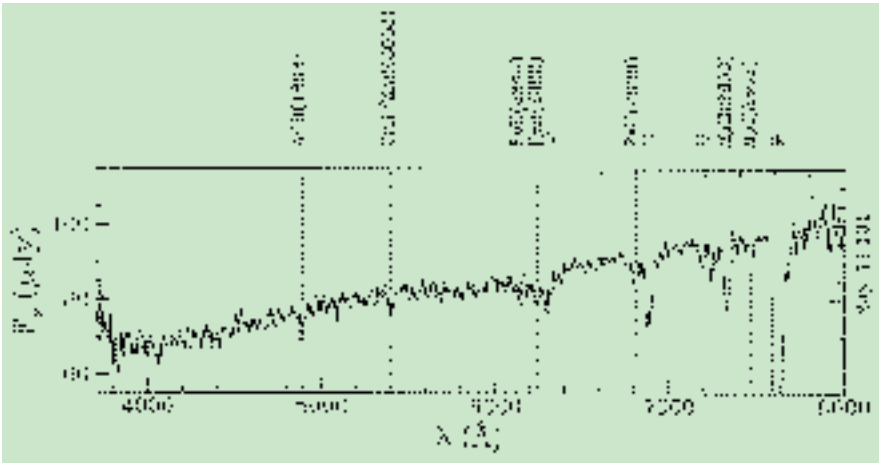

Figure 4: A VLT/FORS1 spectrum of the afterglow of ORB 990510, 20 hours after the burst. Several absorption features are detected, corresponding to the redshift z = 1.6; the OT and the host galaxy may well be more distant. Special symbols mark telluric (atmospheric) absorption bands. Adapted from Vreeswijk et al. (1999b).

nature of the light source. The VLT data showed a significant amount of linear polarisation, 1.6 ± 0.2 per cent, 0.86 days after the burst, and similar, after 1.81 days (Covino et al., 1999; Wijers et al., 1999). It was concluded that the polarisation is intrinsic to the source and that it supports the emission's origin as synchrotron radiation. Polarisation, especially a change in polarisation degree and angle, can also argue for a jet-shaped outflow. The second polarisation measurement, although of lower significance, indeed provides this evidence (see also below). It is clear, though, that this research is in its infancy.[6]

Optical spectra at several epochs were also obtained, displaying several metal absorption lines from e.g. ionised iron, neutral and ionised magnesium. This implies that the OT was at a redshift of $z > 1.6$ (Fig. 4). The neutral magnesium is indicative of a low-ionisation, dense interstellar medium, most likely that of the host galaxy. However, neither the VLT nor Hubble was able to detect a galaxy at the position of the optical afterglow down to V ~ 28. This shows the enormous power of gamma-ray bursts to probe the interstellar medium to high redshifts. The spectral flux distribution and the light curve support the interpretation of the afterglow as synchrotron emission from a jet (Covino et al., 1999; Wijers et al., 1999).

9. NTT and VLT Setting Standards

With less than 20 OTs known, almost any new discovery will strike a record of some kind. In case of GRB 990712, the VLTspectrum gave the redshift $z = 0.43$, corresponding to 4 billion years (Vreeswijk et al. 1999b; Hjorth et al. 2000). This is larger than found for the presumed association GRB 980425 / SN1988bw, but smaller than other OTs, for which the median redshift is near $z = 1$.

The faintest OT at discovery was OT/GRB 980329, measured at R = 23.6 when first detected at the NTT (Palazzi et al., 1999).

Another remarkable NTT discovery was that of OT/GRB 990705; this was the first identification achieved in the near-infrared (Masetti et al., 2000).

Optical spectroscopy of GRB 991216 gave the first indication of multiple absorption line systems, conceivably arising from clouds separate from a host galaxy, and much closer to the Earth. The particular observation was made at the VLT, and showed no less than three absorption line systems, at $z = 0.77$, $z = 0.80$ and $z = 1.02$ (Vreeswijk et al., 1999a). The redshift of the OT must then be $z \geq 1.02$

A record of sorts was due to a gamma-ray burst from January 31, 2000, positioned by means of IPN data; this became the OT identified with the longest delay. When VLT observations could begin, on February 4, it was already more than three days since the burst, and hopes for an optical identification were not high, in particular, since the error box was larger than the FORS1 field of view. Taking two pointings, and repeating them two and four days later, the OT was discovered as a red, fading object, $R > 23$ (Fig. 5) (Pedersen et al., 2000; Andersen et al., 2000).

10. GRB 000301c – a Multi-Site Event

The study of gamma-ray bursts has become a field where contributions from many sites are needed, partly for around-the-clock coverage, partly for wavelength coverage. Observations typically start with a space-borne detection, followed by ground-based optical, infrared, and radio studies.

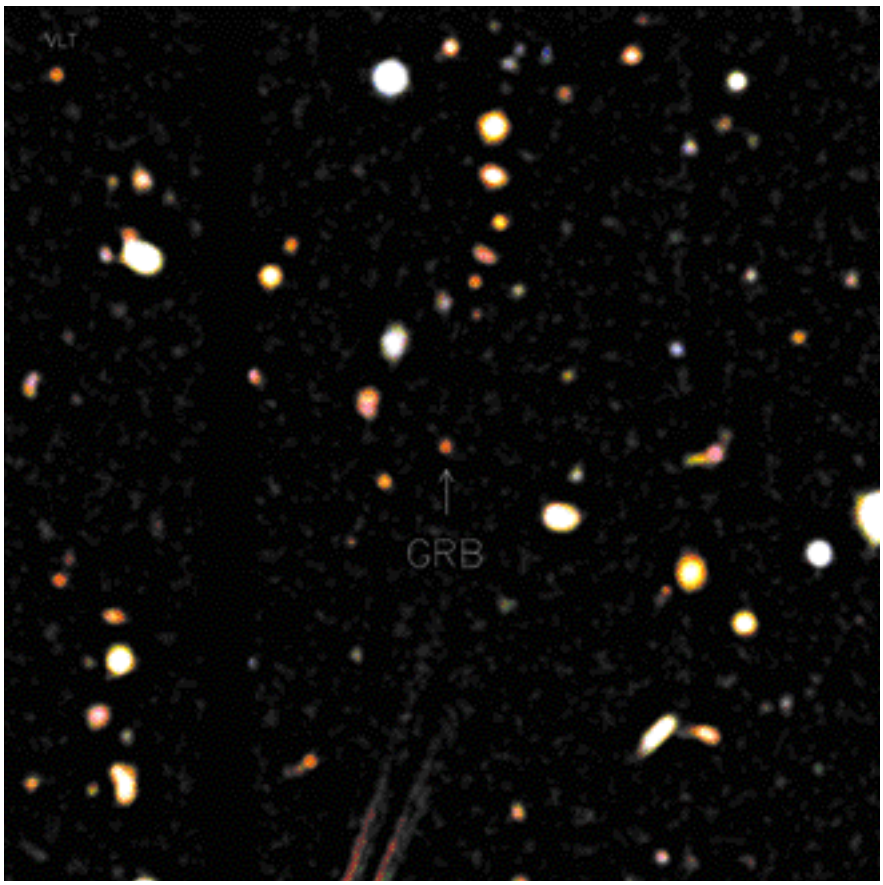

Figure 5: A true colour photograph of GRB 000131, obtained from VLT/FORS1 and 1.54-m Danish observations. From Andersen et al. (2000).

[6] A second, successful polarisation measurement was made on GRB 990712 (Rol et al., *ApJ*, submitted).

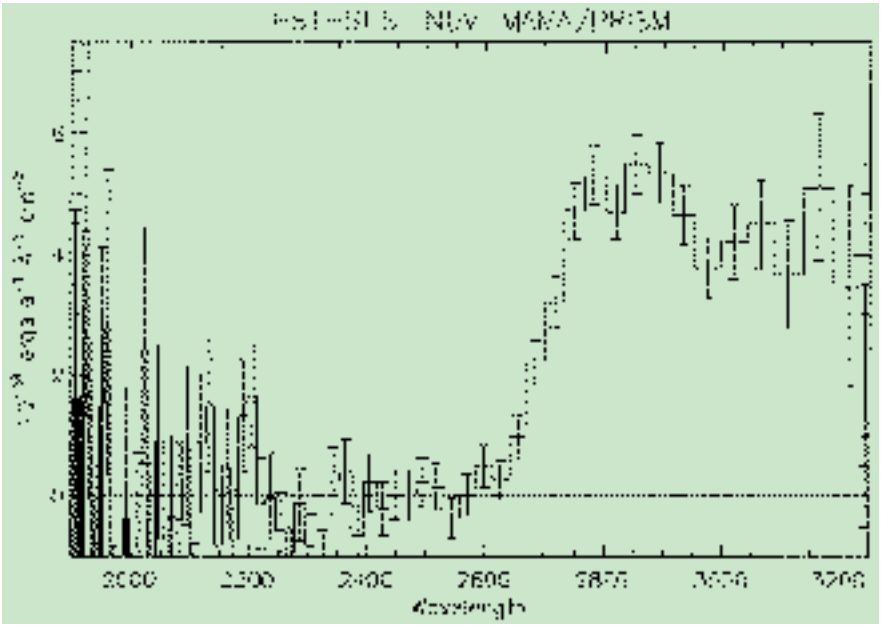

Figure 6: In this spectrum of OT/GRB 000301c, obtained with Hubble Space Telescope 33 days after the outburst, no light is detected below λ = 2600 Å. This has been modelled in terms of redshifted Hydrogen (Lyman edge) absorption, putting the source at z ~ 2 (Fruchter et al., 2000a,b). With kind permission from the STSci GRB team.

GRB 000301c may serve as an illustration. This was a brief (~ 10 s) event, localised by means of data from RXTE, NEAR and Ulysses. The first to react were two Indian observatories, and telescopes at Loiano, Calar Alto and La Palma (NOT). Data from the NOT provided a candidate OT, and confirmation was soon received from elsewhere, including radio-, mm and near-infrared telescopes.

Although the source faded quickly, the VLT could be used to obtain spectra, and other ESO telescopes to acquire multicolour optical photometry (Jensen et al., 2000).

The source has been subject to several runs at the Hubble Space Telescope. This included a remarkable spectroscopic observation with STIS: the Ly-α break was detected at z ~ 2 (Fig. 6) (Fruchter et al., 2000a). This was soon confirmed (and improved upon) with data from Keck-II (Castro et al., 2000) and VLT. Locating the host galaxy, and finding the relative position of the OT within it, turned out to be particularly difficult. Continued imaging by Hubble has failed to show clear evidence for a host, to very deep limits (Fruchter et al., 2000b).

11. Challenging Physics

The pace of discoveries in the field of gamma-ray bursts is truly remarkable. While credit for this goes to many colleagues from the space research community, we wish here to point to the people behind the BeppoSAX satellite, and in particular to Jan van Paradijs. Without his faith in co-ordinated optical observations, we would not have come nearly as far.

Current research falls in two main categories:

• the study of the origin and physical mechanism of gamma-ray bursts and

• the use of gamma-ray bursts as cosmological probes, irrespective of the underlying physical mechanism.

This is indeed what we have in mind for the next two years, during which an approved 'Large Programme' will be conducted. The project includes a study of the preferred locations of the bursts within the host galaxies (central location, in spiral arm, etc.) and also the very nature of the hosts. How do the typical hosts relate to other members of the high-z 'zoo', such as Lyman-break galaxies, Damped Lyman-α Absorbers (DLAs), and the luminous IR galaxies? What is the star-formation rate in these hosts?

The central questions regarding the emission mechanism involves identifying:

• the gamma-ray burst progenitors, the main contenders being merging neutron stars or collapsing massive stars ('collapsars'),

• the emission mechanism, e.g. synchrotron emission,

• the emission geometry, in particular to what extent gamma-ray bursts are collimated and the size of the jet opening angle,

• the density structure and composition of the immediate surroundings of the gamma-ray burst.

There are high hopes that gamma-ray burst afterglows will prove useful in probing hotly debated cosmological questions, such as the large-scale structure of the Universe, the star-formation history of the Universe, the very high-redshift Universe, the effect of extinction at high redshifts, and the nature of DLAs. Gamma-ray bursts could well be among the most distant detectable sources in the Universe; if they come from massive stars they should occur soon after the first stars formed, perhaps at redshifts as high as z ~ 20. With this in mind, future searches at ESO will apply the VLT's ISAAC and NTT's SOFI, in addition to optical instruments.

Our programme also aims to improve on typical response times, so that UVES observations can be conducted in a semi-automated fashion, while the OTs are sufficiently bright, perhaps within 5 minutes from the 'trigger' moment delivered by spacecraft. This may reveal knowledge not only about the OTs and their hosts, but also about the intervening intergalactic medium; in this way, OTs may turn out to be more useful cosmological probes than quasars.

The unpredictable nature of gamma-ray bursts implies that the programme can only be executed under *target-of-opportunity* conditions. We appreciate the kind assistance rendered by ESO staff, and the understanding shown by many regularly scheduled observers, who got bumped.

Within the next few years, several gamma-ray-burst detecting satellites will be launched. First among these are the US/France/Japan mission HETE-2 scheduled for launch later this year; it is expected to provide at least 24 events annually, accurate to 10 arcsec – 10 arcmin. Later come the ESA mission INTEGRAL (launch 2002; ~ 20 events per year), the US/UK/Italy Swift (2003; ~ 100 events per year to arcsecond accuracy), and the Danish Rømer mission, (launch 2003; ~ 70 events per year). All will transmit their data in real-time, over the Internet. The rate of swiftly and precisely located gamma-ray bursts will then increase dramatically. Conducting the necessary ground-based observations in *service mode* will then be the only approach to do basic research in this new and energetic field.

References

Andersen, M.I.A., et al., 2000, in preparation.

Akerlof, C., Balsano, R., Barthelmy, S., et al., 1999, *Nature* **398**, 400.

Beuermann, K., Hessman, F.V., Reinsch, K., et al., 1999, *A&A* **352**, L26.

Bloom, J.S., Kulkarni, S.R., Djorgovski, S.G., et al., 1999, *Nature*, **401**, 453.

Castro, S.M., Diercks, A., Djorgovski S.G. et al., 2000, *GCN* #605 (= http://gcn.gsfc.nasa.gov/gcn/gcn3/605.gcn3).

Covino, S., Davide, L., Ghisellini, S., et al., 1999, *A&A* **348**, 1.

Costa, E., Frontera, F., Heise, J., et al., 1997, *Nature* **378**, 783.

Djorgovski, S.R., Kulkarni, S.R., Bloom, J.S., et al., 1999, GCN #289.

Fruchter, A., Smette, A., Gull, T., et al., 2000a, GCN #627.

Fruchter, A. et al.,2000b, in preparation.

Galama, T.J., Vreeswijk, P., van Paradijs, J., et al., 1998, Nature 395, 670.
Galama, T.J., Vreeswijk, P.M., Rol, E. et al., 1999, GCN #388.
Galama, T.J., Tanvir, N., Vreeswijk, P., et al., 2000, *ApJ.* in press.
Hjorth et al. 2000, in press.
in 't Zand, J., Heise, J., Hoyng, P., et al., 1997, *IAU Circular* #6569.
Jensen, B. L., et al., 2000, in preparation.
Kulkarni, S., Djorgovski, S. G., Ramaprakash, A. N., et al., 1998, *Nature* **393**, 35.
Leibundgut, B., Sollerman, J., Kozma, C., et al., 2000, *The Messenger*, **99**, 36.
Masetti, N., Palazzi, E., Pian, E., et al., 2000, *A&A* **354**, 473.
Mészáros, P., and Rees, M.J., 1997, *ApJ.* **476**, 232.
Palazzi, E., Pian, E., Masetti, N., et al., 1999, *A&A* **336**, L95.
Pedersen, H., Jensen, B.L., Hjorth, J., et al., 2000, *GCN* #534.
van Paradijs, J., Groot, P.J., Galama, T.J., et al., 1997, *Nature* **386**, 686.
Vreeswijk, P.M., Rol, E., Hjorth, J., et al., 1999a, *GCN* #496.
Vreeswijk, P.M., et al., 1999b, *ApJ* submitted.
Wijers, R.A.M.J., Rees, M.J., and Mészáros, P., 1997, *M.N.R.A.S.*, **288**,L51.
Wijers, R.A.M.J., Vreeswijk, P.M., Galama, T.J., et al., 1999, *ApJ.L*. 523, L33.

ISAAC on the VLT Investigates the Nature of the High-Redshift Sources of the Cosmic Infrared Background

Two jewels of European astronomy, ISO and ISAAC, join their capabilities to shed light on one important enigma of present-day cosmology

D. RIGOPOULOU[1], A. FRANCESCHINI[2], H. AUSSEL[3], C.J. CESARSKY[4], D. ELBAZ[5], R. GENZEL[1], P. VAN DER WERF[6], M. DENNEFELD[7]

[1]Max-Planck-Institut für Extraterrestrische Physik, Garching, Germany
[2]Dipartimento di Astronomia, Università di Padova, Vicolo Osservatorio, Padova, Italy
[3]Osservatorio Astronomico di Padova, Vicolo Osservatorio, Padova, Italy
[4]European Southern Observatory, Garching, Germany
[5]CEA Saclay, Gif-sur-Yvette Cédex, France
[6] Leiden Observatory, Leiden, The Netherlands
[7]Institut d'Astrophysique de Paris – CNRS, Paris, France

Abstract

We report on the status of our long-term project aimed at characterising the nature of a new population of galaxies that has emerged from various ISOCAM surveys[1]. In September 1999, we used ISAAC on UT1 and under very good seeing conditions over two nights we obtained the first near-infrared spectra for a sample of ISOCAM galaxies drawn from a deep ISO survey of the Hubble Deep Field South. The Hα emission line was detected in 11 out of the 12 galaxies we looked at, down to a flux limit of 7×10^{-17} erg cm^{-2} s^{-1}, corresponding to a line luminosity of 10^{41} erg s^{-1} at $z = 0.6$ (for an $H_0 = 50$ and $\Omega = 0.3$ cosmology). The rest frame R-band spectra of the ISOCAM galaxies we observed resemble those of powerful dust-enshrouded starbursts. The sample galaxies are part of a new population of optically faint, but infrared luminous starburst galaxies. These galaxies are also characterised by an extremely high rate of evolution with redshift up to $z \sim 1.5$ and significantly contribute to the cosmic far-IR extragalactic background.

[1]ISOCAM was a mid-infrared camera, one of the four instruments on board the Infrared Space Observatory (ISO).

1. New Facts from Deep Sky Explorations at Long Wavelengths

Observations at wavelengths longer than a few μm are essential to study diffuse media in galaxies, including all kinds of atomic, ionic and molecular gases and dust grains. By definition, they are particularly suited to investigate the early phases in galaxy evolution, when a very rich ISM is present in the forming systems.

Unfortunately, the IR and sub-millimetre constitute a very difficult domain to access: astronomical observations are only possible from space, apart from a few noisy atmospheric windows at $\lambda \sim 10$ and 850 μm where they can be done from dry sites on the ground.

1.1 Discovery of the Cosmic Infrared Background

During the last few years, a variety of observational campaigns in the far-IR/sub-mm have started to provide results of strong cosmological impact, by exploiting newly implemented ground-based and space instrumentation.

One important discovery in the field during the last few years concerned an intense diffuse isotropic flux detected at far-IR/sub-mm wavelengths in the all-sky maps imaged by the Cosmic Background Explorer (Puget et al. 1996; Hauser et al. 1998). The isotropy of this background (henceforth the Cosmic IR Background, CIRB) was immediately interpreted as due to an extragalactic source population, but its intensity turned out to be far in excess of the level expected from local galaxies, as observed by IRAS and by millimetre telescopes (e.g. Franceschini et al. 1998). What is remarkable in this context is that the bolometric CIRB flux is at least a factor of two larger than the integrated stellar light from galaxies at any redshifts, as sampled by the HST in ultra-deep imaging surveys.

Then the only viable interpretation for the CIRB was to correspond to an ancient phase in the evolution of galaxies characterised by an excess emission at long wavelengths, naturally interpretable as an effect of a rich and dusty interstellar medium. The large energetic content of the CIRB compared to the optical already sets interesting constraints on galaxy evolution in very general terms, as our team will report in due course.

1.2 Deep SCUBA surveys resolve part of the CIRB at the mm

Particularly relevant have been the deep explorations performed by the

Sub-millimetre Common User Bolometer Array (SCUBA), an imaging camera operating on the JCMT mostly at 850 μm, and by the Infrared Space Observatory (ISO) over a wide wavelength interval from 5 to 200 μm.

Deep surveys by the two observatories have started to provide crucial information on faint distant infrared sources. Because of the different K-corrections, the two source selections probed rather complementary redshift intervals. SCUBA detected at 850 μm redshifted dust-emission from tens of galaxies over a wide redshift interval, mostly between $z \simeq 1$ and $z \simeq 3$, although a completely reliable identification of these faint sub-millimetric sources is still to be definitely established. The most serious limitation of this approach is due to the large error-box for faint SCUBA sources, combined with the extreme optical faintness of their majority, which imply a significant chance of misidentification.

1.3 A population of fast-evolving IR sources discovered by ISO

The IR camera (ISOCAM, P.I. C.J. Cesarsky) on board ISO, with its broad-broad-band filter LW3 sensitive between 12 and 18 μm, provided the most sensitive and spatially accurate way of sampling the far-infrared sky. While designed as an observatory-type mission, the vastly improved sensitivity offered by ISOCAM with respect to the previous IRAS surveys incited us to propose that a significant fraction of the ISO observing time be dedicated to deep surveys (ISOCAM Guaranteed Time Extragalactic Surveys, IGTES, P.I. C.J. Cesarsky). The aim was to parallel optical searches of the deep sky with complementary observations at wavelengths where dust is not only far less effective in extinguishing photons, but is even strongly emissive (in particular through a set of broad emission features peaking at $\lambda \simeq 6$ to 9 μm by as yet unidentified grain species).

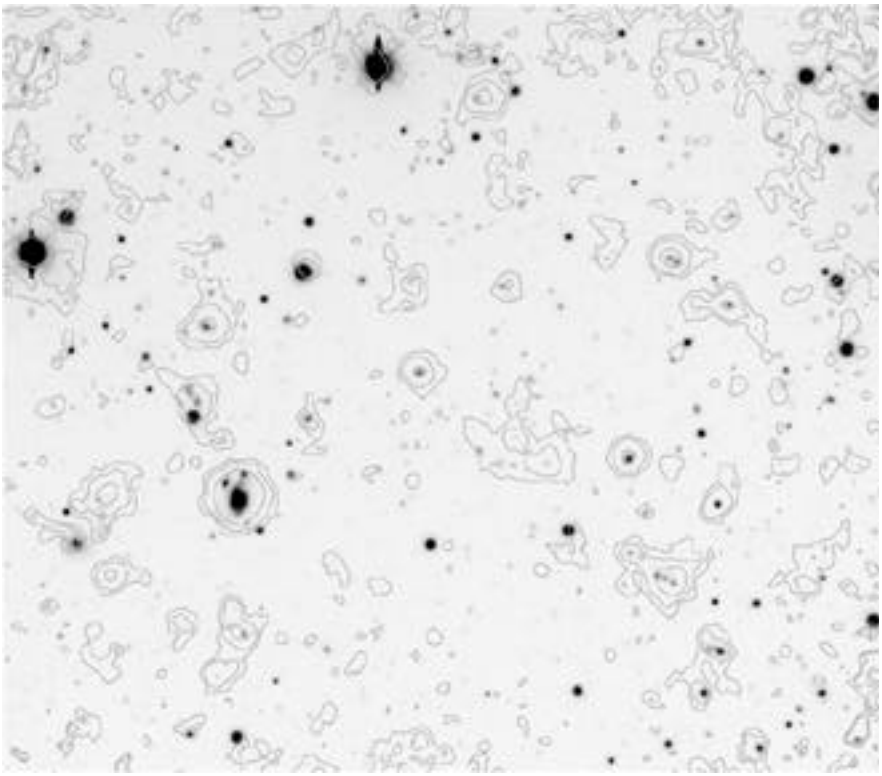

Figure 1: Contours of the ISOCAM LW3 image (15 μm, Aussel et al. 2000) overlaid on the NTT-I band image of Dennefeld et al. (2000).

Table 1. ISOCAM surveys

Name	λ (μm)	Area ($'^2$)	depth (mJy)	# objects [a]	Ref.	coord.(2000)
CAM parallel	7, 15	1.2e5	5	>10000	1	–
ELAIS	7, 15	4e4	1.3	~1000	2	–
Marano2 FIRBACK	15	2700	1.4	29	3	03 13 10 –55 03 49
Lockman Shallow	15	1944	0.72	180	4	10 52 05 +57 21 04
Comet Fields	12	360	0.5	37	5	03 05 30 –09 35 00
Lockman Deep	7, 15	500	0.3	166	6	10 52 05 +57 21 04
CFRS 14+52	7, 15	100	0.3	23, 41	7	14 17 54 +52 30 31
CFRS 03+00	7, 15	100	0.4	8		03 02 40 +00 10 21
Marano2 Deep	7, 15	900	0.19, 0.32	180	9	03 13 10 –55 03 49
A370	7, 15	31.3	0.26	18	10	02 39 50 –01 36 45
Marano Ultra-deep	7, 15	90	0.14	142	11	03 14 44 –55 19 35
Marano2 Ultra-deep	7, 15	90	0.1	115, 137	12	03 13 10 –55 03 49
A2218	7, 15	16	0.12	23	10	16 35 54 +66 13 00
ISOHDF South	7, 15	25	0.1	63	13	22 32 55 –60 33 18
ISOHDF North	7, 15	24	0.05, 0.1	7, 44	14	12 36 49 +62 12 58
Deep SSA13	7	9			15	13 12 26 +42 44 24
Lockman PG	7	9	0.034	15	16	10 33 55 +57 46 18
A2390	7, 15	5.3	0.030	32, 31	17	21 53 34 +17 40 11

[a] If only one number appears, it refers to the longer-λ survey.

References: (1) Siebenmorgen et al. (1996); (2) Oliver et al. (1999); (3), (4), (6), (9), (11), (12): IGTES, see Elbaz et al. (1999); (5) Clements et al. (1999); (7), (8): Flores et al. (1999); (10): Altieri et al. (1999); (13) Elbaz, D., et al, (1999); Oliver et al. submitted (14) Aussel, H., et al. (1999); (16) Taniguchi et al. (1997).

Careful corrections of some transient effects in the detector responsivity (due to the very low temperature and slow electron mobility) and of the non-gaussian noise induced by cosmic-ray impacts are now possible using various independent methods (PRETI developed at the Service d'Astrophysique de Saclay, Stark et al. 1998; a method developed in Bologna by Lari et al. 2000; and one by Desert et al. 1998), all providing consistent results. All this required quite an extensive amount of work (including Monte Carlo simulations of the complex behaviour of the detectors) and fairly long time, but eventually we are in a position to claim that we have now an accurate sampling in the LW3 filter of several independent sky areas down to very faint flux densities and producing highly reliable and complete source catalogues including more than one thousand sources (Elbaz et al. 1999). We report in Table 1 a summary of the surveys performed with ISOCAM during the 2.5 years of the mission lifetime.

An example of the imaging quality achieved is reported in Figure 1, which is the LW3 map of an area centred on the Hubble Deep Field South (Aussel et al. 2000a).

The Euclidean-normalised differential counts provide simple but powerful and robust statistics, useful to evidenciate evolutionary properties in the selected sources. A collection of the LW3 differential counts is reported in Figure 2 based on eight samples of independent sky areas. The first remark is that the counts from all of them are

nicely consistent and support within the statistical uncertainties the accuracy of the adopted methods for source selection. The fact that the observed counts are a factor ten higher around a flux density of 0.3–0.4 mJy provides the first uncontroversial evidence for a drastic increase of the far-infrared emissivity of galaxies going back in cosmic time.

This result is quite consistent with the independent evidence, provided by the CIRB intensity, in favour of very rapid evolution of IR flux from cosmic sources. Indeed, by assuming for the faint ISOCAM sources in Figure 2 the far-IR spectrum of a typical starburst, then these sources would be expected to contribute a substantial part of the CIRB at 140 microns.

Aussel et al. (1998) and Flores et al. (1998) have produced early attempts to identify the ISOCAM sources and to derive their redshifts at the fluxes where the peak excess in the LW3 counts of Figure 2 is observed. Mostly due to the combined effect of K-correction and evolution, these sources are found to range from $z \sim 0.4$ to $z \sim 1.2$, with a median around $z = 0.7$–0.8 (see below).

However, the origin of this energy, either due to stellar nucleosynthesis in star-forming galaxies or to gravitational accretion onto giant black holes as in quasars, is largely unknown. We clearly need a deep spectroscopic survey of these sources to progress in their understanding.

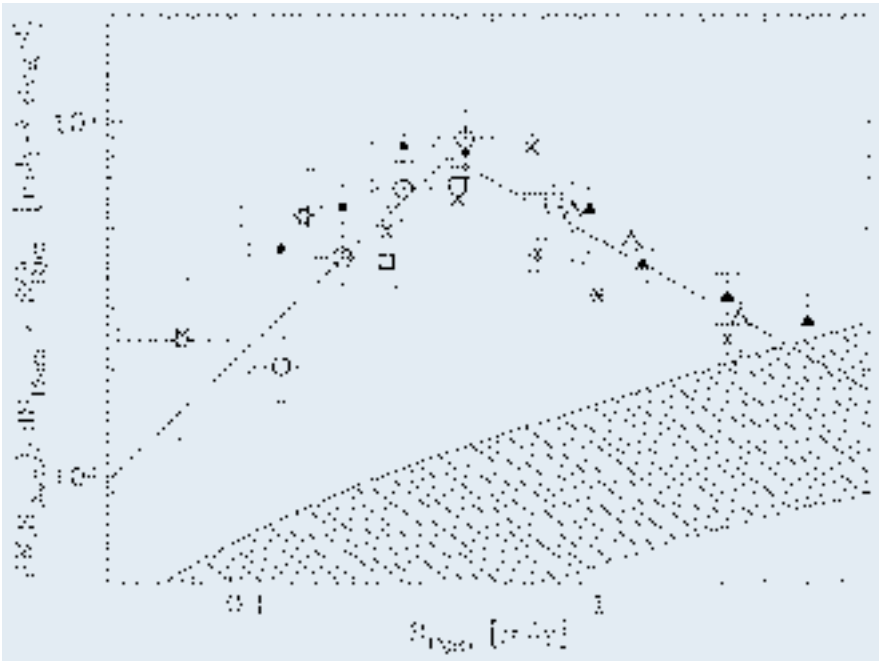

Figure 2: Differential number counts from eight different ISOCAM surveys (from Elbaz et al. 1999).

2. The ISOCAM Survey in the HDFS

The Hubble Deep Field South was observed by ISOCAM at two wavelengths, LW2 (6.75 μm) and LW3 (15 μm), as part of the European Large Area ISO Survey (P.I. M. Rowan-Robinson; see Oliver et al. 2000). ISOCAM detected 63 sources (from the data reduction of Aussel et al. 2000), all brighter than $S_{15\mu m} = 100$ μJy in the LW3 band. Out of this source list we selected the sample for ISAAC follow-up. The selected sources satisfied the following criteria:
(a) they had a reliable LW3 detection, (b) Hα in the wavelength range of ISAAC and, (c) a secure counterpart in the I-band image (Dennefeld et al. 2000) and/or in the K-band image (ESO-EIS Deep, DaCosta et al. 1998). The reference sample contains about 25 galaxies with 15 μm flux densities in the range 100–800 μJy and is therefore a fair representation of the strongly evolving ISOCAM population near the peak of the differential source counts (Elbaz et al. 1999). From these 25 sources we selected randomly 12 sources for our first ISAAC follow-up spectroscopy (hereafter ISOHDFS galaxies).

For the observations and the selection of the exact near-infrared band (Z, SZ, J or H) we used spectroscopic redshifts from optical spectra, where available for $z < 0.7$ (Dennefeld et al. 2000)

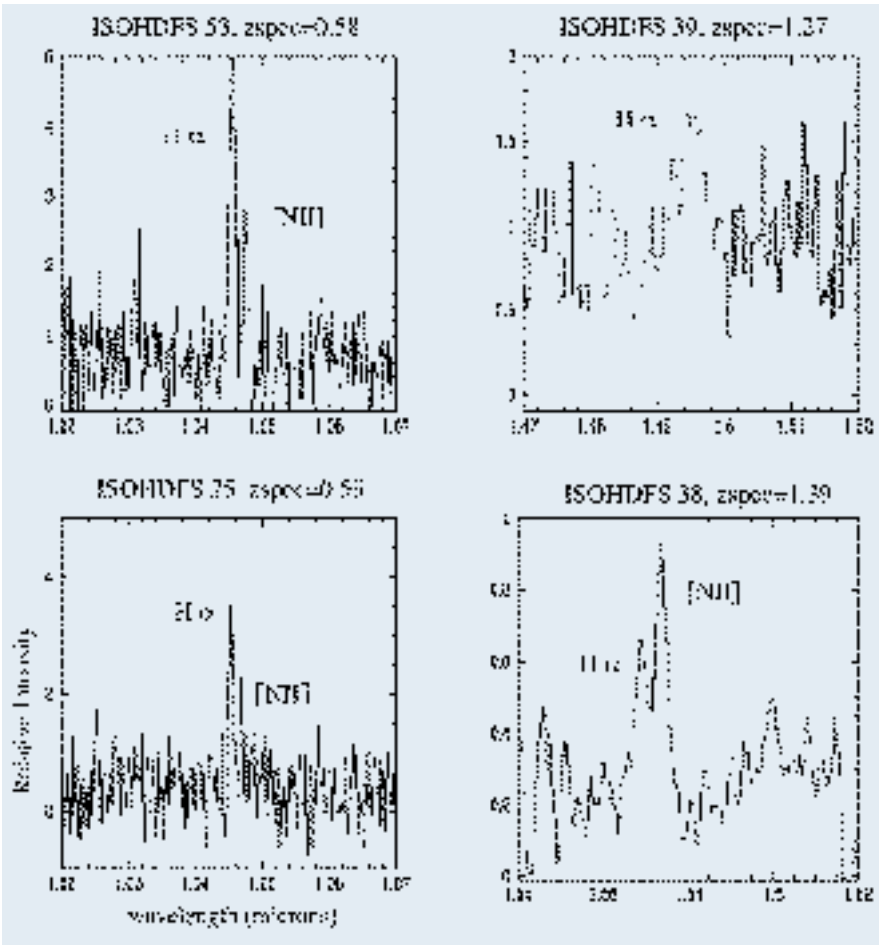

Figure 3: ISAAC-VLT spectra of ISOCAM galaxies, showing two low-z and two high-z sources. The resolution of 600 corresponds to a resolution of about 12Å at the source distance. The H_α and [NII] lines are resolved in three of the spectra. Clockwise from top left: source ISOHDFS 53, at $z_{spec} = 0.58$, source ISOHDFS 39 at $z_{spec} = 1.27$, source ISOHDFS 25 at $z_{spec} = 0.59$, and source ISOHDFS 38 at $z_{spec} = 1.39$ (the H_α/[NII] < 1 implies that this source is an AGN) (spectra from Rigopoulou et al., 2000). ▶

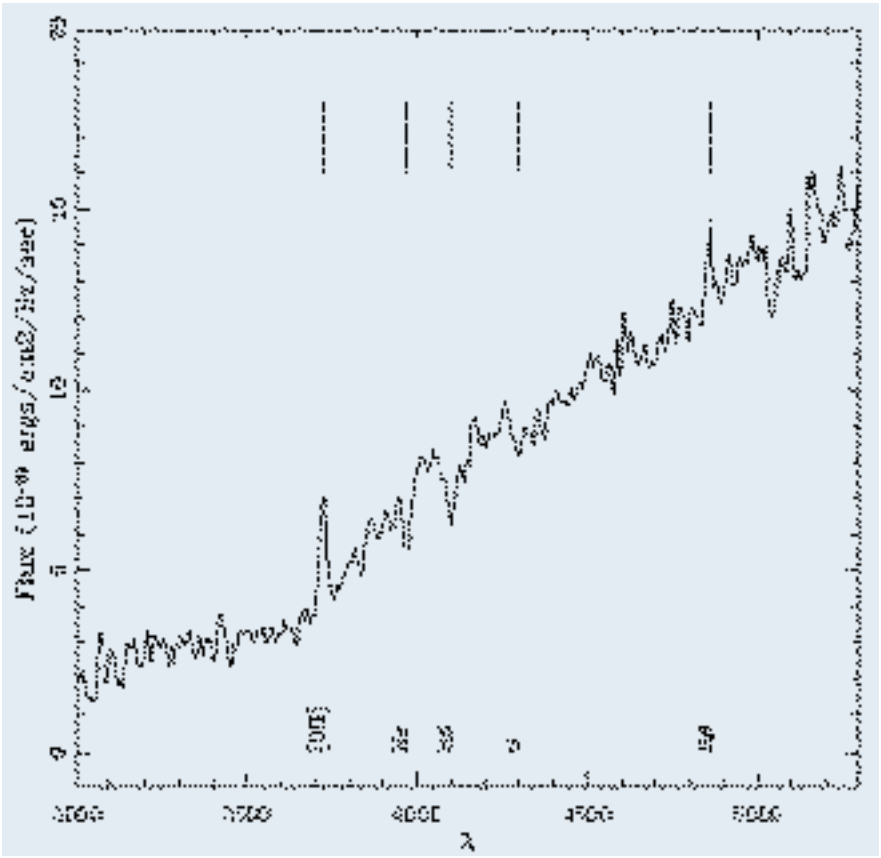

Figure 4: Restframe B-band "averaged" spectrum of ISOCAM galaxies from the CFRS field (from Flores et al. 1999). H_δ and H_ε Balmer absorption features are prominent, alongside a moderately strong [OII] emission.

or photometric redshift estimates. Photometric redshifts have been estimated by using the model PEGASE (Fioc and Rocca-Volmerange 1997). Our photometric redshift determination turned out to be accurate to $\Delta z = \pm 0.1$ and provided a very useful tool for the ISAAC follow-up spectroscopy.

3. The ISAAC Observations

We carried out observations (P.I. A. Franceschini) during 20–24 September 1999 (we observed during the first half of the night). The seeing varied between 0.4–1.00 arcsec and the conditions were generally very good. The good seeing helped us to acquire the very faint objects relatively quickly, our elementary integrations consisted of 1–2 minutes exposure in the H-band. For the observations we used the low-resolution grating $R_s \sim 600$ and a 1-arcsec × 2-arc min long slit. We positioned the slit in such a way as to include on average two galaxies at any given orientation. The choice of filter was dictated by our aim to detect the Hα emission line. Based on the redshift information we had at hand (photometric or spectroscopic) we used the Z (0.83–0.97 μm), SZ (0.98–1.14 μm), J (1.1–1.39 μm) or H (1.42–1.83 μm) filters accordingly.

The H magnitude of our targets (taken from the ESO-EIS Deep) reached down to 22 mag. The very faint objects were acquired by offsetting from a bright star in the field. The individual exposures ranged from 2 to 4 minutes. Most of the spectra were acquired within 1 hour, except for the very faint ones ($H \geq 20.5$ mag) for which we integrated for nearly 2 hours. For each filter, observations of spectroscopic standard stars were made in order to flux calibrate the spectra. The data were reduced using several ECLIPSE applications (Devillard 1998) and standard routines from the IRAF package. We extracted spectra using IRAF-APEXTRACT.

In total we observed 12 galaxies and H_α was successfully detected in all but one of them. [NII] emission is also seen in some spectra. Figure 3 shows some representative spectra.

4. Nature of the Faint ISOCAM Galaxies

Prior to our VLT-ISAAC observations no near-infrared (rest-frame R-band) spectroscopy had been carried out for the ISOCAM population, mostly due to the faintness of the galaxies. Optical spectroscopy (rest-frame B-band) has been done for Hubble Deep Field North (Barger et al. 1999) and the Canada France Redshift Survey (CFRS) field (Flores et al. 1999). The ISOCAM HDF-N galaxies have been cross-correlated with the optical catalog of Barger et al. (1999) resulting in 38 galaxies with confirmed spectroscopic redshifts (Aussel et al. 1999). Flores et al. have identified 22 galaxies with confirmed spectroscopic information. In both of these samples the median redshift is about 0.7–0.8. Our VLT ISOHDFS sample contains 7 galaxies $0.4 < z < 0.7$ and 5 galaxies with $0.7 < z < 1.4$. Thus our sample has a z-distribution very similar to the HDF-N (Aussel et al.) and CFRS (Flores et al.) samples.

Rest-frame B-band spectra host a number of emission and absorption lines related to the properties of the starburst in a galaxy. Based on these features, galaxies can be classified according to their starburst history. Strong H_δ, H_ε Balmer absorption and no emission lines are characteristic of passively evolving k+A galaxies. The presence of significant higher level Balmer absorption lines implies the presence of a dominating A-star population. Such an A-star population may have been created in a burst 0.1–1 Gyr ago (post-starbursts). The simultaneous presence of Balmer absorption and moderate [OII] emission, known as e(a) galaxies, may be characteristic of somewhat younger, but still post-starburst systems or, alternatively, an active but highly dust absorbed tar-bursts. As we will show, the ISOCAM galaxies are in fact powerful starbursts hidden by large amounts of extinction.

Figure 4 shows the average B-band spectrum of the CFRS galaxies (from Flores et al. 1999). The spectrum shows moderate [OII] emission and quite prominent deep Balmer absorption features H_δ, H_ε reminiscent of A stars. Based on this spectrum, Flores et al. suggested that these galaxies look like post-starburst systems. In Figure 5 we plot the B-band and R-band spectrum of the well-known starburst galaxy M82 (spectra from Kennicutt 1992). We note a very similar behaviour: the B-band spectrum of M82 displays characteristics of an e(a) system. At the same time the R-band spectrum displays strong H_α emission with large equivalent widths implying an active on-going star formation. Differential extinction lies at the heart of this apparent disagreement (Poggianti et al 2000): large amounts of dust exist within the HII regions where the H_α and [OII] line emission originates. [OII] emission is affected more than H_α simply because of its shorter wavelength. The continuum is due to A-stars. This A-star signature comes from earlier (0.1–1.0 Gyr) star-formation activity that is not energetically dominant; in fact, it plays a small role once the dusty starburst is dereddened. Such a scenario implies that these galaxies undergo multiple burst events: the less extincted population is due to an older burst while in the heavily dust enshrouded HII regions there is ongoing star formation. Therefore, ISOCAM galaxies are actively star-forming,

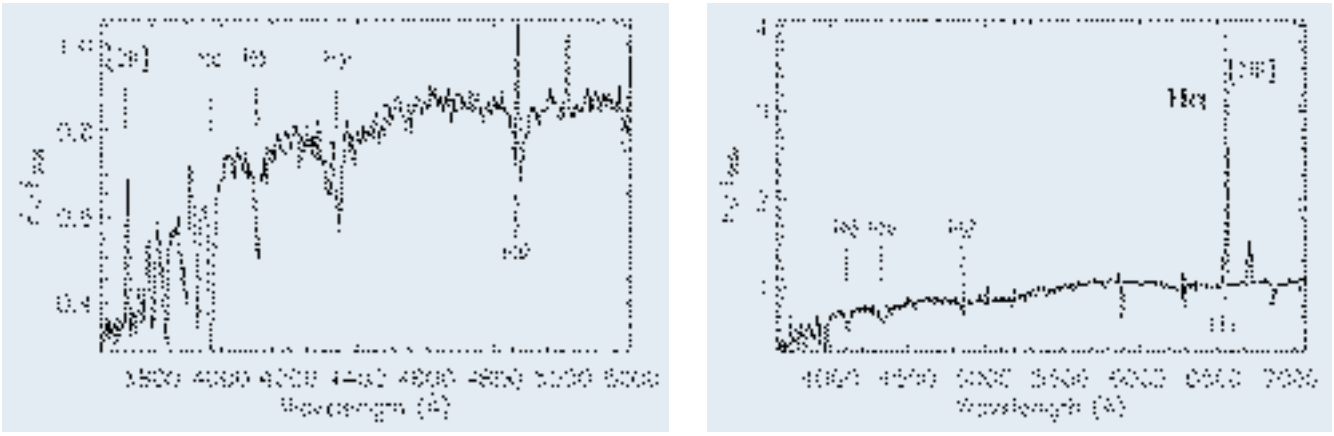

Figure 5: Left panel: B-band spectrum of the well-known starburst galaxy M82. Note the prominent Balmer H_δ and H_ε absorption lines as well as the moderate [OII] emission. Right panel: R-band spectrum of M82. The spectrum is dominated by the very strong H_α emission (spectra from Kennicutt 1992).

dust-enshrouded galaxies, akin to local LIRGs (e.g. NGC 3256, Rigopoulou et al. 1996).

5. Evaluating the Star Formation Activity

Being the strongest of all Balmer lines, the H_α emission line has been traditionally used to derive quantitative star-formation rates in galaxies. However, for $z \geq 0.2$–0.3, H_α redshifts into the near-infrared where spectroscopy with 4-m-class telescopes is inherently much harder and thus less sensitive than in the optical. This is why measurements of the star-formation rates in high redshift galaxies have relied on measurements of the [OII] λ3727 doublet. The advent of 8-m-class telescopes such as the VLT allows us for the first time to use H_α as a measure of the star-formation activity in distant galaxies.

In ionisation bounded HII regions, the H_α luminosity scales directly with the ionising luminosity of the embedded stars and is thus proportional to the star-formation rate (SFR). The conversion factor between ionising luminosity and SFR is computed with the aid of an evolutionary synthesis model. The prime contributors to the integrated ionising flux are massive stars ($M > 20\ M_\odot$) with relatively short lifetimes (≤ 10 million years). Using any stellar synthesis model (we have used the code of Sternberg 1998) for solar abundances, a Salpeter IMF (1–100 $M_\odot$) and for a short-duration burst (a few 10^7 yrs) we obtain:

$$SFR(M_\odot/yr) = 5 \times 10^{-42} L(H_\alpha)(ergs^{-1}). \quad (1)$$

Using this formula we estimate that the SFR rates in our ISOHDFS galaxies range between 2–50 $M_\odot$/yr, corresponding to total luminosities of ~ 1–10 × 10^{42} erg s^{-1} (assuming $H_0 = 50$ km/s/Mpc, $\Omega = 0.3$).

The SFR estimates based on eq. (1) represent only a *lower limit* of the real SFR in these galaxies. To get an estimate of the extinction, we use V–K colour indices (magnitudes taken from the ESO-EIS survey) and using STARBURST99, the evolutionary synthesis code of Leitherer et al. (1999), for various star-formation histories we calculated the range of intrinsic (extinction-free) colours. By comparing the observed V–K colours to the model-predicted ones we derive a median extinction A_V of 1.8 assuming a screen model for the extinction. This A_V value corresponds to a median correction factor for the SFR(H_α) of ~ 4.

But the far-infrared luminosities can also be used to infer SFR, especially since the ISO-HDFS galaxies are dust enshrouded. For the same IMF as above, the SFR scales with the FIR luminosity as:

$$SFR(M_\odot/yr) = 2.6 \times 10^{-44} L_{FIR}(ergs^{-1}) \quad (2)$$

The L(FIR) in equation (2) is calculated based on the method of Franceschini et al. (2000) which uses the 15 μm flux and assumes an L_{FIR}/L_{MIR} ratio of ~ 10. We find that the SFR(FIR) estimates are on average a factor of 5 to 50 higher than the SFR estimates inferred from H_α uncorrected for extinction. The ratio SFR(FIR)/SFR(H_α) drops to 3 if we use extinction-corrected H_α values, confirming that the extinction in these galaxies is much higher than inferred from UV or optical observations alone. Thus, ISOCAM galaxies are in fact actively star-forming dust-enshrouded galaxies. We finally note that the factor 3 inconsistency noted above for the FIR-based SFR is consistent with the value obtained by Poggianti et al. (2000) for a sample of luminous IRAS starbursts.

6. Conclusions and Future Plans

We have obtained the first near-infrared spectra (rest-frame R-band) of a sample of 12 ISO selected far-IR galaxies from the Hubble Deep Field South. The detection of strong H_α emission lines with large EW in all but one is consistent with these ISOCAM sources being powerful dust enshrouded starburst galaxies.

In only one object (see Fig. 3) we find evidence for the presence of an AGN, as inferred from the inverted NII/H_α line ratio and the peculiar and high 6.7 μm to 15 μm flux ratio, indicative of very hot AGN-like dust. In general, we do not find evidence for broad H_α components as would be expected from classical AGNs, but this will require further NIR spectra at high resolution for confirmation. Our result echoes recent reports about ultra-deep CHANDRA hard X-ray surveys of high-*z* SCUBA sources, in which no high-X-ray-energy emission was detected as would be expected if even a fraction of the FIR flux would be due to an AGN (Hornschemeier et al. 2000). Generalising these results, we may tentatively conclude that the large energy content of the CIRB originates from stellar activity.

Based on the H_α emission line intensity we estimate star-formation rates in the range 2–50 $M_\odot$/yr, which are a factor of 5–50 times lower than the SFR we derive based on FIR luminosities. If we correct the H_α for extinction, we deduce SFR(FIR)/SFR(H_α) ~ 3, confirming that the extinction in the ISOCAM galaxies is much higher than can be predicted using UV or optical data alone. This result demonstrates that deriving star-formation rates from UV/optical data alone is incorrect for this class of sources. A fraction of star formation, hard to quantify at the moment but probably quite significant, is entirely missed by optical surveys.

We plan to continue our project by increasing our statistics on ISOCAM galaxies. In our upcoming August 2000 run we will supplement our sample with low-resolution spectroscopy of new ISOCAM targets. Meanwhile, we will also attempt to obtain higher-resolution spectra to probe the gas kinematics and ionisation stage in these galaxies.

The unique combination offered by ISO and ISAAC instruments promises a decisive progress in our understanding of the origin of the vast amount of energy released by starburst galaxies during their main activity phases.

References

Altieri, B., et al., 1999, *A&A* **343**, L65.
Aussel, H., Elbaz, D., Cesarsky, C.J., Starck, J.L., 1999, In The Universe as seen by ISO, eds. P. Cox, M.F. Kessler, ESA SP **47**, 1023.
Aussel, H., Cesarsky, C.J., Elbaz, D. and Starck, J.L.,1999, *A&A* **342**, 313.
Aussel, H. et al., in preparation.
Da Costa et al., 1998, *http://www.eso.org/science/eis/eis-rel/deep/HDF-Srel.html*
Clements, D., et al., 1999, *A&A* **346**, 383.
Dennefeld et al. 2000, in prep.
Devillard N., 1998, *The Messenger* No. **87**, March 1997.
Desert, F.X., et al., 1999, *A&A* **342**, 363.
Elbaz, D., Cesarsky, C.J., Fadda, D., Aussel, H., et al. 1999 *A&A* **351**, L37.
Fioc, M., Rocca-Volmerange, B., 1997, *A&A* **326**, 950.
Flores, H., Hammer, F., Thuan, T.X., Cesarsky, C., 1999 *Ap.J.*, **517**, 148.
Franceschini et al. (2000) in prep.
Kennicutt, R.C., (1992) *Ap.J.*, **388**, 310.
Hornschemeier, A.E., et al., 2000, astroph/0004260.
Lari, C., et al., 2000, in prep.
Leitherer, C., et al., 1999 *ApJS* **123**, 3.
Oliver, S., et al., 2000., in prep.
Oliver, S., et al., 2000, MNRAS, in press, astroph.
Poggianti B., Bressan A., Franceschini A., 2000, *ApJL* submitted.
Rigopoulou, D., et al, 1996, *A&A*, **305**, 747.
Rigopoulou, D., Franceschini, A., Aussel, H., et al. 2000, *ApJL,* in press.
Siebenmorgen, R., et al., 1996, *A&A* **315**, L169.
Starck, J.L., et al., *A&A* **134**, 135.
Sternberg, A., 1998, *ApJ* **506**, 721.
Taniguchi,Y., Cowie, L.L., Sato, Y., Sanders, D.B., et al., 1997, *A&A* **318**, 1.

The Deep Eclipse of NN Ser

R. HÄFNER, Universitäts-Sternwarte München

The elusive nature of NN Ser was discovered in July 1988 (Häfner, 1989a, 1989b) in the course of a search for eclipses in faint cataclysmic variables using the CCD camera on the Danish 1.5-m telescope at La Silla. This target (V ~ 17), then named PG 1550+131 and thought to be such a variable, turned out to exhibit a sine-shaped light curve and a very deep eclipse of short duration repeating once every 3 hours and 7 minutes. Due to the low time resolution of the photometry (3.5 min), the duration of the eclipse (separated by half a period from maximum light) as well as its depth could only be roughly estimated to be about 12 min and at least 4.8 mag respectively. During mid-eclipse no signal from the object was recordable. Two spectra (resolution about 12 Å) obtained near maximum light (A) and near the onset of the eclipse (B) using EFOSC at the 3.6-m telescope revealed mainly narrow emission lines of the Balmer series superimposed on broad absorptions (A) and shallow Balmer absorptions without emission (B). It was immediately clear that such an object could not be a cataclysmic system. The data were rather interpreted in terms of a pre-cataclysmic binary, an evolutionary precursor of a cataclysmic system, consisting of a white dwarf/late main-sequence detached pair. Thus all observed properties of the system find a consistent explanation: the sine-shaped light curve (full amplitude ~ 0.6 mag) is caused by a strong heating effect, the emission lines originate in the heated hemisphere of the cool star and cannot be seen near primary eclipse, the absorption lines originate in the hot star, the steep (ingress/egress ~ 2 min) and deep eclipse of short duration are due to the obscuration of a very hot small object by a much cooler and larger star, a secondary eclipse is not detectable since the cool star does not contribute much to the flux. Based on these observations and assuming M_{hot} = 0.58 $M_\odot$ (mean value for DAwhite dwarfs), T_{hot} = 18,000 K, inclination close to 90º and a circular orbit, a first crude estimate of the system parameters yielded the following results: separation ~ 0.92–1.03 $R_\odot$, R_{hot} ~ 0.01–0.14 $R_\odot$, R_{cool} ~ 0.06–0.33 $R_\odot$, M_{cool} ~ 0.03–0.28 $M_\odot$, T_{cool} (unheated hemisphere) ~ 2600–3300 K, T_{cool} (heated hemisphere) ~ 4300–6600 K, spectral type of cool star ~ M3–M6. The evolution of the system into the semi-detached (cataclysmic) state is only possible via radiation of gravitational waves and was estimated to take some 10^9 years.

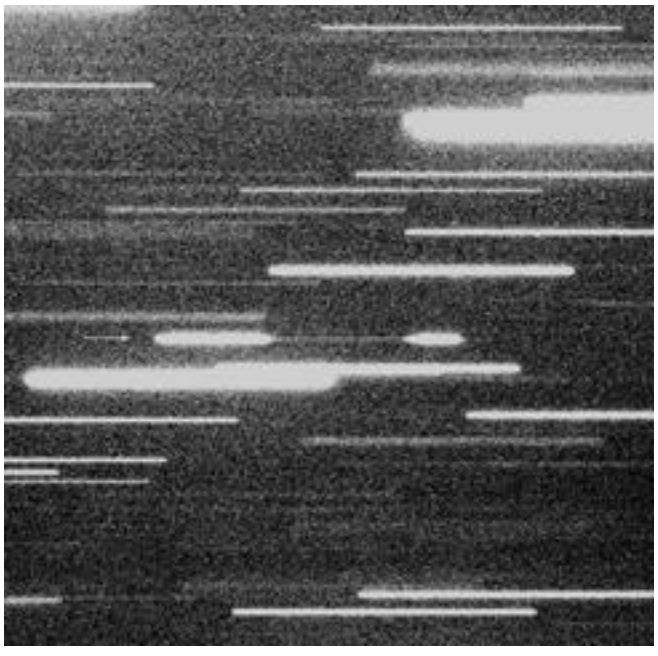

Figure 1: The drift exposure of the sky field around NN Ser (arrow).

Based on optical and IUE spectroscopy as well as further photometry (Wood and Marsh, 1991; Catalan et al., 1994), the pre-cataclysmic nature of NN Ser was confirmed and the range of system parameters could be narrowed down. The IUE data as well as fits of some Balmer absorptions via model atmospheres hint at a white dwarf temperature in the range 47,000–63,000 K, much more than previously assumed. But all studies so far performed were hampered by the fact that the true depth of the eclipse and the duration of the totality (if any), i.e. the inner contact phases of the white dwarf, were not known. This crucial information, important for the determination of the radii of the components, could not be obtained using telescopes of the 4-m class, as several attempts by the author revealed. Even applying sophisticated observing methods and/or using a special photometer, several observing runs (ESO 3.6-m telescope, NTT and Calar Alto 3.5-m telescope) were not successful in this respect.

The powerful combination of the first VLT 8.2-m Unit Telescope (ANTU) and the multi-mode FORS1 instrument (Appenzeller et al., 1998) offered now the opportunity for a new experiment. Since the HIT mode, allowing photometry and spectroscopy with high time resolution, was not yet available at the scheduled time of observation (June 1999) another technique had to be applied: the trailing method, where the tel-

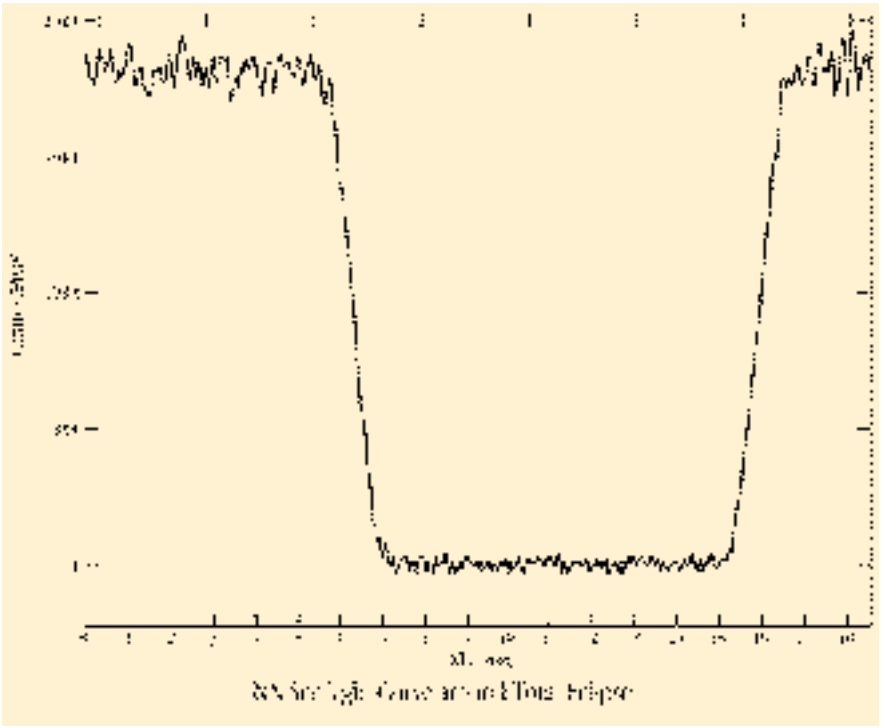

Figure 2: The eclipse light curve of NN Ser as extracted from the drift exposure.

escope performs a controlled continuous motion in RA and DEC, thus registering the light of the targets in the field of view along lines on the same frame. Direction and drift rate had to be chosen very carefully to avoid interference with stars in the neighbourhood of NN Ser and to ensure a reasonable recording of the inner contact phases. Since the brightness of the cool star was unknown, the latter was a tricky task. Using the ETC, the drift rate was eventually fixed at 1 pixel (25 µm) per 3 seconds, a compromise between the presumed integration time and the desired time resolution. Another point of uncertainty was the autoguiding system which was not known to work properly for the drift rate chosen beforehand. It had to be much faster than that needed to follow solar system objects.

However, with no technical problems and aided by excellent seeing of 0.5 arcsec, a 18.5-min drift exposure (SR collimator, V filter) could be obtained in the night 10/11 June 1999. Figure 1 shows the resulting star trails of the field around NN Ser. The trail of the eclipsing system is indicated with an arrow. Figure 2 gives the eclipse light curve of NN Ser as extracted from that trail. The recorded signal during eclipse is well measurable and amounts to about 70 counts/pixel (barely visible in Figure 2, since the full range of the eclipse is shown) down from about 18,300 counts/pixel outside eclipse. This corresponds to an eclipse depth of $\Delta V = 6.04$ and constitutes one of the deepest eclipses if not actually the deepest eclipse ever measured for a binary. Trails of comparison stars on the same frame allow the brightness shortly before/after and during eclipse to be fixed at V = 16.98 and 23.02 respectively. Since the light curve is perfectly flat at the bottom, the eclipse is total, i.e. the white dwarf disappears completely behind the red star. The contact phases are now easily measurable: Totality lasts 7^m37^s, ingress/egress take 1^m26^s each, and the whole eclipse duration amounts to 10^m28^s. These numbers now allow the radii of the involved stars to be derived: R_{hot} = 0.0204 ± 0.0021 $R_\odot$ and R_{cool} = 0.1595 ± 0.0155 $R_\odot$ (about 1.5 times the radius of Jupiter).

Furthermore, it seemed extremely interesting to obtain spectral information on the cool component: With M_{cool} ~ 0.09–0.14 $M_\odot$ (Wood and March, 1991), its mass is very near the upper limit (~ 0.08 $M_\odot$) for brown dwarfs. Even if the object turned out to be 'only' a normal late main-sequence star, with known mass and radius at hand, a spectrum could allow a critical check of current theories of atmospheres and evolutionary computations for late M stars. Since the spectrum had to be taken during the phase of totality, the exposure time had consequently to be limited to about 5 min to avoid any contamination by the white dwarf. Although this seemed to be quite short for a 23-mag object, a faint noisy spectrum could be recorded in the 600–900 nm wavelength region even under mediocre seeing conditions (0.95 arcsec) using the FORS1 longslit option combined with grism 150I+OG590 (0.55 nm/pixel, SR collimator). Figure 3 shows the resulting slightly smoothed tracing together with a spectrum of a M6.5 dwarf star. Several molecular bands of TiO are well visible, additionally some VO bands may also be present. The spectrum does not resemble that of a brown dwarf, it rather hints at a very late dwarf star of spectral type M6 or later. Of course, many such spectra have to be superimposed to allow a definite spectral classification of the cool component in NN Ser which, despite a strong irradiation on one hemisphere, constitutes a 'normal' main-sequence star on the un-heated side.

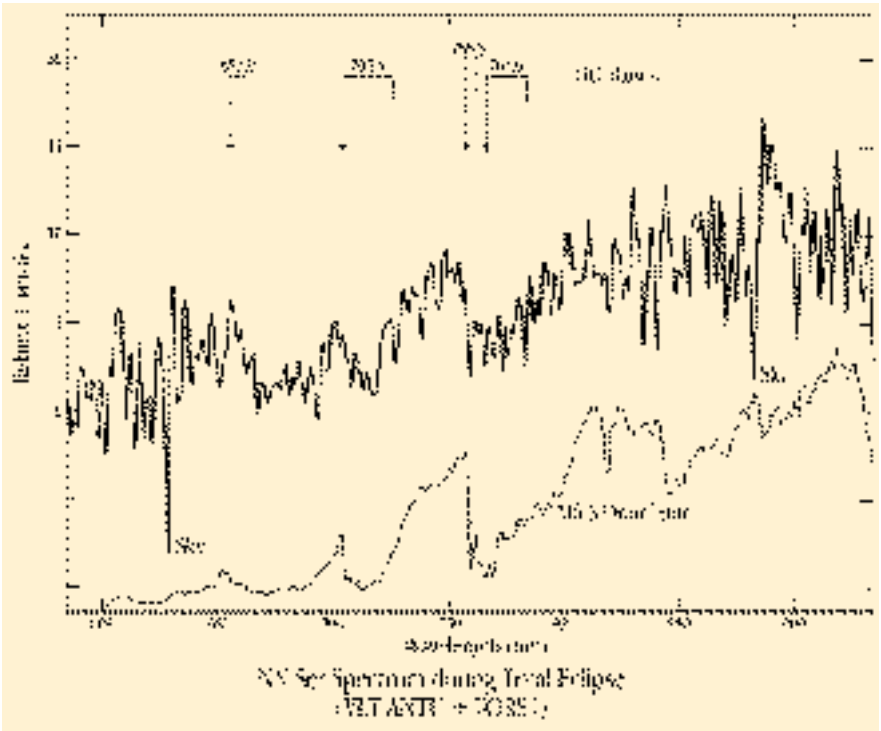

Figure 3: The spectrum of the cool component of NN Ser compared with a spectrum of a M6.5 dwarf star. Residuals from sky subtraction are indicated.

As previously stated, NN Ser belongs to the class of pre-cataclysmic binaries. These systems are thought to be born after the common-envelope evolution of originally wide pairs of unequal mass with orbital periods in the order of a few days. In the pre-cataclysmic state, the binaries exhibit shorter periods, consist then of a hot subdwarf or white dwarf primary and a main-sequence secondary and are surrounded by a planetary nebula which may later disperse. The secondary is believed to remain basically unaffected by this binary evolution process. Presently, we have at least some information on about 50 candidates, about one dozen being still associated with planetary nebulae. Only nine of these 50 systems show eclipses and provide sufficient spectral information to allow the determination of fairly reliable values of masses and radii of the components. Five systems are hot subdwarf/main-sequence binaries, the remaining four (including NN Ser) harbour white dwarf/K-M components. A thorough study of NN Ser will, therefore, also contribute to our knowledge of this interesting evolutionary state of binaries.

References

Appenzeller, I. et al.: 1998, *The Messenger* No. **94**, 1.

Catalán, M.S., Davey, S.C., Sarna, M.J., Smith, R.C., Wood, J.H.: 1994, *Mon.Not. R.Astron.Soc.* **269**, 879.

Häfner, R.: 1989a, *Astron.Astrophys*. **213**, L15.

Häfner, R.: 1989b, *The Messenger* No. **55**, 61.

Wood, J.H., Marsh, T.R.: 1991, *Astrophys. J.* **381**, 551.

E-mail: haefner@usm.uni-muenchen.de

The FORS Deep Field

I. APPENZELLER[1, 5], R. BENDER[3], A. BÖHM[2], N. DRORY[3], K. FRICKE[2], R. HÄFNER[3], J. HEIDT[1], U. HOPP[3], K. JÄGER[2], M. KÜMMEL[5], D. MEHLERT[1], C. MÖLLENHOFF[1], A. MOORWOOD[4], H. NICKLAS[2], S. NOLL[1], R. SAGLIA[3], W. SEIFERT[1], S. SEITZ[3], O. STAHL[1], E. SUTORIUS[1], T. SZEIFERT[4], S. WAGNER[1], B. ZIEGLER[2]

[1]Landessternwarte Heidelberg, [2]Universitäts-Sternwarte Göttingen, [3]Universitäts-Sternwarte München, [4]ESO Garching, [5]MPIA Heidelberg

1. Deep Fields

Watching the sky with the naked eye we can detect several thousand galactic stars but never more than two or three objects beyond our Milky Way galaxy. On the other hand, already images taken with small telescopes and photographic plates record in fields well outside the galactic plane more distant galaxies than galactic stars. Obviously, an increased sensitivity does not only allow us to see more objects, but, more importantly, we can look deeper into space. During the period when photographic plates were still the prime optical detectors, deep observations were usually carried out using Schmidt telescopes which allowed us to combine a deep look with a large field of view. Telescopes with larger apertures did not provide a great advantage since (because of the non-linearity and poor reproducibility of the photographic process) the flux (or magnitude) limit of photographic imaging was determined by the sky background, which could not be subtracted accurately. Only with the introduction of the essentially linear CCD detectors it became possible to observe objects with a surface brightness well below that of the sky. However, for manufacturing reasons, the achievable dimensions of CCDs are much smaller than those of large photographic plates. Therefore, imaging surveys reaching very faint magnitudes have, so far, been restricted to relatively small *Deep Fields.* Nevertheless, such deep-field surveys have proven to be exceedingly valuable in producing complete inventories of faint objects, for finding very distant objects, and for studying the properties and statistics of galaxies as a function of the evolutionary age of the universe.

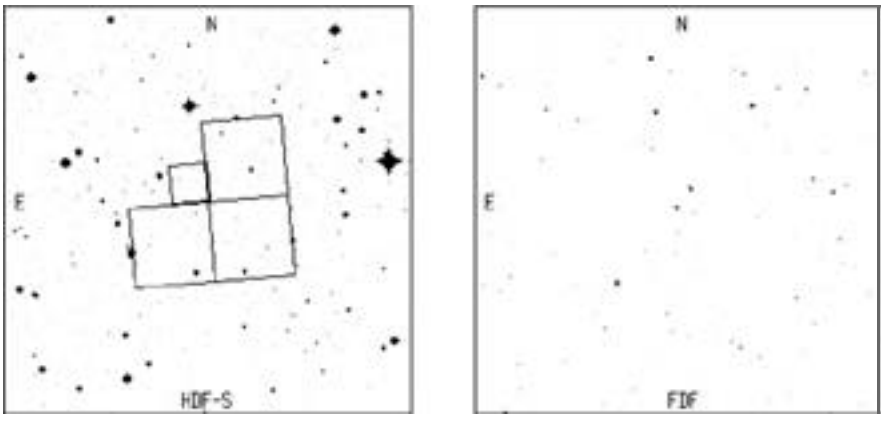

Figure 1: Digital Sky Survey plots of the FDF and of a field of the same size surrounding the HDF-S. Note the lower surface density of bright foreground objects and the absence of bright stars in the FDFregion.

Although the mean sky background can be determined and subtracted reliably from CCD frames, the photon noise of the sky, being of stochastic nature, cannot be eliminated. Therefore, even with CCDs, the achievable accuracy of faint-object photometry still depends on the amount of sky flux underlying the object images. Therefore, observations from space provide particularly favourable conditions for deep imaging and photometry since at most visual wavelengths the sky background is lower and since the absence of atmospheric seeing effects normally results in sharper images. It is not surprising, therefore, that two HST-based deep-field surveys (HDF and HDF-S) had a particularly strong scientific impact, providing a wealth of information and inspiring many follow-up studies.

2. Motivation for a FORS Deep Field

In spite of their great importance and success, the Hubble Deep Fields have some drawbacks. One obvious disadvantage is the, compared to modern ground-based faint-object cameras, relatively small field of view of the HST WFPC which limited the Hubble Deep

Figure 2: True colour image of the inner 6′ × 6′ of the FORS Deep Field. North is up, East to the left.

Fields to areas of only about 6 square arcminutes. Moreover, the compared to present large ground-based telescopes relatively modest aperture of the HST requires very long integration times to collect a sufficient number of photons from faint objects. Finally, under optimal atmospheric conditions today's large ground-based telescopes with high quality cameras at good sites can reach practically the same image quality as the HST. This has been demonstrated during the past months with the combination of the ESO VLT and the HR mode of the FORS focal plane instruments where the best stellar images obtained so far showed FWHM values below the 2 × 0.1 arcsec pixel sampling resolution limit of the CCD. Since the HST WFPC has the same pixel size (which again undersamples the instrumental PSF), the images obtained with the FORS HR mode during the best seeing experienced so far at Paranal just match the resolution of single HST WFPC frames. Hence, by selecting observing periods of optimal seeing, at least at wavelength bands where the sky background is produced mainly outside the earth's atmosphere, modern ground-based telescopes with high-quality focal-plane instruments can in principle observe as deep as, or deeper than, the HST.

Unfortunately, a quick look at the Paranal seeing statistics shows that periods of seeing below 0.2 arcsec are so rare that observing programmes requiring such good seeing for sizeable amounts of time would require years to complete, even if all the time with excellent seeing would be allocated to one such a programme. On the other hand, moderately good seeing occurs relatively often. According to ESO's VLT Site Selection WG report, seeing below 0.6 arcsec is to be expected for about 40 % of the time. At 0.6 arcsec the well-sampled VLT PSF is about 3 times larger and its surface about 10 times larger than for the HST WFPC, resulting for unresolved objects in a 10 times larger sky background. In wavelength bands with no significant atmospheric sky contribution, this results in an increase of the noise level by about a factor 3 and in a correspondingly lower signal-to-noise ratio. On the other hand, the VLT has an about 10 times larger collecting area, resulting in an increase of S/N by a factor 3. Therefore, for point sources at 0.6 arcsec seeing (and with no significant atmospheric contribution to the

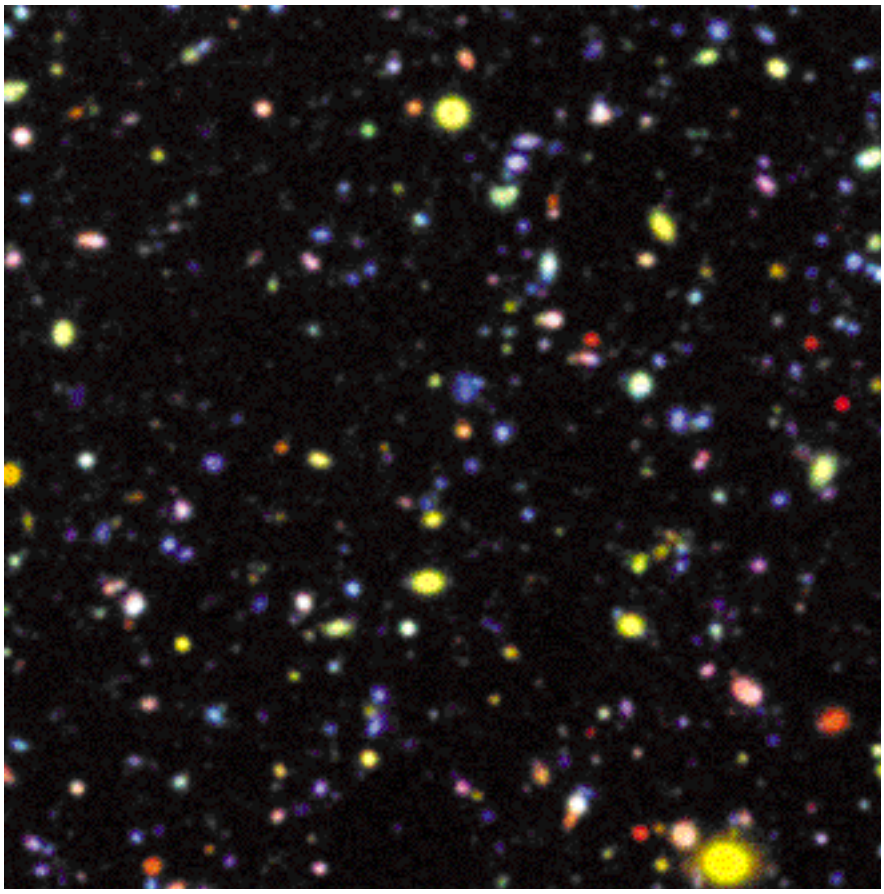

Figure 3: Enlargement of a 100″ × 100″ area of Figure 2.

sky background), the larger collecting area of the VLT just compensates the seeing effect on the photometric S/N. Hence for equal exposure times we get the same S/N as with the HST. For extended sources we in fact gain with the VLT. In the red spectral range, where we have strong atmospheric contributions to the sky background, the HST has a larger advantage compared to the VLT. At these wavelengths, the VLT is competitive only at better seeing conditions or with an increased total exposure time. Nevertheless, if periods of good seeing are selected and if a sufficient amount of observing time is invested, the VLT can look as deep as the HST. But with the larger FOV of the FORS instruments significantly larger statistical samples can be obtained in a single FORS field.

The above estimates show that FORS and the VLT provide an attractive alternative to HST for deep-field studies. But the estimates also show that in order to reach similar limiting magnitudes, comparable amounts of observing time have to be invested. Such large projects cannot be carried out easily as normal General Observer programmes at the VLT. For this reason, the consortium of German astronomical institutes (comprising the Heidelberg State Observatory (LSW) and the University Observatories of Göttingen and München) which – in co-operation with ESO – built the FORS instruments, decided to devote a significant fraction of the guaranteed observing time, which the three institutes received for their effort, to observe a FORS Deep Field (FDF).

3. Field Selection and Observing Programme

Although under optimal seeing conditions the FORS instruments are most sensitive using the HR imaging mode, all FDF observations were carried out in the Standard Resolution (SR) mode. There were two reasons for using this mode: Firstly, the HR mode becomes superior only during periods of seeing below 0.4 arcsec, which at the VLT occurs only during less than 4 per cent of the time. Secondly, with the SR mode, having a FOV covering about 46 square arcmin (about 8 times that of the HST WFPC), we can potentially observe more objects and, by covering a larger volume of space, we may be less affected by local density variations and peculiarities.

A major disadvantage of the larger aperture of the VLT is that even moderately bright objects will produce CCD saturation effects already during relatively short exposure times. Moreover, because of the larger field, the chances of finding a bright star in the FORS FOV are greater than for the WFC. In order to keep the ratio between exposure times and readout periods of the individual frames at an acceptable value, deep photometry can be carried out with FORS economically only in fields which are free of stars brighter than about 19 mag. Therefore, apart from the usual criteria of the absence of significant galactic extinction, the absence of IR emission, and the absence of foreground galaxy clusters, the main criterion for the FDF was the absence of stars brighter than 19 mag. For this reason, it was not possible to use the surroundings of the southern Hubble Deep Field (HDF-S) for the FDF programme. As shown in Figure 1, there are too many bright foreground stars in and near the HDF-S to allow deep VLT exposures of this region. An additional criterion for the selection of the FDF was the presence of a distant (z > 3) QSO, which

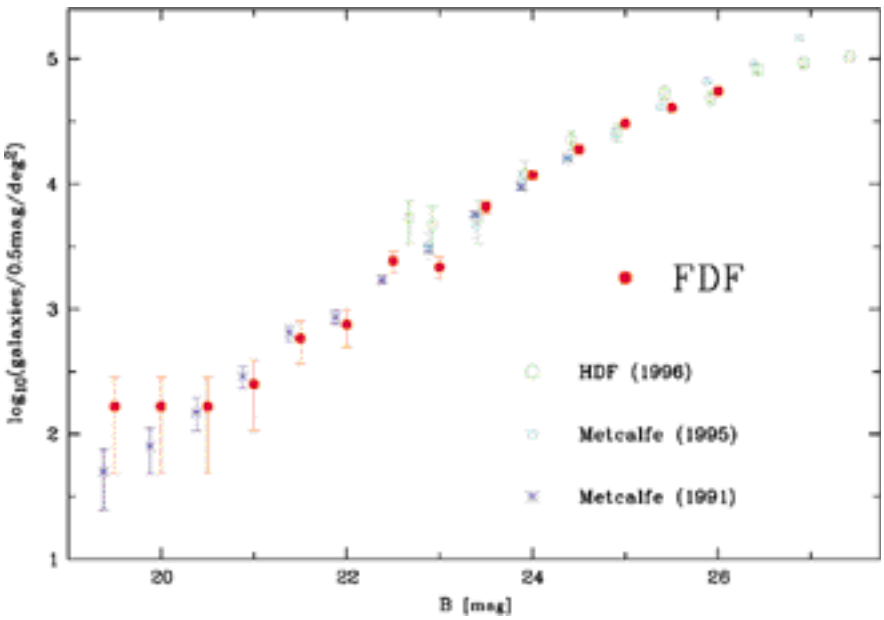

Figure 4: Comparison of preliminary (bright) galaxy counts in the FDF with results from other deep surveys.

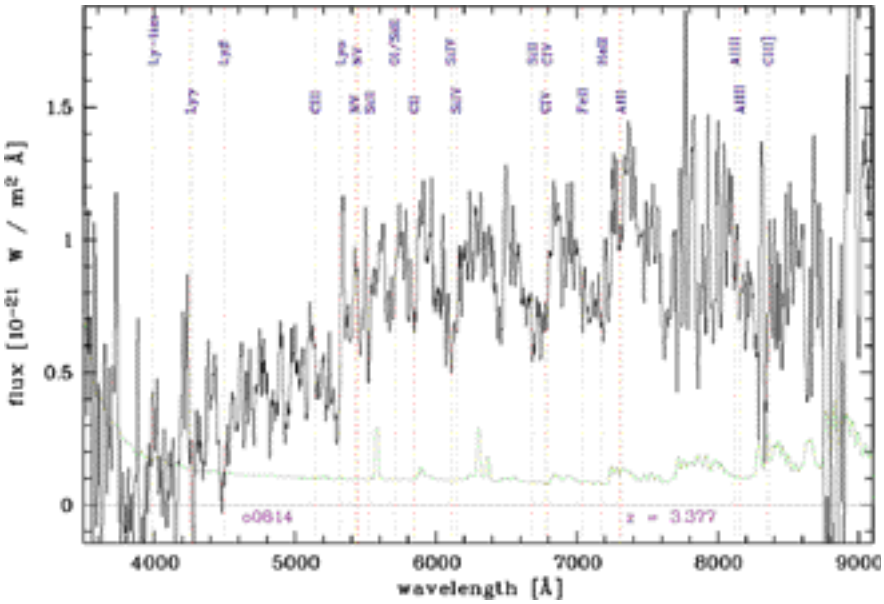

Figure 5: Spectrum of a distant (z = 3.377) galaxy found in the FDF. The green line indicates the noise level, which varies with wavelength due to the night sky spectrum and the wave - length-dependent instrumental efficiency.

would allow us to study the intergalactic gas distribution along the line of sight. Finally, the field had to be observable well from Paranal. An analysis of various digital sky maps resulted in four fields matching these criteria. Test observations then showed that only one of the four field candidates was fully suited for our purpose. A true-colour image of this field (located at α_{2000} = $01^h06^m03.6^s$, δ_{2000} = –25° 45′ 46″) containing about 10^4 galaxies is reproduced in Figure 2. Figure 3 shows an enlarged subimage of a 100″ × 100″ area in the SE quadrant of Figure 2. The conspicuous blue galaxies have in most cases significant redshifts and are intrinsically UV-emitting galaxies with enhanced star formation at earlier cosmic epochs.

4. First Results

During the second half of 1999, we carried out a programme to obtain deep photometry in the U, B, g, R, and I bands (as well as in some selected narrow bands) of the FDF. In each of these filter bands we constructed deep images based on several hours of exposures obtained during good seeing conditions. Using an automatic extraction programme, we are presently generating a catalogue of the observed galaxies and their colours in the FDF. As soon as the catalogue is complete and in its final form, these data will be made public. We also started a statistical analysis of the detected objects and a photometric classification and photometric redshift derivation of all galaxies in the field. Since for the reliable classification of certain galaxy types NIR colours are of crucial importance, we also obtained in the fall of 1999 J- and K-band frames of the FDF using SOFI at the NTT at ESO La Silla.

Figure 4 shows preliminary galaxy number counts (based on a small subset of the data) in the B band. As shown by the figure, at brighter magnitudes, the observed distribution fits well the galaxy surface density derived by other authors, indicating that the FDF is well suited as a study region. Although the observations revealed the presence of a moderately distant galaxy cluster in the SW corner of the field, this cluster is not rich enough to disturb the number counts significantly. With our final data, we hope to extend the comparison to the whole magnitude range observed with the HST.

For subsamples of objects found to be of particular interest from the photometric data, we began obtaining FORS low-resolution spectra. The main objective of this spectroscopic programme will be to study the dependence of the physical properties of galaxies on the cosmic age. According to present plans, most of the spectroscopy will be carried out during two GTO runs in fall 2000. A few MOS spectroscopic frames were already obtained in periods of poor seeing or non-photometric conditions during the 1999 photometric runs. Among the more than one hundred spectra thus obtained so far, we found already some interesting high-redshift galaxies and QSOs. In Figures 5 and 6, we present two examples of high-redshift galaxy spectra showing strong Lyman and high ionisation metallic lines and a strong UV continuum (indicating intense starburst activity) but no or only weak emission lines.

As already noted, the FDF was selected to include a known high redshift (z = 3.36) QSO. Figure 7 presents a blue FORS spectrum of this object. The figure clearly shows the presence of a rich forest of intergalactic lines of various types. A detailed study of these lines requires a higher spectral resolution than is feasible with FORS. Therefore, we applied for time with UVES at the VLT to obtain high-resolution spectra of this QSO. The resulting spectra will allow us to derive redshifts for the Lyα absorbers, which will be compared to the redshifts of the galaxies along the line of sight. In this way, we hope to identify some of the absorbers and to compare the distribution of galaxies and the absorbing gas clouds in the direction of the FDF. Finally, we note that we also

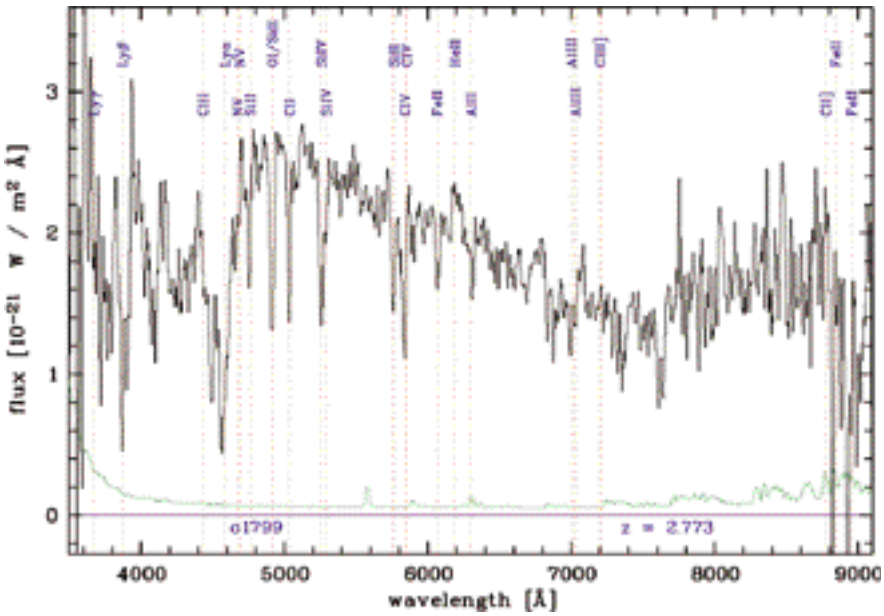

Figure 6. The spectrum of a z = 2.773 FDF galaxy. Note the strong (rest frame) UV continu - um and absence of strong line emission.

initiated FDF follow-up investigations in other wavelength ranges. The most extensive of these follow-up studies is a mapping of the FDF at radio wavelengths which is being carried out in co-operation with colleagues from the MPI for Radioastronomy, Bonn, at the VLA.

At present our FDF project is still work in progress. While our deep photometric study can probably be completed within the next few months, the spectroscopic programme and the follow-up investigations may keep us (and other interested groups) busy for years to come. We hope – and are optimistic – that these studies will eventually result in new and important insights into the evolution of our universe, which will perhaps be reported in future issues of *The Messenger*.

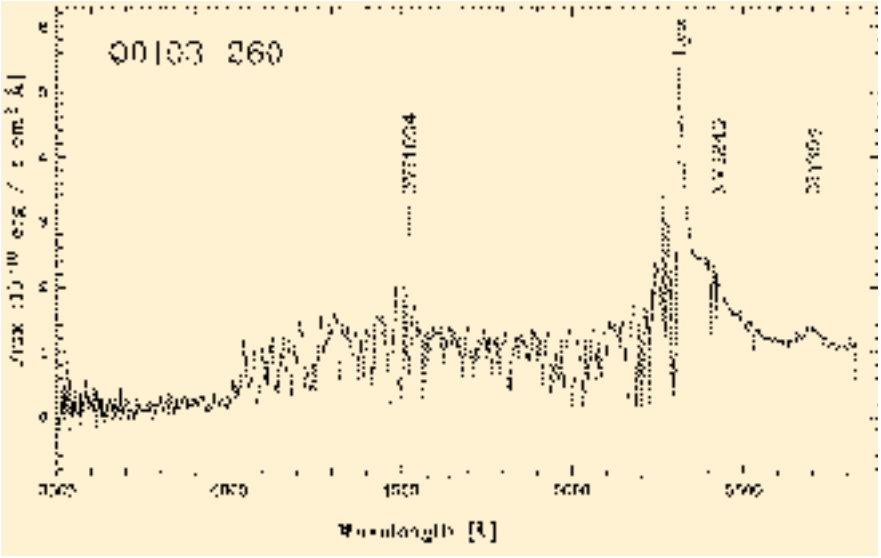

Figure 7: FORS spectrum of the Lyman forest of the FDF quasar Q0103-260.

DATA MANAGEMENT & OPERATIONS DIVISION

Astronomical Image Resampling

N. DEVILLARD, ESO

1. Introduction

Resampling an image is a standard operation used in astronomical imaging for various tasks: changing the scale of an image to superimpose it on another, shifting an image by a non-integer offset, rotating an image by an arbitrary angle, or deforming an image to counter detector or optical deformations, are the usual operations in need of image resampling. In a more general way, this operation is referred to as *image warping* in the digital image processing world.

2. Sampling a Signal

The stellar light landing on an astronomical detector is a continuous optical signal. It is sampled by the detector at precise positions, yielding a regular grid of intensity values also known as pixels (for *picture elements,* often abbreviated to *pel).* The initial signal carries by definition an infinite amount of information (because of its continuity), but it has been reduced to a finite number of values by the detector system. The sampling theory has proved that it is possible to reconstruct the initial signal from the knowledge of its samples only, provided that a certain number of assumptions are fulfilled.

In our case, we will assume that this is always the case, i.e. that the pixel sampling frequency is always greater than twice the greatest spatial frequency of the image (Shannon or Nyquist sampling). This is true for most ground-based telescopes because the instruments have been designed so, but this does not apply to some HST instruments for example. In that case, it is still possible to retrieve the signal, modulo some assumptions. This is not discussed in this paper.

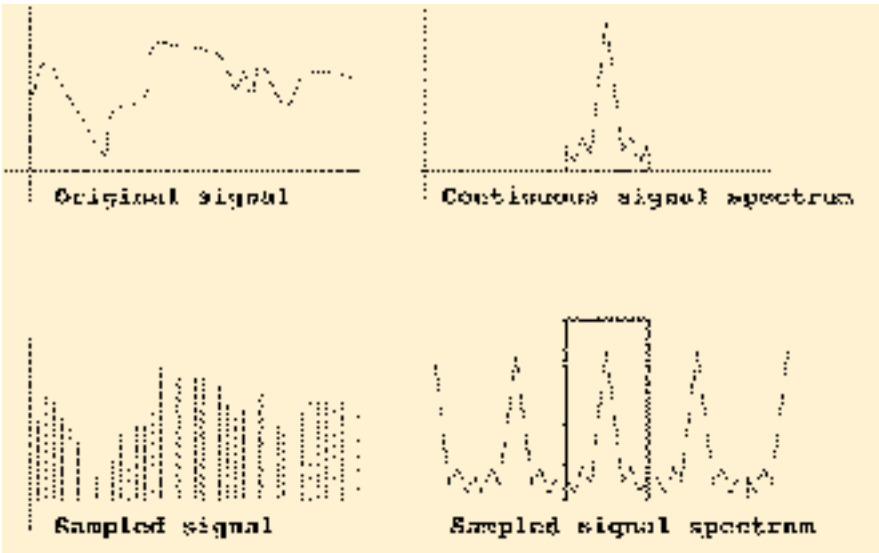

Figure 1: Top left is the original signal, top right its Fourier transform. Bottom left is the sampled signal and bottom right the Fourier transform of the sampled signal.

3. Sampling Theory

This section provides some background about the sampling theory in general. For convenience, a simple 1-dimensional signal S(t) will be used as a conventional signal, because in this case the same rules apply to images understood as 2-dimensional signals (an intensity as a function of the pixel position on the detector).

The Fourier transform is a very convenient tool to perform an academic study of this case. It also helps to see the signal in another space to understand exactly what is happening during the various operations performed on it.

The representation of a signal *S*(*t*)in Fourier space is a distribution that has no energy outside of a certain frequency range, i.e. it has non-zero values

only inside a given range. This representation is symmetrical for real-life signals, so the non-zero support is completely defined by the cut-off frequency f_c. Figure 1 shows what a time signal might look like, and what its representation in Fourier space would be. Now, what happens when this continuous signal is sampled? According to Fourier theory, sampling a signal with an ideal sampler is equivalent to convolving it with a delta function, which is equivalent in Fourier space to multiplying the signal by a comb function (a regularly-spaced collection of diracs).

The idea for reconstruction is that we would like at some point to reconstruct completely the continuous signal, and then re-sample it, i.e. take new samples at arbitrary positions. The sampling theory enables that the right assumptions are fulfilled. What it means in practice in Fourier space, is that side replica of the sampled signal spectrum should be removed (the central part of the spectrum isolated).

This is easily achieved in Fourier space by multiplying the sampled spectrum by a door function (a function that is 0 everywhere but 1 where the central spectrum is, see on figure 1 the box around the central spectrum replica). Unfortunately, this ideal door function corresponds to a *sine* function in the real space, which has infinite support and is thus not implementable in real-life. In other words, perfect reconstruction can only be achieved mathematically. To build a system that would achieve the same, we need to have an infinite quantity somewhere in the system, which does not belong to our real-life domain.

This ideal door function can be approximated by functions that do not have an infinite support, though. But as approximations are not truly the function, the reconstruction will not exactly stick to the real signal. The amount of errors in the reconstructed signal will depend on how the approximation is done. The approximated door function is usually called a *kernel* in the literature.

The search for “good” kernels has lead to a veritable zoo of functions fit for one purpose or another. Many authors in very different fields have found kernels that have some interesting properties that pair ideally with some characteristics of the signals they studied. The filter domain is one of the key fields in digital electronics, whether it applies to sound machines (stereo systems), to images (television) or any kind of sampling machine. Various kernels are reviewed in the next section.

4. Image-Space Interpolation

Another way of reconstructing the missing parts of the signal between samples, is to stay in the real space and create the missing information based on e.g. some assumptions on the signal smoothness. In electronics, the following reconstruction schemes are often used for reconstruction:

4.1 Nearest neighbour

Maybe the simplest idea is to say that the signal value is the one of the closest sample. This is known as a zero-order blocking filter, or nearest-neighbour interpolation. If we study that carefully, we see that this is strictly equivalent to applying a box kernel to the real space, thus a sine function in the Fourier space.

It means that the central replica of the sampled spectrum will be multiplied by a sine function, which is actually a very bad approximation of the ideal box kernel. This leads to obvious artefacts like jagged edges in images or granularity in sound. You can actually hear that kind of artefact when using noisy digital telephone lines like mobile phones: your voice appears deformed as if it were ringing.

This is due to the fact that the mobile phone receives voice samples one by one, and if the line is cut for a tiny amount of time (some samples are missing), it keeps emitting the same sound until it receives more information. This comes back to subsampling the voice, and reconstructing it with a very bad reconstruction approximation. The voice spectrum is folded and you get that kind of nasty artefacts.

Nearest-neighbour interpolation is the cheapest way of reconstructing a signal and also the dirtiest. It might be OK if you need speed (e.g. to display a zoomed image), but certainly not if you want to preserve the smoothness of the input signal.

4.2 Linear interpolation

One idea is to draw slope segments between samples. This corresponds strictly to a linear approximation of the values between known samples. In electronics, this is also referred to as a first-order blocking filter. Now what is the quality of a linear interpolation in real space, if we try to compare it to other kernels in Fourier space?

Drawing line segments between samples is strictly equivalent to convolving the input signal with a triangle function (demonstration left to the reader). Convolving the signal with a triangle function is then equivalent to multiplying its spectrum by the Fourier transform of a triangle, which is a *square sinc* function.

A *square sinc is* better than a *sinc*: it is never negative and goes to zero much faster, which means that other replica of the central spectrum are less likely to be included in the reconstructed spectrum. However, it is still a very bad approximation of the ideal box function. It obviously attenuates high frequencies and tends to deform low-frequencies. The ringing goes towards zero but not that fast, which tends to include other replica in the reconstructed signal.

Linear interpolation is another cheap way of reconstructing a signal and might be a good candidate when artefacts are not so much an issue. For every-day digital pictures (television or photos), this is still valid, but for signals like astronomical images it is more reasonable to use a smoother reconstruction.

4.3 Spline interpolation

To preserve a certain smoothness of the signal between samples, one can use a set of smooth functions such as splines. Describing the maths behind these functions is outside the scope of this article, it is enough to know that they tend to reproduce quite well signal variations, and they are expensive to compute.

What do they correspond to in Fourier space? A spline function is usually obtained by convolving a box function with itself a certain number of times. How many times the convolution is applied determines the level of the spline functions, which are also referred to as N-order blocking filters in electronics.

In Fourier space, that means the N-th power of the *sinc* function. As N goes to higher degrees, the kernel tends to looks more and more like a gaussian shape with steep slopes. This is a much better approximation of an ideal box function and usually yields the best visual results with normal images.

Because they are expensive to compute, splines are usually used in their third order (cubic splines). You can find that kind of interpolation for images in all respectable image-processing software packages (like PhotoShop or GIMP). For astronomical images, this is still a questionable method due to the noise in images, bringing very high frequencies which are not so well handled by cubic splines.

4.4 Fourier-based kernels

These interpolation methods are based on some study happening in Fourier space, but they are nonetheless implemented in the image space without ever having the need to convert the whole image by use of FFT or equivalent means.

As mentioned above, interpolation kernels can be found by hundreds in various fields. The most appropriate for image processing are quoted here:

• Lanczos2 or Lanczos3: these kernels are based on cosine functions, they are shown to respect quite well the low-frequency parts of the signal but

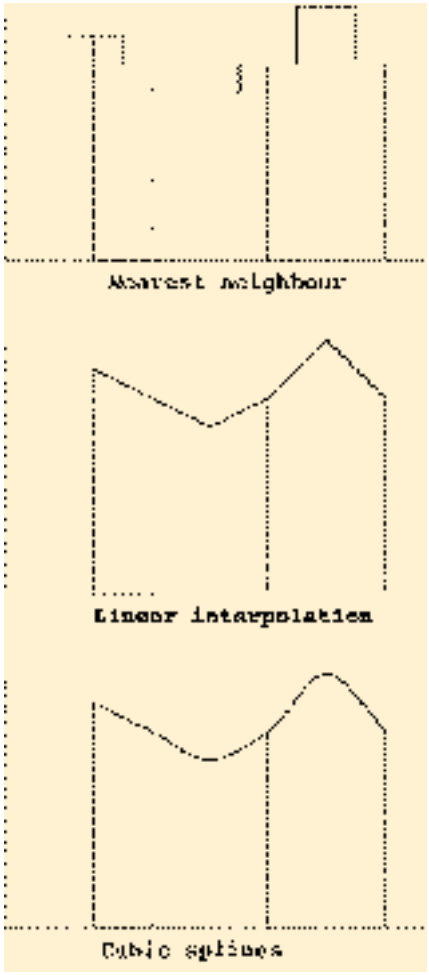

Figure 2: Three different interpolation schemes.

smooth a little bit the high-frequencies. This is an issue for noisy images such as astronomical images.

• Hann and Hamming kernels are also based on truncated cosine functions. They also tend to smooth out high frequencies and induce some rippling in the image space, but produce very acceptable quality for usual images.

• Hyperbolic tangent kernel: this is one of the best-known approximations of the ideal box function, obtained by multiplying symmetric hyperbolic tangent functions. It preserves quite well both high and low frequencies (as expected for a faithful approximation of a box function) and induces almost no rippling in the image space.

The latter kernel (hyperbolic tangent) is the one implemented in the jitter imaging recipe in the ISAAC pipeline. More information can be found about its definition, implementation, and evaluation in the corresponding article: http://www.eso.org/projects/dfs/papers/jitter99/

4.5 Examples

Figure 2 shows an example of the nearest neighbour, linear, and spline interpolations of the same signal.

Figure 3 shows various examples of image interpolations applied to zoom an example image. Top left is nearest neighbour, top right is linear, bottom left is cubic spline, and bottom right is a hyperbolic tangent based interpolation kernel.

5. Spatial Transformations

Now that we know how to create new samples out of a sampled signal, the next question is: where do we want to place these new samples? This of course depends on the nature of the operation to be performed on the image.

Shifting an image by a non-integer offset for example, is a typical operation in need of pixel interpolation. Obviously, the worst case is when the shift must be done up to exactly half a pixel. This is the place that is the furthest from the real known samples, thus having the most invented properties.

Scaling an image (i.e. zooming it in or out) is also a common operation that involves interpolation. In your favourite image displayer (RTD or Saoimage), when you request to double the zoom on your image, the software behind actually performs a pure pixel replication, which is the same as nearest-neighbour interpolation. While this is very bad for signal properties, it is acceptable for a user display since you can very easily see where artefacts are. If you need to scale an image by a non-integer factor e.g. to superimpose it with another image taken with a different pixel scale on the sky, you will need more accurate interpolation methods.

Correcting an image for detector deformations (pincushion or barrel, depending on the orientation) will most likely require a 2d polynomial of second degree at least. A true mapping of the deformation is more easily expressed in radial co-ordinates and yields complicated deformation formulas. Whatever the deformation you choose to correct for, you will end up with a formula that explains how to compute the one-to-one correspondence between a pixel in the deformed image and a pixel in the corrected image.

Other deformations can easily be implemented if they can be expressed as a one-to-one relationship between pixels in the original image, and pixels in the deformed (warped) image.

6. Possible Implementations

There are only two ways of implementing a resampling scheme for images: direct or reverse. The direct way is going from the original image to the deformed one, literally spraying the input pixels onto an output grid. The reverse way is going from the deformed image back to the original one, computing samples only where they are needed.

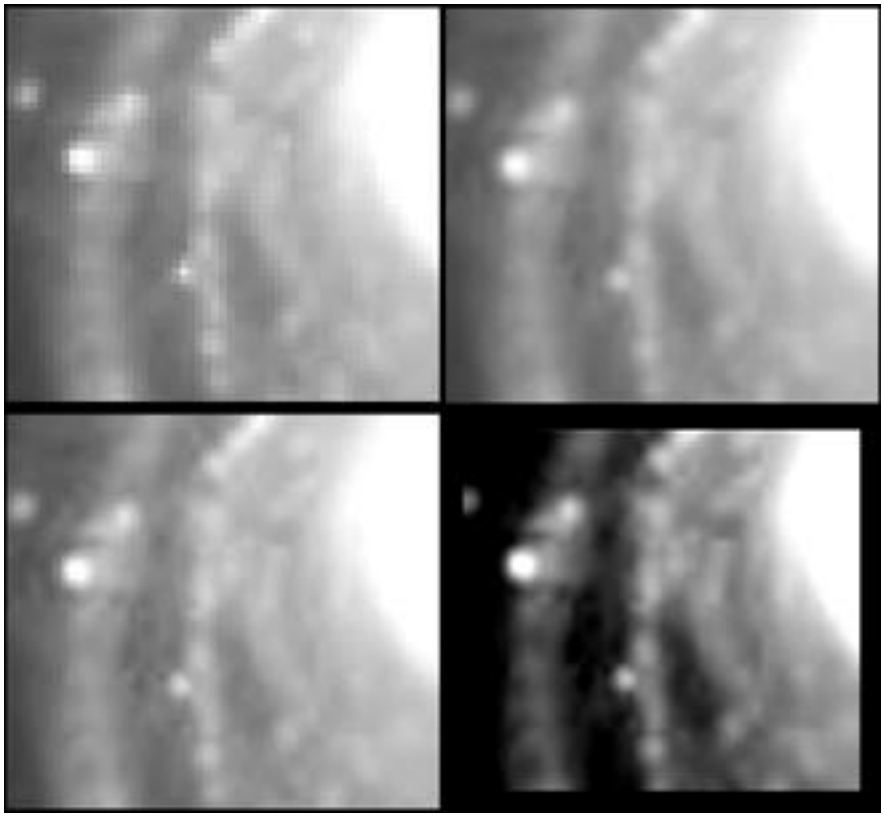

Figure 3: Various interpolation schemes. Top left is nearest neighbour, top right is linear, bottom left is cubic spline and bottom right is hyperbolic tangent.

6.1 Direct warping

Direct warping is taking pixels from the original image and trying to throw them onto an output grid that represents the output, warped image. The main drawbacks of this method are the following:

• The output grid needs to keep track of how many pixels have landed in each section, to be able to correctly normalise the output value. This can be a nightmare to implement efficiently.

• There might be some deformations that will leave holes in the output grid. If for some reason the output grid is denser than the input one, the risk is to have so many holes that the output image does not make sense. To avoid that, one can oversample the input image to make it of similar density to the output image, but then the memory consumption is growing by the same amount. For large images, this is not a solution.

• If there is no possible assumption about the way input pixels are thrown onto the output grid, it is impossible to guarantee that the output pixels will be written sequentially. This makes it hard to optimise I/O accesses, and slow down to the extreme the processing of large images, even for simple transformations.

Direct warping is usually considered too dangerous to implement because of potential holes in the resulting image, and because of speed concerns. Image processing is a domain that needs optimisation no matter what the underlying hardware is. A pixel operation that needs a millisecond to run will have you wait more than 17 minutes in front of your screen if you have to process an ISAAC image, or 71 hours if you are processing a VST image.

The best optimisations in the image processing domain usually reach about a hundred clock ticks to achieve. On a modern PC running at 500 MHz, considering that the image processing software is alone running on the CPU, you will still have to wait 2 seconds per ISAAC image and 54 seconds per VST image. And that is for CPU time only, a bad I/O optimisation forcing the software to go to the disk regularly would multiply these figures by a factor thousand at least.

Direct warping is at the heart of the "drizzle" method implemented for HST image reconstruction. Drizzle makes use of a convolved linear interpolation scheme that brings more artefacts than simple linear interpolation. If big images are involved, or tricky (non-linear) deformations, or bad pixels, or large amounts of noise, this method is likely to create false information in the output image. The same is valid for almost all astronomical image processing packages: most of them use a linear reconstruction scheme for default interpolation method.

6.2 Reverse warping

Reverse warping is considering first the output grid as the image to obtain. The size of the grid can be determined by observing the transformation function between deformed and corrected image. For example: if the transformation is a scaling by a factor 2, the output grid will simply be 2 times bigger than the input image, containing 4 times more pixels.

The method is looping over all output pixels, computes by means of a reverse transformation which are the contributing pixels from the original image, applies an interpolation scheme as described above, and writes the result to the output image.

This has several advantages:

• The output grid cannot have holes, since all output pixels are reviewed.

• The output grid will be sequentially visited, allowing to cache the results to avoid going to disk too often.

• Because of the sequential nature of the operation (no matter what the transformation is), it is relatively easy to optimise the pixel accesses in a generic way, helping to achieve optimised but also portable code (i.e. a software that is fast no matter what the underlying hardware and OS are).

• The implementation is relatively easy to write and read, allowing a better maintenance.

If you implement a generic interpolation kernel scheme that allows the user to select the kernel to use, reverse warping becomes an easy task to implement and allows for large gains in speed in the resulting software.

This is the method implemented in the warping tool offered in the eclipse package (http://www.eso.org/eclipse/), and at the heart of the ISAAC imaging pipeline. The default kernel is the hyperbolic tangent mentioned above.

7. Conclusions

Astronomical image resampling is a complex operation that involves recent theorems in the field of signal and image processing, together with information theory knowledge to be carried out properly.

No information was given about the various methods that can be used to identify the transformation between two images. This is a complete research domain in itself, refer to the appropriate literature for more information. The emphasis in this article has been put on the various methods that can be used to interpolate pixels in an image, and efficient ways to implement them.

Usual interpolation schemes are shown to be insufficient in the usual noisy astronomical images, adding aliasing and other various artefacts into the images. There are more precise kernels such as the hyperbolic tangent, that are more suitable for astronomical image handling. It might also be a good idea to look into pre-processing filters to apply to the input images before trying to re-sample them.

If you care about the quality of your images whenever you have to apply resampling operations, you should query your favourite data reduction package to check out what kind of interpolation scheme is actually implemented behind the scenes. Choosing linear interpolation is rarely a good solution in the case of noisy images.

OTHER ASTRONOMICAL NEWS

Portugal to Accede to ESO *(from ESO Press Release 15/00, 27 June 2000)*

The Republic of Portugal will become the ninth member state of the European Southern Observatory.

On Tuesday, June 27, during a ceremony at the ESO Headquarters in Garching (Germany), a corresponding Agreement was signed by the Portuguese Minister of Science and Technology, José Mariano Gago, and the ESO Director General, Catherine Cesarsky, in the presence of other high officials from Portugal and the ESO member states .

Following subsequent ratification by the Portuguese Parliament of the ESO Convention and the associated protocols, it is foreseen that Portugal will formally join this organisation on January 1, 2001.

Signing of the Portugal-ESO Agreement on June 27, 2000, at the ESO Headquarters in Garching. At the table, the ESO Director General, Catherine Cesarsky, and the Portuguese Minister of Science and Technology, José Mariano Gago. Photographer: H.-H. Heyer

Uniting European Astronomy

In his speech, the Portuguese Minister of Science and Technology, José Mariano Gago, stated that "the accession of Portugal to ESO is the result of a joint effort by ESO and Portugal during the last ten years. It was made possible by the rapid Portuguese scientific development and by the growth and internationalisation of its scientific community."

He continued: "Portugal is fully committed to European scientific and technological de velopment. We will devote our best efforts to the success of ESO".

Catherine Cesarsky, ESO Director General since 1999, warmly welcomed the Portuguese intention to join ESO. "With the accession of their country to ESO, Portuguese astronomers will have great opportunities for working on research programmes at the frontiers of modern astrophysics."

"This is indeed a good time to join ESO", she added. "The four 8.2-m VLT Unit Telescopes with their many first-class instruments are nearly ready, and the VLT Interferometer will soon follow. With a decision about the intercontinental millimetre-band ALMA project expected next year and the first concept studies for gigantic optical/infrared telescopes like OWL now well under way at ESO, there is certainly no lack of perspectives, also for coming generations of European astronomers!"

Portuguese Astronomy: a Decade of Progress

The beginnings of the collaboration between Portugal and ESO, now culminating in the imminent accession of that country to the European research or ganisation, were almost exactly ten years ago.

On July 10, 1990, the Republic of Portugal and ESO signed a Co-operation Agreement, aimed at full Portuguese membership of the ESO organisation within the next decade. During the interim period, Portuguese astronomers were granted access to ESO facilities while the Portuguese government would provide support towards the development of astronomy and the associated infrastructure in this country.

A joint Portuguese/ESO Advisory Body was set up to monitor the development of Portuguese astronomy and its interaction with ESO. Over the years, an increasing number of measures to strengthen the Portuguese research infrastructure within astrophysics and related fields were proposed and funded. More and more, mostly young Portuguese astronomers began to make use of ESO's facilities at the La Silla observatory and recently, of the Very Large Telescope (VLT) at Paranal.

Now, ten years later, the Portuguese astronomical community is the youngest in Europe with more than 90% of its PhD's awarded during the last eight years. As expected, the provisional access to ESO telescopes – especially the Very Large Telescope (VLT) with its suite of state-of-the-art instruments for observations at wavelengths ranging from the UV to the mid-infrared – has proven to be a great incentive to the Portuguese scientists.

As a clear demonstration of these positive developments, a very successful Workshop entitled "Portugal – ESO – VLT" was held in Lisbon on April 17–18, 2000. It was primarily directed towards young Portuguese scientists and served to inform them about the ESO Very Large Telescope (VLT) and the steadily evolving, exciting research possibilities with this world-class facility.

Scientific Preprints

(March – June 2000)

1364. E. Pancino et al.: New Evidence for the Complex Structure of the Red Giant Branch in ω Centauri. *ApJ*.
1365. S. Bagnulo et al.: Modelling of Magnetic Fields of CP Stars. III. The combined interpretation of five different magnetic observables: theory, and application to β Coronae Borealis. *A&A*.
1366. M. Chadid: Irregularities in Atmospheric Pulsations of RR Lyrae Stars. *A&A*.
1367. T. Broadhurst et al.: Detecting the Gravitational Redshift of Cluster Gas. *ApJL*, and
A Spectroscopic Redshift for the CL0024+16 Multiple Arc System: Implications for the Central Mass Distribution. *ApJL*.
1368. R. Falomo and M.-H. Ulrich: Optical Imaging and Spectroscopy of BL Lac Objects. *A&A*.
1369. O.R. Hainaut et al.: Physical Properties of TNO 1996 TO_{66}. Lightcurves and Possible Cometary Activity. A&A.
1370. B. Leibundgut: Type Ia Supernovae. *The Astronomy and Astrophysics Review*.
1371. Contributions of the ESO Data Management and Operations Division to the SPIE Conference "Astronomical Telescopes and Instrumentation 2000". Conference 4010.
D.R. Silva et al.: VLT Science Operations: The First Year.
P. Quinn et al.: The ESO Data-Flow System in Operations: Closing the Data Loop.
A.M. Chavan et al.: A Front-end System for the VLT's Data-Flow System.
P. Amico and R. Hanuschik: Operations of the Quality Control Group: Experience from FORS1 and ISAAC at VLT Antu.
P. Ballester et al.: Quality Control System for the Very Large Telescope.
1372. S. Hubrig et al.: Magnetic Ap Stars in the H-R Diagram. *ApJ*.
1373. J.U. Fynbo et al.: The Sources of Extended Continuum Emission Towards Q0151+048A: the Host Galaxy and the Damped Lyα Absorber. *A&A*.
1374. S. Stefl et al.: The Circumstellar Structure of the Be Shell Star φ Per. *A&A*.
1375. M. Kissler-Patig: Extragalactic Globular Cluster Systems. A New Perspective on Galaxy Formation and Evolution. Reviews in Modern Astronomy, vol 13.
1376. E. Scannapieco et al.: The Influence of Galactic Outflows on the Formation of Nearby Galaxies. *ApJ*.
1377. J.D. Landstreet et al.: Magnetic Models of Slowly Rotating Magnetic Ap Stars: Aligned Magnetic and Rotation Axes. *A&A*.
1378. S. Cristiani et al.: The First VLT FORS1 Spectra of Lyman-Break Candidates in the HDF-S and AXAF Deep Field. *A&A*.
1379. D. Hutsemékers and H. Lamy: The Optical Polarization of Radio-Loud and Radio-Intermediate Broad Absorption Line Quasi-Stellar Objects. *A&A*.
1380. C. Stehlé et al.: Polarised Hydrogen Line Shapes in a Magnetised Plasma. The Lyman α Line.

About The ESO Messenger

K. KJÄR, Technical editor, ESO

The present *Messenger* is the hundredth issue to be published. This may be a good moment to look back to the beginning and to the development of this publication.

The idea of an internal ESO newsletter was born in the early seventies. Using the words of Professor Blaauw, Director General of ESO at that time and the person who launched *The Messenger* in its orbit, the purpose of The ESO Messenger should be "first of all, to promote the participation of ESO staff in what goes on in the Organization, especially at places of duty other than our own. Moreover, The Messenger may serve to give the world outside some impression of what happens inside ESO. The need for more internal communication is felt by many of the staff. The dispersion of our resources over several countries in widely separated continents demands a special effort to keep us aware of what is going on at the other establishments..."

The first issue of *The Messenger* appeared in May 1974. It was printed without colour, had six pages and a circulation of about 1100 copies. It was distributed to ESO staff, to the members of the ESO Council and the various ESO committees, and to astronomical institutes.

Blue as a second colour was introduced for the first time in *The Messenger* No. 4, but only on the upper part of the cover page and for the description of ESO on the last page. The upper part of the cover has essentially remained unchanged until today, except for small changes in connection with the location of the various ESO establishments.

The first five issues were done in letterpress printing. From No. 6 until today it has been printed in offset. The first colour pictures were reproduced in the December 1982 issue (No. 30). Colour was used occasionally, and then with increasing tendency. Now, the use of colour has become standard. The number of pages has varied greatly over the years – from 6 pages (No.1) to a record number of 88 pages (No. 70).

Until No. 70, *The Messenger* was produced in the traditional way. That is, after preparation by the editors, all manuscripts were retyped at the publishers, then proofread and checked with the manuscript. The layout was done at ESO by pasting the corrected proofs and copies of the figures on paper sheets. The publisher then put the text into pages according to this layout. Since more and more authors of Messenger articles provided electronic files (in LaTeX format), from No. 71 (March 1993) to No. 78 (December 1994), the text columns of those articles were prepared in LaTeX. These texts were then exposed on film with the printer's high-resolution output device, and the film mounted on pages the same way as before. Trials to prepare the three-column layout entirely in LaTeX format were not successful.

At the end of 1994, following the example of some of his colleagues, the technical editor acquired a Power Macintosh with the necessary desk-top publishing tools. So, starting with No. 79 (March 1995), the layout of *The Messenger* has been produced in-house, using the electronic files provided by the authors or scanning the hard copies in those cases where the authors are not able to provide text in a format compatible with the layout programme (QuarkEXpress). The whole publication on CD ROM (~ 650 Mbytes) is taken to the publisher, which means that only printing and bookbinding are done outside ESO. This way, savings of printing costs of the order of 30,000 DM per year are realised for *The Messenger*.

As activities increased and more and more scientific results were produced at ESO, the interest of the press, of amateur astronomers, physics teachers, etc. in The Messenger also increased. In the course of the years, the distribution list gradually increased from about 800 addresses at the beginning to almost 4000 today. Including the copies distributed to ESO staff and at ESO exhibitions and other PR or astronomical events, the total circulation is now 5000 and sometimes even more.

However, the number of readers may be considerably higher. Agreat number of copies is sent to institutes and libraries where they are read by several people. In addition, from No. 81, September 1995, *The Messenger* can also be accessed via Internet (http://eso.org/gen-fac/pubs/messenger/) Due to internal problems, No. 82 was produced by the publisher in the traditional way and is therefore available only on paper.

Two people at ESO regularly work on *The Messenger*: the Editor (about 0.3 FTE = Full Time Equivalent) and the technical editor (about 0.5 FTE). It would be interesting to know the total time spent for the preparation of The Messenger. However, it is not possible to evaluate the time needed by the authors and the people who assist them (secretaries, draughtsmen, etc.) in preparing their contributions.

Until today, four editors were alternately responsible for The Messenger: Editor of the first three issues was Francis Walsh; Editor of Nos. 4 to 19 and again of Nos. 43 to 72: Richard West; Editor of Nos. 21 to 39: Philippe Véron, and from No. 73: Marie-Hélène Ulrich (Demoulin). The Nos. 20 and 40 to 42 were prepared by the technical editor without official editorship (contributions approved by the Director General).

Some Mishaps in Connection with the Production of The Messenger

It is probably not surprising that during the production of 100 issues of The Messenger, also a number of mishaps have occurred. Perhaps the most serious one happened with Messenger No. 4, when an object fell on the printing form, damaging part of the first Messenger page. The damaged letters were exchanged by the printers without submitting a new proof to the editors. All the damaged letters were correctly exchanged, except that the Messenger No. 4 was printed and distributed again as No. 1.

But errors are not only due to negligence – too much thoughtfulness can also produce errors. For example: on two occasions the discovery trails of minor planets disappeared from the Schmidt plates that were reproduced in The Messenger because the printers thought that the printing plates had been scratched. Without telling the editors, the plates were retouched, and the discovery trails, well described in the captions, had gone. However, these errors were discovered in time.

A similar case that was not discovered in time happened in No. 19, in an article about neutron stars. The author of that article provided a number of figures accompanying his text. On one of them, a drawing of the optical companion of the neutron star and the neutron star itself (seen from two different directions) was presented. The author was probably well aware that the small neutron star – just a dot on the figure – might get lost in the printing process. He drew the attention of the editors to the importance of the dots in the figure. The technical editor, for his part, told the printers to see to it that the two dots on the figure would not disappear. The neutron star remained at its place until the last revision of that Messenger issue. However, when The Messenger was finally delivered, the neutron stars had disappeared! Investigating the matter more closely, it was found that the printer, at the last moment before running the printing machine, had discovered two "dust grains" on one of the figures and eliminated them… In order not to lose time, the technical editor, with the help of the three kind ladies of the ESO Secretariat that served as reception and typing pool at that time, took some drawing pencils, and put the neutron stars back in place. Fortunately, the circulation then was only about 1200 copies, and the work was done in less than one day. It is hoped that the author will forgive us if the neutron stars may not have had exactly the right size or not been at their exact position…

The last anecdote is only indirectly related to The Messenger and happened in early 1977 and with the same publisher. It shows that public-relations activities should not be neglected in an organisation like ESO. In order to better understand the situation, the reader should know that at that time the ESO scientific and technical divisions were still at the CERN premises near Geneva, and the Office of the Director General with the Administration had shortly before moved from Hamburg to Garching. The ESO Headquarters was in its construction phase and the Garching staff (22 or 23 people) was provisionally housed in an apartment building in Garching. Only a small, discreet sign identified the place as ESO offices. One day, the manager of the publishing firm came to ESO to bring the blue prints of The Messenger and to discuss some matters with the technical editor. To see someone of ESO, a visitor had first to ring the bell outside the building. Then a member of the ESO Secretariat, located in a flat on the ground floor of the building, opened the door and asked whom he wanted to see. Then the secretary by telephone informed the staff member concerned. The visitor went up to the apartment in which the staff member had his office. Here, he had to ring the bell again and wait a moment to be let in.This all must have appeared very strange and mysterious to the man. He said nothing while he was at ESO. But some weeks later, when the technical editor had matters to discuss with him at his place, he said: "Now I know what ESO is all about – you can't fool me – astronomy is just a pretext. ESO is a secret-service agency!…."

ESO Fellowship Programme 2000/2001

The European Southern Observatory (ESO) awards up to six postdoctoral fellowships tenable at the ESO Headquarters, located in Garching near Munich and up to seven postdoctoral fellowships tenable at ESO's Astronomy Centre in Santiago, Chile. The ESO fellowship programme offers a unique opportunity for young scientists to pursue their research programmes while learning and participating in the process of observational astronomy with state-of-the-art facilities.

ESO facilities include the Very Large Telescope (VLT) Observatory on Cerro Paranal, the La Silla Observatory and the astronomical centres in Garching and Santiago. The VLT consists of four 8-m-diameter telescopes. Normal science operations are now conducted on the first two and will start on the third on 1 April 2001. At La Silla, ESO operates five optical telescopes with apertures in the range from 1.5 m to 3.6 m, the 15 m SEST millimetre radio telescope and smaller instruments.

The main areas of activity at the Headquarters and in Chile are:

- research in observational and theoretical astrophysics;
- managing and constructing the VLT;
- developing the interferometer and adaptive optics for the VLT;
- operating the La Silla Observatory;
- development of instruments for current ESO telescopes and for the VLT;
- calibration, analysis, management and archiving of data from the current ESO telescopes;
- developing the Atacama Large Millimetre Array (ALMA);
- fostering co-operation in astronomy and astrophysics within Europe and Chile.

The main scientific interest of ESO Faculty astronomers in Garching and in Chile are given in the ESO web site http://www.eso.org/science/facultymembers.html.

Both the ESO Headquarters and the Astronomy Centre in Santiago offer extensive computing facilities, libraries and other infrastructure for research support.

There are ample opportunities for scientific collaborations. The ESO Headquarters host the Space Telescope European Co-ordinating Facility (ST-ECF), are situated in the immediate neighbourhood of the Max-Planck Institutes for Astrophysics and for Extraterrestrial Physics and are only a few kilometres away from the Observatory of the Ludwig-Maximilian University. In Chile, ESO fellows have the opportunity to collaborate with the rapidly expanding Chilean astronomical community in a growing partnership between ESO and the host country's academic community.

Fellows in Garching spend up to 25% of their time on the support or development activities mentioned above, in addition to personal research. They can select functional activities in one of the following areas: instrumentation, user support, archive, VLTI, ALMAor science operations at the Paranal Observatory. Fellowships in Garching are granted for one year with the expectation of a second year and exceptionally a third year.

In Chile, the fellowships are granted for one year with the expectation of a second and third year. During the first two years, the fellows select to be assigned to either a Paranal operation group or a La Silla telescope team. They support the visiting astronomers at a level of 50% of their time, with 80 nights per year at either the Paranal or La Silla Observatory and 35 days per year at the Santiago Office. During the third year, two options are provided. The fellows may be hosted by a Chilean institution and will thus be eligible to propose for Chilean observing time on all telescopes in Chile; they will not have any functional work. The second option is to spend the third year in Garching where the fellows will then spend 25% of their time on the support of functional activities.

The basic monthly salary will be not less than DM 4,970 to which is added an expatriation allowance of 9–12% in Garching, if applicable, and up to 35% in Chile. The remuneration in Chile will be adjusted according to the cost of living differential between Santiago de Chile and Munich. An annual allocation of DM 12,000 (somewhat higher for a duty station in Chile) for research travel is also available. Additional information on employment conditions/benefits can be found on the ESO web site http://www.eso.org/gen-fac/adm/pers/fellows.html

Candidates will be notified of the results of the selection process in January 2001. Fellowships begin between April and October of the year in which they are awarded. Selected fellows can join ESO only after having completed their doctorate.

Applications must be made on the ESO Fellowship Application Form (postscript) which can be obtained from the ESO web site http://www.eso.org/gen-fac/adm/pers/forms/. The applicant should arrange for three letters of recommendation from persons familiar with his/her scientific work to be sent directly to ESO. Applications and the three letters must reach ESO by October 15, 2000.

Completed applications should be addressed to:

European Southern Observatory, Fellowship Programme
Karl-Schwarzschild-Str. 2, D-85748 Garching bei München, Germany
vacancy@eso.org

Contact person: Angelika Beller – E-mail: abeller@eso.org – Tel: 0049-89-3200-6553, Fax: 0049-89-3200-649

PERSONNEL MOVEMENTS

International Staff (April – June 2000)

ARRIVALS

EUROPE

BAARS, Jacob (NL), Systems Engineer, as of 1.11.99
GAILLARD, Boris (F), Coopérant
KEMP, Robert (UK), Application Software Designer and Developer
PIERFEDERICI, Francesco (I) Data Archive and Pipeline Software Specialist
SIEBENMORGEN, Ralf (D), Infrared Instrumentation Scientist
TAN, Gie Han (NL), Project Engineer

CHILE

AGEORGES, Nancy (F), Operation Staff Astronomer
CURRAN, Stephen (UK), Associate (SEST)

DEPARTURES

EUROPE

BELETIC, James (USA), Senior Astronomer
CABILLIC, Armelle (F), Programme Manager
KIM, Young-Soo (Korean), Associate
LOMBARDI, Marco (I), Student
PRIMAS, Francesca (I), Fellow
RAUCH, Michael (D), User Support Astronomer
TOLSTOY, Elizabeth (NL), Fellow

CHILE

LUNDQVIST, Göran (S), System Analyst

Local Staff (April – May 2000)

ARRIVALS

ACEVEDO, Maria Teresa, Telescope Instrument Operator, Paranal
BAEZA, Silvia, Software Engineer Developer, La Silla
CASTILLO, Monica, Telescope Instrument Operator, La Silla
COSTA, Jaime, Electrical Engineer, Paranal
SALDIAS, Christian, System Administrator, Vitacura

DEPARTURES

KAISER, Cristian, Personnel Assistant, Vitacura

TRANSFERS

KASTINEN, Ismo, Software Engineer Developer, La Silla
PAVEZ, Marcus, System Administrator, La Silla

ESO, the European Southern Observatory, was created in 1962 to "… establish and operate an astronomical observatory in the southern hemisphere, equipped with powerful instruments, with the aim of furthering and organising collaboration in astronomy …" It is supported by eight countries: Belgium, Denmark, France, Germany, Italy, the Netherlands, Sweden and Switzerland. ESO operates at two sites. It operates the La Silla observatory in the Atacama desert, 600 km north of Santiago de Chile, at 2,400 m altitude, where several optical telescopes with diameters up to 3.6 m and a 15-m submillimetre radio telescope (SEST) are now in operation. In addition, ESO is in the process of building the Very Large Telescope (VLT) on Paranal, a 2,600 m high mountain approximately 130 km south of Antofagasta, in the driest part of the Atacama desert. The VLT consists of four 8.2-metre and three 1.8-metre telescopes. These telescopes can also be used in combination as a giant interferometer (VLTI). The first 8.2-metre telescope (called ANTU) is since April 1999 in regular operation, and also the second one (KUEYEN) has already delivered pictures of excellent quality. Over 1200 proposals are made each year for the use of the ESO telescopes. The ESO Headquarters are located in Garching, near Munich, Germany. This is the scientific, technical and administrative centre of ESO where technical development programmes are carried out to provide the La Silla and Paranal observatories with the most advanced instruments. There are also extensive astronomical data facilities. In Europe ESO employs about 200 international staff members, Fellows and Associates; in Chile about 70 and, in addition, about 130 local staff members.

The ESO MESSENGER is published four times a year: normally in March, June, September and December. ESO also publishes Conference Proceedings, Preprints, Technical Notes and other material connected to its activities. Press Releases inform the media about particular events. For further information, contact the ESO Education and Public Relations Department at the following address:

EUROPEAN
SOUTHERN OBSERVATORY
Karl-Schwarzschild-Str. 2
D-85748 Garching bei München
Germany
Tel. (089) 320 06-0
Telefax (089) 3202362
ips@eso.org (internet)
URL: http://www.eso.org

http://www.eso.org/gen-fac/pubs/messenger/

The ESO Messenger:
Editor: Marie-Hélène Demoulin
Technical editor: Kurt Kjär

Printed by
J. Gotteswinter GmbH
Buch- und Offsetdruck
Joseph-Dollinger-Bogen 22
D-80807 München
Germany

ISSN 0722-6691

Tragic Car Accident Involves ESO Employees

Saturday, May 27, turned into a tragic day for ESO. The team installing TIMMI2 at La Silla, went on an excursion to the Elqui valley, 70 km east of the city of La Serena and suffered a serious car accident, crashing against another car driving from the opposite direction.

Dr. Hans-Georg Reinmann, from the University of Jena, died in the crash, while Mr. Ralf Wagner (ESO Associate), from Germany, was seriously injured and had to be taken to the intensive care unit of the Hospital de Coquimbo. The other three persons travelling in the car, Helena Relke, from the University of Jena, Ulrich Käufl and Armin Silber, from ESO Garching, were injured to a lesser degree.

Ralf Wagner remained in a critical condition for a period of three weeks. He was eventually transferred to the Clínica Alemana in Santiago, where he is slowly recovering from multiple lesions and fractures.

During the process, a large amount of blood was requested and donated by the ESO staff, in order to support the case.

A family with two children travelled in the other car involved in the crash. One of the children was critically injured. He is now out of danger, but unfortunately may remain seriously impaired.

We would like to thank the ESO staff who provided blood and personal assistance in this emergency. It should also be mentioned that the Chilean authorities and medical services assisted us beyond their call of duty.

Contents

R. Gilmozzi and P. Dierickx: OWL Concept Study 1
Paranal Impressions 11

TELESCOPES AND INSTRUMENTATION

D. Currie et al.: The ESO Photometric and Astrometric Analysis Programme for Adaptive Optics 12
E. Diolaiti et al.: StarFinder: a Code to Analyse Isoplanatic High-Resolution Stellar Fields 23
D. Bonaccini et al.: VLT Laser Guide Star Facility: First Successful Test of the Baseline Laser Scheme 27

THE LA SILLA NEWS PAGE

H. Jones: 2p2 Team News 29
M. Sterzik, M. Kürster: News from the 3.6-m Telescope 30
La Silla under the Milky Way 31

REPORTS FROM OBSERVERS

H. Pedersen et al.: Gamma-Ray Bursts – Pushing Limits with the VLT 32
D. Rigopoulou et al.: ISAAC on the VLT Investigates the Nature of the High-Redshift Sources of the Cosmic Infrared Background . . 37
R. Häfner: The Deep Eclipse of NN Ser 42
I. Appenzeller et al.: The FORS Deep Field 44

DATA MANAGEMENT AND OPERATIONS

N. Devillard: Astronomical Image Resampling 48

OTHER ASTRONOMICAL NEWS

Portugal to Accede to ESO 51

ANNOUNCEMENTS

Scientific Preprints (March–June 2000) 52
K. Kjär: About The ESO Messenger 53
A Challenge for Engineers and Astronomers 54
ESO Fellowship Programme 2000/2001 55
Personnel Movements 55
Tragic Car Accident Involves ESO Employees 56